

KIT SCIENTIFIC REPORTS 7703

Redox, solubility and sorption chemistry of technetium in dilute to concentrated saline systems

Ezgi Yalçıntaş

Ezgi Yalçıntaş

**Redox, solubility and sorption chemistry of technetium
in dilute to concentrated saline systems**

Karlsruhe Institute of Technology
KIT SCIENTIFIC REPORTS 7703

Redox, solubility and sorption chemistry of technetium in dilute to concentrated saline systems

by
Ezgi Yalçıntaş

Report-Nr. KIT-SR 7703

Dissertation, Karlsruher Institut für Technologie (KIT)
Fakultät für Chemie und Biowissenschaften, 2015

Tag der mündlichen Prüfung: 13. April 2015

Dekan: Prof. Dr. Peter Roesky

Referenten: Prof. Dr. Horst Geckeis, Prof. Dr. Petra Panak

Impressum



Karlsruher Institut für Technologie (KIT)
KIT Scientific Publishing
Straße am Forum 2
D-76131 Karlsruhe

KIT Scientific Publishing is a registered trademark of Karlsruhe
Institute of Technology. Reprint using the book cover is not allowed.

www.ksp.kit.edu



*This document – excluding the cover – is licensed under the
Creative Commons Attribution-Share Alike 3.0 DE License
(CC BY-SA 3.0 DE): <http://creativecommons.org/licenses/by-sa/3.0/de/>*



*The cover page is licensed under the Creative Commons
Attribution-No Derivatives 3.0 DE License (CC BY-ND 3.0 DE):
<http://creativecommons.org/licenses/by-nd/3.0/de/>*

Print on Demand 2015

ISSN 1869-9669

ISBN 978-3-7315-0412-2

DOI: 10.5445/KSP/1000048085

Redox, solubility and sorption chemistry of technetium in dilute to concentrated saline systems

Zur Erlangung des akademischen Grades eines
DOKTORS DER NATURWISSENSCHAFTEN
(Dr. rer. nat.)

Fakultät für Chemie und Biowissenschaften
Karlsruher Institut für Technologie (KIT) - Universitätsbereich
genehmigte

DISSERTATION

von

Ezgi YALÇINTAŞ

aus

Izmir, TÜRKEI

Dekan: Prof. Dr. Peter Roesky

Referent: Prof. Dr. Horst Geckeis

Korreferent: Prof. Dr. Petra Panak

Tag der mündlichen Prüfung: 13.04.2015

Acknowledgments

This PhD work was performed at the Institute for Nuclear Waste Disposal (INE) of the Karlsruhe Institute of Technology (KIT) under the supervision of Prof. Dr. Horst Geckeis. I would like to thank him for giving me this opportunity to do my PhD in his institute. I had a chance to contribute to high level scientific research. I have gathered a lot of valuable experience working with several advanced scientific methods and technologies.

I am also delighted to thank Dr. Marcus Altmaier head of the Radiochemistry Division at KIT-INE. I am very grateful to him for many scientific discussions and suggestions, the most important is for his always positive and constructive support.

I especially would like to thank my direct supervisor, Dr. Xavier Gaona, for his scientific advices, for the time which he was always able to find for my questions and discussions in his busy schedule, for his support whenever I started to fade, and the most for his limitless patience and kindness. I am honoured to be supervised by him during my PhD work.

I would like to thank Dr. Taishi Kobayashi for introducing me to fundamentals of technetium chemistry in the beginning of my PhD. I would like to thank Dr. David Fellhauer for guiding me in the Pitzer calculations. I would like to thank Ms. Melanie Böttle for the quick material support in the lab. I would like to thank all the members of the Aquatic Chemistry and Thermodynamics group in INE for sharing their knowledge, experience and time professionally and personally.

I appreciate Dr. Andreas Scheinost for giving me a great opportunity to work with advanced spectroscopic techniques (XAFS) in ESRF-ROBL, Grenoble, France. I am grateful for his contribution to my thesis and EXAFS data evaluation.

I would like to thank the KIT-INE beamline scientists, Dr. Kathy Dardenne and Dr. Joerg Rothe for XAFS measurements at INE-beamline for Actinide Research at ANKA and their contribution to EXAFS data evaluation. I would like to thank Ms. Sylvia Moisei-Rabung for ICP-OES measurements, Ms. Eva Soballa for SEM-EDS measurements, Dr. Nicolas Finck for XRD measurements. I would like to thank Dr. Robert Polly for quantum chemical calculations.

I am very thankful to the Radiation Protection Group of INE, with special thanks to Mr. Gerhard Christill for helping me with transferring my samples and his lovely personality.

The biggest thank is to my dear mother, Ayse Yalcintas, for being always by my side with her own way when I was in good and bad moods, for her support and trust, which makes me stronger and keep going.

I would like to thank all my family members and friends in Turkey who never stop taking care of me and supporting me from far away. I would like to thank my precious friends in Karlsruhe for their never ending support, keeping me always cheered, their limitless patience and understanding during stressful periods. They made the life easier and liveable here.

Abstract

This PhD thesis addresses the (i) redox chemistry, (ii) solubility and (iii) sorption behaviour of technetium in dilute solutions to concentrated salt brine systems. These processes are of high importance for the long-term performance assessment of nuclear waste repositories. The investigation of concentrated brine solutions in addition to diluted systems provides direct input to assess the chemistry of Tc in the framework of waste repositories designed in salt-rock formations, but also allows to derive accurate thermodynamic and precise activity models using SIT and Pitzer approaches to treat ion-interaction processes. Provided the redox sensitivity of Tc, all experiments presented in this work were performed in glove boxes under Ar-atmosphere at room temperature. The results are systematized in terms of equilibrium thermodynamics of aqueous systems.

^{99}Tc is a fission product of ^{235}U and ^{239}Pu forming with a high yield in nuclear reactors. The behavior of ^{99}Tc in repositories for radioactive waste needs to be properly assessed due to its redox sensitive character, very long half-life ($t_{1/2} \sim 2.13 \cdot 10^5$ a) and contribution to the potential radiological risk. Two different oxidation states of Tc (+VII and +IV) control the potential release and migration of this radionuclide from the repository to the biosphere, each showing markedly different solubility, complexation and sorption behaviour. In this context, an **improved understanding of Tc redox chemistry and transformation processes as function of the potential geochemical boundary conditions** (pH, E_h or p_e , ionic strength, etc.) expected for the various repository concepts and scenarios is mandatory for analysing the long-term safety. The first part of this PhD thesis provides a comprehensive evaluation of the redox behaviour of Tc in the presence of several reducing systems in dilute to concentrated NaCl and MgCl_2 solutions from acidic to hyperalkaline pH region. The pH, p_e and Tc concentration in the different systems were measured until attaining equilibrium conditions, allowing a first assessment of reaction kinetics. The effect of specific reducing systems, pH and ionic strength on the redox state of Tc was evaluated and compared to the thermodynamically calculated Tc(VII)/Tc(IV) redox transformation borders using the thermodynamic data selection in NEA–TDB. The results highlight the feasibility and reliability of $p_e + \text{pH}$ measurements for the prediction of Tc redox states in dilute to concentrated aqueous systems, whilst further confirming the predominance of Tc(IV) under the pH and redox conditions expected for the disposal in deep underground facilities.

In spite of the relevance of Tc(IV) in all the repository concepts for radioactive waste disposal, little is known on the solubility and hydrolysis of Tc(IV) in concentrated brine systems and aqueous systems of intermediate ionic strength. As the aquatic Tc chemistry in dilute systems is rather well understood, there is a decisive lack of knowledge for conditions where significant ion-interaction processes may drastically impact the stability of aqueous species and also affect solid phase characteristics. The second part of this thesis is therefore devoted to comprehensively **investigate the solubility and hydrolysis of Tc(IV) in dilute to concentrated NaCl, MgCl_2 and CaCl_2 solutions**, the later constituting the main matrix elements in several high ionic strength scenarios. The study is based upon detailed and highly systematic measurements of pH, E_h and Tc concentration in the different samples, but also investigates the aqueous Tc speciation using solvent extraction and EXAFS spectroscopy and performs accurate solid phase characterization based on SEM–EDS, XRD and chemical analysis. The formation and predominance of the ternary complexes $\text{Ca}_3[\text{TcO}(\text{OH})_5]^{3+}$ and $\text{Mg}_3[\text{TcO}(\text{OH})_5]^{3+}$ in alkaline concentrated CaCl_2 and MgCl_2 solutions, was proposed based on the slope analysis of

solubility data and in analogy with previous observations for other tetravalent metal cations (*e.g.* Th⁴⁺, Np⁴⁺, Pu⁴⁺, Zr⁴⁺). According to the newly generated experimental solubility data and spectroscopic evidences, complete chemical models, **thermodynamic data and activity models using SIT and Pitzer are derived for the system Tc⁴⁺-Na⁺-Mg²⁺-Ca²⁺-H⁺-Cl⁻-OH⁻-H₂O at 25 °C**. The thermodynamic data derived in this work are contributing to national (THEREDA) and international (NEA-TDB) database projects, and are made available for geochemical calculations of systems relevant for radioactive waste disposal, for the first time including concentrated salt brines.

The third part of this PhD is investigating the **Tc reduction and uptake mechanisms of Tc by Fe(II) minerals**. The study was performed in close collaboration with the ROBL beamline at ESRF (HZDR). A number of Fe(II) minerals are expected to form under reducing conditions through the anoxic corrosion of steel components present in the repository. These solid phases are expected to play a relevant role in the retention of radionuclides due to the large surface and strong sorption capacity, but also because of their possible contribution to the reduction of redox-sensitive radionuclides to lower and thus less mobile oxidation states (*e.g.* U, Np, Tc). Tc(VII) batch sorption experiments were performed in the presence of magnetite (Fe₃O₄), mackinawite (FeS) and siderite (FeCO₃) in 0.1 M NaCl, 5.0 M NaCl and 4.5 M MgCl₂. The quantitative analysis of the sorption using distribution coefficients (*R_d* values) confirms the reduction of Tc(VII) to Tc(IV) by all the minerals evaluated both in dilute and concentrated brine systems. Advanced spectroscopic techniques (XANES/EXAFS) provide key inputs for the identification of the retention mechanisms of Tc, and confirm that both surface complexation and incorporation in the mineral structure contribute in the uptake process by Fe(II) minerals.

This PhD work represents the (to date) most comprehensive evaluation of redox processes, solubility and sorption behaviour of Tc in the absence of complexing ligands extending from dilute to concentrated NaCl, MgCl₂ and CaCl₂ systems. The complete thermodynamic and activity models derived represent an important step forward with respect to geochemical calculations for Tc in concentrated brine systems. The mechanistic information achieved for the sorption processes of Tc in Fe mineral phases help to clarify this relevant retention process and represents a first step towards a more fundamental description of the uptake processes, besides the purely empirical “*K_d*-approach”.

Table of Contents

Acknowledgments	i
Abstract	iii
1 Introduction	1
1.1 Background of the work.....	1
1.2 Basic knowledge and aquatic chemistry of Tc.....	2
1.2.1 Fundamental Tc chemistry	2
1.2.2 Tc redox chemistry	4
1.2.2.1 Definition of redox equilibrium	4
1.2.2.2 Redox chemistry of technetium.....	6
1.2.3 Solubility and hydrolysis	8
1.2.3.1 Solubility and hydrolysis reactions: definition of equilibrium constants	8
1.2.3.2 Activity models	10
SIT model	10
Pitzer model.....	11
1.2.3.3 Solubility and hydrolysis of Tc(IV) in the absence of complexing ligands	12
1.2.4 Sorption processes	13
1.2.4.1 Sorption of Tc on Fe minerals.....	13
1.3 Thermodynamics of Tc. Thermodynamic databases (TDB).....	15
1.4 Aim of the present work.....	16
2 Experimental	19
2.1 Chemicals and analytical methods.....	19
2.1.1 Chemicals	19
2.1.2 ⁹⁹ Tc	20
2.1.3 Fe minerals.....	20
2.1.4 pH measurements.....	21
2.1.4.1 General definition.....	21
2.1.4.2 pH measurements with glass electrode.....	22
2.1.4.3 pH measurements in saline solutions	23
2.1.4.4 pH measurements in this work	23
2.1.5 <i>E_h</i> measurements.....	24
2.1.6 Determination of total concentration and redox speciation of Tc in solution.....	25
2.1.6.1 Liquid scintillation counting (LSC).....	25
2.1.6.2 Solvent extraction.....	25
2.1.7 Solid phase characterization (XRD, SEM–EDS, chemical analysis).....	26
2.2 Tc redox experiments in the presence of reducing chemicals.....	27
2.3 Tc(IV) solubility experiments.....	29
2.3.1 Tc(IV) solid phase preparation	29

2.3.2	Sample preparation	30
2.4	Reduction and uptake of Tc by Fe(II) minerals	32
2.5	EXAFS/XANES.....	34
2.5.1	ANKA, INE-beamline	34
2.5.1.1	Sample Preparation.....	34
2.5.1.2	XAFS measurements.....	34
2.5.1.3	Data evaluation.....	35
2.5.2	ESRF, ROBL-beamline	35
2.5.2.1	Sample Preparation.....	35
2.5.2.2	XAFS measurements.....	36
2.5.2.3	Data evaluation.....	36
3	Redox behaviour of Tc(VII)/Tc(IV) in dilute to concentrated NaCl and MgCl₂ solutions.....	37
3.1	Tc(VII)/Tc(IV) redox border: thermodynamic and activity models in NaCl and MgCl ₂	37
	SIT model	37
	Pitzer model.....	38
3.2	Redox behaviour of Tc(VII)/Tc(IV) in dilute to concentrated NaCl and MgCl ₂ solutions: comparison of experimental p <i>H</i> _c , <i>E</i> _h and [Tc] _{aq} with thermodynamic calculations	40
3.2.1	Na ₂ S ₂ O ₄ systems	40
3.2.2	Sn(II) systems	43
3.2.3	Hydroquinone	44
3.2.4	Fe(II)/Fe(III) systems.....	47
3.2.5	Corroding Fe powder systems	48
3.3	Conclusions on Tc(VII)/Tc(IV) redox processes	51
4	Solubility and hydrolysis of Tc(IV) in dilute to concentrated NaCl, MgCl₂ and CaCl₂ solutions	53
4.1	Solubility data of Tc(IV) in dilute to concentrated NaCl, MgCl ₂ and CaCl ₂ solutions.....	53
4.1.1	Solubility data of Tc(IV) in dilute to concentrated NaCl solutions	53
4.1.1.1	Acidic to weakly alkaline pH (1.5 ≤ p <i>H</i> _m ≤ 9)	53
4.1.1.2	Alkaline pH (p <i>H</i> _m ≥ 9).....	54
4.1.2	Solubility data of Tc(IV) in dilute to concentrated MgCl ₂ solutions	56
4.1.3	Solubility data of Tc(IV) in dilute to concentrated CaCl ₂ solutions	58
4.2	Tc aqueous and solid phase characterisation	59
4.2.1	Tc aqueous phase characterisation.....	59
4.2.1.1	Tc redox speciation (solvent extraction)	59
4.2.1.2	XANES/EXAFS.....	59
4.2.2	Solid phase characterization (XRD, SEM–EDS and chemical analysis).....	62
4.3	Tc(IV) chemical, thermodynamic and activity models.....	66
4.3.1	Chemical and thermodynamic model reported in Neck and Fanghänel (1999).....	67
4.3.2	Use of chemical and thermodynamic models reported in Hess et al. (2004).....	69

4.3.3 Improved chemical, thermodynamic and activity models derived in this work	71
4.3.3.1 Acidic pH conditions ($\text{pH}_m \leq 4$)	72
4.3.3.2 Weakly acidic to weakly alkaline pH conditions ($4 \leq \text{pH}_m \leq 8 / 10$)	76
4.3.3.3 Alkaline pH conditions ($\text{pH}_m \geq 10$) in NaCl system	77
4.3.3.4 Alkaline pH conditions ($\text{pH}_m \geq 8$) in MgCl_2 and CaCl_2 systems.....	79
4.4 Chemical, thermodynamic and activity model for the system Tc^{4+} – Na^+ – Mg^{2+} – Ca^{2+} – H^+ – Cl^- – OH^- – H_2O	86
4.5 Conclusion for Tc(IV) solubility.....	91
5 Reduction and uptake of Tc by Fe(II) minerals in dilute to concentrated saline systems.....	93
5.1 Reduction and uptake of Tc by magnetite and mackinawite in 0.1 M NaCl	93
5.1.1 Quantitative evaluation of the wet chemistry data.....	93
5.1.2 Structural interpretation of Tc uptake: EXAFS/XANES.....	96
5.1.2.1 Magnetite.....	96
5.1.2.2 Mackinawite.....	99
5.2 Reduction and uptake of Tc by magnetite, mackinawite and siderite in concentrated NaCl and MgCl_2 solutions	101
5.2.1 Quantitative evaluation of the wet chemistry data.....	101
5.2.2 Redox speciation of Tc taken up by Fe(II) minerals: XANES	103
5.3 Conclusion for Tc uptake studies by Fe(II) minerals.....	104
6 Summary and Conclusion.....	105
Appendix.....	107
Appendix I.....	107
Appendix II	108
References	109

1 Introduction

1.1 Background of the work

Many processes related to the use of radioactive materials, such as nuclear power plants, nuclear fuel fabrications, reprocessing plants, dismantling of nuclear weapons, medical applications and nuclear research produce long-lived radioactive waste which needs to be safely disposed to avoid human exposure. Deep underground repositories are accepted by the international community as the safest option for the final disposal of radioactive waste. These repositories are normally designed between 250 m and 1000 m underground in stable host-rock formation. The design of underground repositories follows a multi-barrier concept, with the aim of minimizing the likelihood of radionuclide mobilization into the biosphere. Iron inserted stainless steel or copper canister are an important barrier where the nuclear waste is placed in. The waste canisters will further be surrounded by the engineered (buffer/backfilled material) barriers with improved properties such as mechanical stability, high radionuclide sorption capacity and low hydraulic conductivity. The type of waste canisters as well as the design and composition of backfill materials vary depending on the type of waste to be disposed and the nature of the host rock-type available. The selection of host-rock formations vary among countries, with three main formations being considered: crystalline (granite), clay rock and salt-rock.

- Crystalline formations are the most widely found rock type on the Earth, and have been chosen or are under consideration for the construction of nuclear waste repositories in countries such as Sweden, Finland, Canada and Japan. Due to its crystalline structure, it is mechanically stable with very low mineral solubilisation and low heat sensitivity. On the other hand, the fractured structure of crystalline rocks provides natural pathways for gases and solutions [1].
- Indurated and plastic clay formations present relevant advantages such as tightness, plasticity, hydraulic permeability, swelling capacity, low solubility and high radionuclide retention capacity. However, mining usually needs advanced engineering efforts because of their high plasticity. Due to the larger differences in the properties of clay rocks, the type of canister and engineered materials are also subjected to relevant variations depending upon repository site. The use of clay formations has been selected or is under assessment in Switzerland, France and Belgium [1].
- Salt-rocks show favourable rock-mechanical properties such as self-sealing feature, high temperature resistance and good deformation behaviour. A repository in rock salt is expected to be dry, with scenarios including water intrusion being clearly less likely or unlikely. As rock salts have limited radionuclide retention capacity, a demand for an accurate knowledge of the solubility and sorption behaviour of radionuclides in saline brines is given [1]. Nuclear waste repositories in salt-rock formations have been already licensed for permanent disposal of low- and intermediate level radioactive waste in Germany (Morsleben) and USA (WIPP; Waste Isolation Pilot Plant).

An appropriate understanding of the migration paths of radionuclides from the repository to the biosphere is mandatory for the long-term safety assessment of nuclear waste repositories. One of the considered migration scenario involves the water inflow into the repository and the contact with the radioactive waste. In this framework, the adequate understanding of the solution processes of dominating the release/retention of radionuclides, i.e., redox transformations, solubility, colloid formation, sorption/precipitation, dissolution/desorption under repository relevant conditions are of special importance for long-term performance assessment exercises.

The geochemical conditions in the nuclear waste repositories can be complex and vary as a function of the groundwater, host-rock formation, backfilled material and waste form, among others. The composition of intruding water in all considered systems may include dilute dissolved salts ($I < 0.1$ M). In the particular case of the nuclear waste repositories in salt-rock formations, aqueous systems with high ionic strength ($5 \text{ M} < I < 15 \text{ M}$) are expected to form in certain scenarios, i.e. with mostly the presence of Na^+ , Mg^{2+} , K^+ , Cl^- , SO_4^{2-} and with lower concentrations of Ca^{2+} , HCO_3^- , F^- and Br^- ions [2]. The use of cement-based materials for the solidification of waste package, as a backfill material or for construction purposes represents an additional alteration of the geochemical media which buffers the pH in the hyperalkaline range and induces a significant increase in Ca concentration [3]. The solution chemistry of radionuclides in saline system of high ionic strength cannot be predicted straightforwardly from dilute systems because of strong ion interaction processes. Concentrated dissolved ions can significantly affect the chemical behaviour and thermodynamic stability of radionuclides because of ion interaction processes, but, like in the case of chloride, can also act as ligands which may interact with the radionuclides to form more stable aqueous species or solid compounds. This can lead to a completely different chemistry and consequently different migration behaviour of the radionuclides in the salt brines which need dedicated experimental efforts.

In the near-field of deep geological repositories, the anoxic corrosion of metallic iron canisters leads to the release of Fe(II)(aq) and formation of Fe(II) -bearing solid phases, buffering the redox conditions of the system to very reducing conditions. Fe(II)(aq) and the corresponding secondary phases are of high importance in the safety assessments of a repository due to its impact on migration behaviour of radionuclides through redox transformations and sorption processes. The redox state of radionuclides play an important role on mobility because of their different solubility, complexation and sorption behaviour. Therefore, investigations focussing on possible redox transformations of radionuclides, their solubility, hydrolysis and complexation behaviour in equilibrium with corresponding solid forms, sorption/incorporation processes at solid/water interface are necessary under repository relevant dilute to concentrated salt brine conditions.

1.2 Basic knowledge and aquatic chemistry of Tc

1.2.1 Fundamental Tc chemistry

Technetium was the first artificially produced element by Emilio Segrè and Carlo Perrier in scrap metal parts from Ernest Lawrence's cyclotron located in the Radiation Laboratory in Berkeley, California. It is the lightest element in the periodic table without stable isotopes. Technetium ($Z = 43$)

has an electronic structure of $[\text{Kr}] 4d^5 5s^2$ and is located in the periodic table between rhenium and manganese. Chemically, technetium shows more analogy with rhenium than its lighter homologue manganese.

Tc exists in several oxidation states ranging from 0 to +VII. Tc(0) exists as a shiny grey metal which shows a high tendency to oxidise under sub oxidic/oxidising or high temperature conditions. In contrast to the actinides, low valence states of Tc (I, II) can be observed under specific conditions in the presence of soft-donor (CO, CN⁻, etc.) and organic ligands (EDTA, NTA, DBP, etc.) [4, 5]. Lower valence Technetium complexes containing CO are mainly synthesized to use in the medical applications [6-9]. However, the presence of these complexes has been detected under the specific conditions in the waste tanks of Hanford Site, and in the last decades has become an issue in terms of Tc separation from the tank waste [10-12]. Tc(III) is reported in literature [13] as Tc(IV)/Tc(III) or Tc(III)/Tc(III) polymeric forms in in-situ experiments under very acidic and reducing conditions ($\text{pH} \leq 1$), whereas no evidence of stable Tc(III) species exists for longer periods of time or under higher pH conditions. Tc(IV) forms sparingly soluble oxides $\text{TcO}_2 \cdot x\text{H}_2\text{O}(\text{s})$, and is one of the most stable oxidation states of Tc under reducing conditions. Tc(V) and Tc(VI) can be observed by one and two electron reduction steps of Tc(VII), respectively. However, they are known to rapidly disproportionate to Tc(VII) and Tc(IV) in the absence of strong complexing ligands. Tc(VII) is the most stable oxidation state of Tc in suboxic/oxidising environments, forming mobile TcO_4^- anions over the entire pH range of aqueous solutions with very high solubility and very weak sorption properties [14]. Tc redox chemistry and its importance for nuclear safety assessments are discussed in Section 1.2.2.2.

Most of the Tc oxidation states have an octahedral coordination. The ionic radii and the coordination number of Technetium in selected oxidation states as summarized in Shannon [15] are shown in Table 1.1. The nominal charge of the hypothetical bare ions and their charge dependent ionic radii, (Z^2/r) gives the stability of different chemical species according to their electrostatic energy. In this context, the aquatic chemistry of tetravalent Tc shows certain analogies with that of tetravalent actinide ions, but also with lighter elements such as Zr [16].

Table 1.1 Coordination numbers and ionic radii reported in Shannon [15] for different oxidation states of Tc.

Oxidation state	Coordination	Ionic Radius
+4	VI	0.65
+5	VI	0.60
+7	IV	0.37
	VI	0.56

All known isotopes of technetium are radioactive. Most of these isotopes have a short half-life of only few seconds to few days (e.g. ^{110}Tc $t_{1/2} \sim 0.82$ sec; $^{97\text{m}}\text{Tc}$ $t_{1/2} \sim 61.2$ days) [17, 18]. $^{99\text{m}}\text{Tc}$ ($t_{1/2} \sim 6.02$ h) which is produced by neutron bombardment of various molybdenum isotopes, is a very relevant short-lived isotope of Tc with applications in nuclear medicine as radioactive tracer. Tc has three long-lived isotopes ^{97}Tc ($t_{1/2} \sim 2.6 \cdot 10^6$ a), ^{98}Tc ($t_{1/2} \sim 4.2 \cdot 10^6$ a) and ^{99}Tc ($t_{1/2} \sim 2.13 \cdot 10^5$ a) which are produced

in nuclear reactors, but the β -emitter ($E_{\max} = 0.292$ MeV) ^{99}Tc is the most important because the significant amounts are produced by neutron-induced fission of both ^{235}U and ^{239}Pu in nuclear reactors with the fission yield of about 6.1%. This corresponds to approximately one kg of ^{99}Tc generated from the fission of one ton of 3.2 wt % ^{235}U -enriched UO_2 fuel with a typical burn up rate (33000 MWd/MT) [19]. ^{99}Tc is also the daughter nuclide of the short-lived $^{99\text{m}}\text{Tc}$. All produced ^{99}Tc needs to be disposed with L/ILW (low- and intermediate level waste) or HLW (high level waste) depending on its activity and amount. Due to its long-half life and redox sensitive character, an adequate understanding of ^{99}Tc solution chemistry is of high relevance in the long-term performance assessment of nuclear waste repositories.

1.2.2 Tc redox chemistry

1.2.2.1 Definition of redox equilibrium

The redox state of radionuclides is of high importance for the safety assessments of nuclear waste repositories since the solubility, complexation and sorption behaviour vary depending on their oxidation states. In general, redox reactions are based on the equilibrium of redox couples consisting of oxidised and reduced forms:



The electrode (half-cell) potential of a redox couple can be defined by the Nernst equation as shown in Eq (1.2).

$$E = E^\circ + \frac{RT \ln(10)}{nF} \log\left(\frac{a_{\text{ox}}}{a_{\text{red}}}\right) \quad (1.2)$$

where E is the redox potential for a given medium, E° is the redox potential under standard conditions, n is the number of transferred electrons in the redox reaction, R is the ideal gas constant, T is the absolute temperature in Kelvin and F is the Faraday constant.

The absolute value of the electrode potential cannot be experimentally measured. Therefore, the electrode potential is determined as reduction potential relative to the standard hydrogen electrode (which is zero by definition) and quoted as E_h value. The redox potential of a system is defined as the negative logarithm of the electron activity in analogy to pH and expressed as pe:

$$\text{pe} = -\log a_{e^-} \quad (1.3)$$

The correlation between E_h and pe values is provided in equations (1.4) and (1.5):

$$E_h = -\frac{RT}{F} \ln(a_{e^-}) = \frac{RT \ln(10)}{F} \text{pe} \quad (1.4)$$

$$\text{pe} = 16.9 E_h [\text{V}] \quad \text{at } T = 25 \text{ }^\circ\text{C} \quad (1.5)$$

Measuring E_h (pe) and pH of an aqueous system can be used to assess the stability field of different (redox) species of a given element by systematizing the pe-pH in so called *Pourbaix* diagrams. The predominance area of different (redox) species is separated by the (redox) borderlines reflecting a 50:50 % distribution between these two species. These borderlines are calculated using the stability constants of equilibrium under standard state or at given I conditions (see example for Tc in Figure 1.1). The presentation of pe-pH measurements in a *Pourbaix* diagram is systematically used throughout this work to compare experimentally measured data (pH, E_h , [Tc], redox speciation) with thermodynamic calculations. It should be noted that the redox potential of an aqueous solution is limited within the borders for water reduction and water oxidation provided in the *Pourbaix* diagram.

The lower stability line of water corresponds to a hydrogen partial pressure $P(\text{H}_2(\text{g})) = 1$ bar which leads to the reduction of water to $\text{H}_2(\text{g})$ according to the reaction:

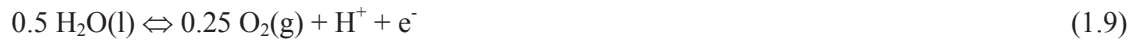


with

$$\log K^{\circ}(\text{red}) = 0.5 \log P(\text{H}_2(\text{g})) + \text{pH} + \text{pe} = 0 \quad (1.7)$$

$$(\text{pe} + \text{pH}) = -0.5 \log P(\text{H}_2(\text{g})) \quad (1.8)$$

The upper stability line of water corresponds to an oxygen partial pressure $P(\text{O}_2(\text{g})) = 1$ bar which leads to the oxidation of water to O_2 according to the reaction:



with

$$\log K^{\circ}(\text{ox}) = 0.25 \log P(\text{O}_2(\text{g})) - 0.5 \log a_w - \text{pH} - \text{pe} = -20.77 \quad (1.10)$$

$$(\text{pe} + \text{pH}) = 20.77 + 0.25 \log P(\text{O}_2(\text{g})) - 0.5 \log a_w \quad (1.11)$$

The lower and upper stability limits of water are determined as $(\text{pe} + \text{pH}) = 0$ and $(\text{pe} + \text{pH}) = 20.77$, respectively, at $I = 0$ and $T = 25$ °C.

Besides the borders of water reduction and oxidation, the theoretical “redox neutral line” [20] is also systematically considered in the *Pourbaix* diagram in this work. It represents a redox-neutral solution without the addition of reducing and oxidising agents where $P(\text{H}_2(\text{g})) = P(\text{O}_2(\text{g}))$ in analogy to a pH neutral solution ($\text{pH} = 7$ with $[\text{H}^+] = [\text{OH}^-]$). The redox-neutral line of a solution under inert atmosphere also can be calculated as following:



$$\log K^{\circ} = \log P(\text{H}_2(\text{g})) + 0.5 \log P(\text{O}_2(\text{g})) = -41.55 \quad (1.13)$$

With hypothetical partial pressure of $P(\text{H}_2(\text{g})) = -27.6$ and $P(\text{O}_2(\text{g})) = -27.9$,

$$(\text{pe} + \text{pH}) = 13.8 \quad (1.14)$$

pe and pH measurements of inert (HCl, NaCl, NaOH, etc.) background solutions under Ar atmosphere show usually this ‘‘redox-neutral’’ line with pe + pH close to 13.8. The value of pe + pH is constant for many other redox couples and gives a hint about the reducing capacity of the related buffer and therefore, is used to identify the predominant oxidation states of an element in a *Pourbaix* diagram [20].

1.2.2.2 Redox chemistry of technetium

The redox behaviour of Tc is of high importance for the safety assessments of nuclear waste repositories since the mobility of Tc is highly depending on its oxidation states. Comprehensive thermodynamic data on Tc redox chemistry are reported within the NEA–TDB series [14]. In aqueous solutions, the dominant long-term stable oxidation states are Tc(VII) and Tc(IV). The main redox reaction between the most stable oxidation states of $\text{TcO}_4^-/\text{TcO}_2 \cdot x\text{H}_2\text{O}(\text{s})$ is summarized in the NEA–TDB as:



The standard potential selected in the NEA–TDB is $E^\circ = 0.747 \pm 0.004 \text{ V}$, which leads to $\log^* K^\circ = 37.8 \pm 0.6$ for reaction (1.15).

Figure 1.1 shows the *Pourbaix* diagram of Tc calculated within $0 \leq \text{pH} \leq 14$ and $-14 \leq \text{pe} \leq 14$ using the thermodynamic data selected in the current NEA–TDB data selection. Only Tc(VII) and Tc(IV) species appear in the diagram, although aqueous Tc(III) species (not currently selected in the NEA–TDB) have been reported to form under very acidic and reducing conditions [21, 22]. The aqueous Tc(IV) species in equilibrium with $\text{TcO}_2 \cdot 1.6\text{H}_2\text{O}(\text{s})$ are calculated with the hydrolysis species reported in NEA–TDB (see Section 1.3).

The redox behaviour of the Tc(VII)/Tc(IV) couple was investigated by several authors in different reducing systems. Owunwanne et al. (1977) [23] and Warwick et al. (2007) [24] used Sn(II) to reduce Tc(VII) under highly acidic ($\text{pH} < 2$) and highly alkaline ($\text{pH} > 13.3$) conditions, respectively. A fast and complete reduction of Tc(VII) was observed in both cases, although no solid phase characterization was performed in these studies. Cui et al. (1996) [25] observed that the reduction of Tc(VII) to Tc(IV) by Fe(II)(aq) was kinetically hindered, whereas Fe(II) precipitated or sorbed on the vessel walls rapidly reduced Tc(VII). Zachara et al. (2007) [26] also studied the reduction of Tc(VII) in presence of Fe(II)(aq) in the neutral pH region (6-8). The authors reported that reaction kinetics were strongly pH dependent and reduction of Tc(VII) was a combination of a homogenous and heterogeneous reaction. Ben Said et al. (1998) [27] investigated the reduction of Tc(VII) in acidic solutions as a function of [Tc], [Fe(II)(aq)] and Fe(II)/Fe(III) ratio. Several studies have also focussed on the reduction/sorption mechanisms of Tc on solid iron phases of special relevance for nuclear waste disposal [28-33]. A detailed discussion of this phenomenon is provided in Section 1.2.4.1. Recently, Kobayashi and co-workers [34] systematically assessed the reliability of E_{h} -pH measurements and

reaction kinetics to explain the redox behaviour of Tc(VII)/Tc(IV) in dilute solutions (0.1 M NaCl) in the presence of homogeneous (reducing chemicals) and heterogeneous (Fe minerals) reducing systems. The authors compared their experimental data with available thermodynamic predictions for Tc [35], and reported an experimental borderline for Tc(VII)/Tc(IV) reduction about 100 mV below the borderline calculated thermodynamically. This observation was explained by the formation of $\text{TcO}_2 \cdot x\text{H}_2\text{O}(\text{coll,hyd})$ colloidal particles with higher solubility than the solid phase $\text{TcO}_2 \cdot 1.6\text{H}_2\text{O}(\text{s})$ selected in the NEA–TDB review.

Although there are several number of experimental Tc redox studies, the understanding of Tc(VII)/Tc(IV) redox behaviour is currently rather restricted to dilute aqueous systems. For the waste disposal in underground salt-rock formations, Tc(VII)/Tc(IV) redox behaviour needs to be systematically investigated in dilute to concentrated saline systems.

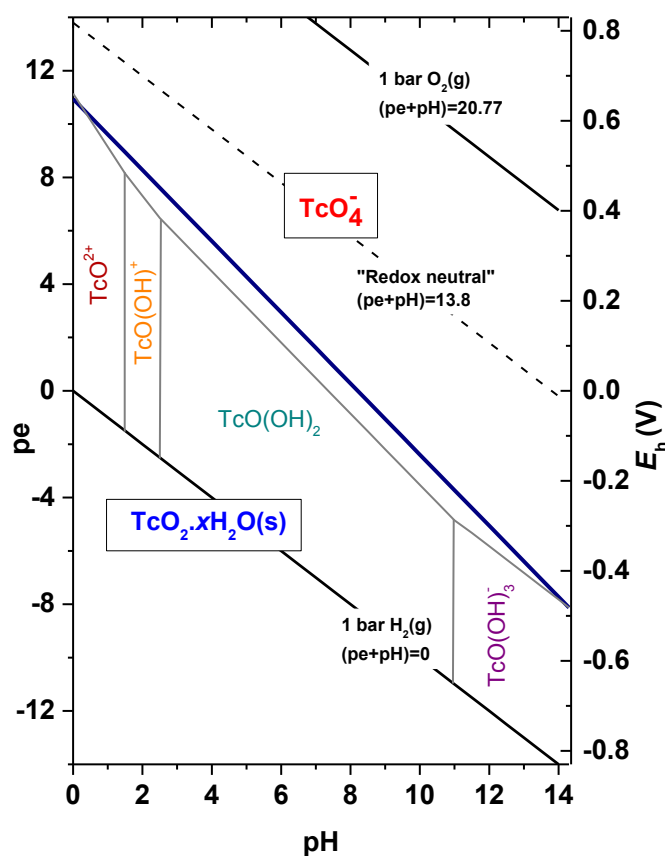
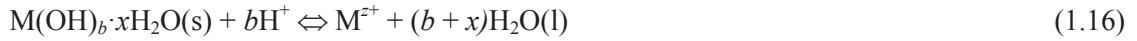


Figure 1.1 *Pourbaix* diagram of Tc calculated for $I = 0$ with thermodynamic data selected in NEA–TDB [22]. Bold blue line corresponds to Tc(VII)/Tc(IV) equilibrium considering reaction (1.15) calculated for $I = 0$. Thin dark grey lines correspond to 50:50 distribution borderlines between aqueous Tc species at $I = 0$. Black lines indicate upper and lower decomposition lines of water and “redox neutral” ($\text{pe} + \text{pH} = 13.8$) conditions. All calculations performed at $[\text{Tc}]_{\text{tot}} = 10^{-5} \text{ M}$.

1.2.3 Solubility and hydrolysis

1.2.3.1 Solubility and hydrolysis reactions: definition of equilibrium constants

In this part of the thesis, the main equilibrium reactions for solubility and hydrolysis are presented in the aqueous systems in the absence of other complexing ligands than the hydroxide anion. Solubility of metal hydroxides conventionally can be defined as Eq (1.16) with $\log K'$ referring to conditional constants in a given medium and $\log K^\circ$ to standard state conditions.



with

$$K'_{\text{sp}} = [\text{M}^{z+}][\text{H}^+]^{-b} \quad (1.17)$$

or

$$\log K'_{\text{sp}} = \log[\text{M}^{z+}] - b\log[\text{H}^+] \quad (1.18)$$

The standard state solubility constant of reaction (1.16) at $I=0$ and $T=25^\circ\text{C}$ is written as a function of activity coefficients (γ_i) of ion i and activity of water (a_w):

$$\log K^\circ_{\text{sp}} = \log K'_{\text{sp}} + \log \gamma_{\text{M}^{z+}} + (b+x)\log a_w - b\log \gamma_{\text{H}^+} \quad (1.19)$$

In the absence of complexing ligands, the aqueous metal phases react with water by hydrolysis. The hydrolysis reactions can be written in terms of protons or hydroxides. Reaction (1.20) shows the hydrolysis of metal cations with the $\log {}^*\beta'$ referring to formation constant in a given medium and $\log {}^*\beta^\circ$ to standard state conditions.



with

$${}^*\beta'_{(1,y)} = [\text{M(OH)}_y^{(z-y)}][\text{H}^+]^y[\text{M}^{z+}]^{-1} \quad (1.21)$$

or

$$\log {}^*\beta'_{(1,y)} = \log [\text{M(OH)}_y^{(z-y)}] + y\log[\text{H}^+] - \log[\text{M}^{z+}] \quad (1.22)$$

and

$$\log {}^*\beta^\circ_{(1,y)} = \log {}^*\beta'_{(1,y)} + \log \gamma_{\text{M(OH)}_y^{(z-y)}} + y\log \gamma_{\text{H}^+} - \log \gamma_{\text{M}^{z+}} - y\log a_w \quad (1.23)$$

The value of $\log {}^*K'_{sp}$ and $\log {}^*K'_{(1,y)} (= \log {}^*K'_{sp} + \log {}^*\beta'_{(1,y)})$ can be obtained from experimental data in a given medium and extrapolated to standard state conditions ($\log {}^*K_{sp}^0$ and $\log {}^*K_{(1,y)}^0$) at $I = 0$ using the activity coefficients calculated with SIT or Pitzer activity models (see Section 1.2.3.2). The total metal concentration can be written as sum of aquo ions and hydrolysis species as shown in Eq (1.24) and correspondingly in Eq (1.25) in case there are no other complexes or colloidal species.

$$[M]_{tot} = [M^{z+}] + \sum [M(OH)_y^{(z-y)}] \quad (1.24)$$

$$[M]_{tot} = K'_{sp}[H^+]^b + \sum K'_{sp}[H^+]^b \beta'_{(1,y)}[H^+]^{-y} \quad (1.25)$$

Since $[M]_{tot}$ in Eq (1.25) is a function of $[H^+]$, the experimentally obtained relation between $[M]_{tot}$ and $[H^+]$ can be used to determine the unknown thermodynamic data in Eq (1.25). If the experimentally measured metal concentration follows a well-defined slope as a function of pH (see example in Figure 1.2), this behaviour can be interpreted as the formation/predominance of only one aqueous species in equilibrium with a specific solid phase at the related pH range. Simple linearization ($y = mx + n$) of the solubility and hydrolysis constants of the metal hydroxides, where $y = \log [M]_{tot}$; $x = -\log [H^+]$ as shown in Eq (1.26), allows to do slope analysis.

$$\log [M^{z+}] = b \log [H^+] + \log {}^*K'_{sp} \quad (1.26)$$

In this case, the slope of the solubility data represents the number of exchanged protons in the solubility reaction and the intercept represents the $\log {}^*K'_{sp}$ under given conditions. This information contributes to define solubility and hydrolysis reactions as well as equilibrium constants, and therefore to derive chemical, thermodynamic and activity models. It is to note that slope analysis requires the knowledge of the solubility limiting solid phases and must be performed at constant ionic strength conditions / background electrolyte concentrations.

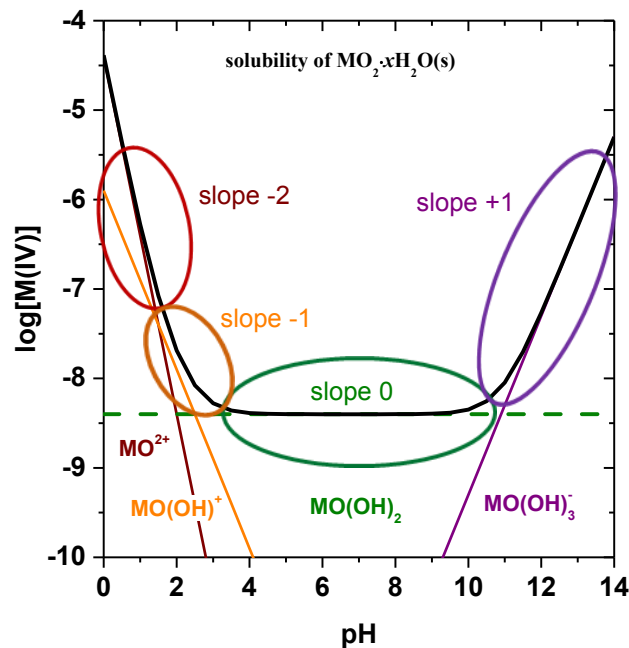


Figure 1.2 An example solubility curve of $MO_2 \cdot xH_2O(s)$ derived by the solubility and hydrolysis species formed in the entire pH region.

1.2.3.2 Activity models

In general, for an aqueous system with $I \geq 0$, the activity coefficients have to be taken into account because of non-negligible interactions between the ions. The activity coefficient of an ion is calculated for the corresponding electrolyte system and its concentration. SIT and Pitzer activity models are used for activity coefficient calculations in this study and are explained in detailed in the following subsections.

SIT model

The specific ion interaction theory (SIT approach) [36] is the method adopted by the NEA–TDB [35] for the treatment of ion interaction processes and ionic strength effects for the real systems at $I > 0$. The SIT approach which is based on the extended Debye-Hückel law, reflects the influence of electrostatic, non-specific long-range, binary interactions between charged ions to calculate activity coefficient. The activity coefficient of a j ion is defined as;

$$\log \gamma_j = -z_j^2 D + \sum_k \varepsilon(j, k) m_k \quad (1.27)$$

where z_j is the charge of the ion j , m_k is molality of the oppositely charged ion k and $\varepsilon(j, k)$ is the specific ion interaction parameter for a given electrolyte, D is the Debye-Hückel term with:

$$D = \frac{A\sqrt{I_m}}{1 + B_{aj}\sqrt{I_m}} \quad (1.28)$$

A and B_{aj} in the Debye-Hückel term are constants which are temperature and pressure dependent, and equal to $0.509 \pm 0.001 \text{ kg}^{1/2} \cdot \text{mol}^{-1/2}$ and $1.5 \text{ kg}^{1/2} \cdot \text{mol}^{-1/2}$ at 25°C and 1 bar, respectively. Ionic strength is defined as:

$$I = 1/2 \sum_i m_i z_i^2 \quad (1.29)$$

Considering the Eq (1.27) and Eq (1.28) together, the activity coefficient of j ion can be written as:

$$\log \gamma_j = -z_j^2 \frac{0.509\sqrt{I_m}}{1+1.5\sqrt{I_m}} + \sum_k \varepsilon(j, k) m_k \quad (1.30)$$

Since the ionic strength dependence of $\varepsilon(j, k)$ is negligible, the contribution of m_k term as $\sum_k \varepsilon(j, k) m_k$ reflects mainly the ionic strength effect in $\log \gamma_j$. For example, $I_m \approx m_j = m_k$ for a 1:1 electrolyte, while $I_m \approx 3 m_j = 1.5 m_k$ for a 1:2 electrolyte. The validity of SIT is normally limited to $I_m \leq 3.5 \text{ M}$ [37] and the Pitzer model is suggested for higher ionic strength conditions due to non-negligible effect of the concentration on ion-interaction coefficients. However, recent thermodynamic publications based on comprehensive experimental data and spectroscopic analysis have shown a good performance of SIT far beyond this limit in concentrated MgCl_2 and CaCl_2 solutions at $I_m \leq 13.5 \text{ M}$ [38-40].

Pitzer model

The use of the Pitzer formulism is recommended for thermodynamic calculations and geochemical modelling in concentrated salt brine solutions [41]. Since the electrolyte interactions in the Debye-Hückel law are unspecific, the calculated ion interaction coefficients for different ions with the same charge are identical. However, the Pitzer approach identifies the effect of ionic strength depending on short-range binary interactions (i.e., the second virial coefficient) and additionally interactions between ions with the same charge, between charged ions and neutral species as well as the triple-interactions. This results a more realistic modelling of mean activity coefficients especially in the medium and high ionic strengths at the cost of having a significantly larger number of parameter for calculating the activity of a given ion.

The semi-empirical activity model of Pitzer allows the thermodynamic description of aqueous electrolyte systems, in particular for the system of oceanic salts at $T=25\text{ }^\circ\text{C}$, which is covering the entire concentration range (dilute to highly concentrated) [41]. The approach is based on a virial expansion of the excess Gibbs energy:

$$\frac{G^{ex}}{w_w RT} = f(I) + \sum_i \sum_j m_i m_j \lambda_{ij}(I) + \sum_i \sum_j \sum_k m_i m_j m_k \mu_{ijk} + \dots \quad (1.31)$$

where the w_w is the number of kilograms of water and $m_i, m_j, m_k \dots$ are the molalities of all solute species. The first term is the Debye-Hückel limiting law, which depends only on ionic strength and not on individual species. $\lambda_{ij}(I)$ and μ_{ijk} are the virial coefficients and represent the short-range interaction between the solute particles.

For the mixed electrolytes in the presence of cations M, c, c' and anions X, a, a', the individual activity coefficients are described by Eq (1.32) and Eq (1.33) for a cation M and an anion X, respectively:

$$\begin{aligned} \ln \gamma_M = & z_M^2 F + \sum_a m_a (2 B_{Ma} + Z C_{Ma}) + \sum_c m_c (2 \Phi_{Mc} + \sum_a m_a \psi_{Mca}) \\ & + \sum_{a < a'} \sum_{a'} m_a m_{a'} \psi_{Ma a'} + z_M \sum_{c < a} m_c m_a C_{ca} + 2 \sum_n m_n \lambda_{nM} \end{aligned} \quad (1.32)$$

$$\begin{aligned} \ln \gamma_X = & z_X^2 F + \sum_c m_c (2 B_{cX} + Z C_{cX}) + \sum_a m_a (2 \Phi_{Xa} + \sum_c m_c \psi_{cXa}) \\ & + \sum_{c < c'} \sum_{c'} m_c m_{c'} \psi_{cc'X} + |z_X| \sum_{c < a} m_c m_a C_{ca} + 2 \sum_n m_n \lambda_{nX} \end{aligned} \quad (1.33)$$

where $Z = \sum_i m_i |z_i|$ and F term represents the Debye-Hückel term and the ionic strength dependence specific to the salt. Pitzer model defines binary parameters $\beta^{(0)}_{ij}$, $\beta^{(1)}_{ij}$, $\beta^{(2)}_{ij}$ and $C^{(\phi)}_{ij}$ specific to the interacting ions. $\beta^{(0)}_{ij}$ represents mainly the effect of repulsive forces between the similar ions, while the main contribution comes from the attractions between oppositely charged ions in parameter $\beta^{(1)}_{ij}$ [41]. $\beta^{(2)}_{ij}$ is considered only for 2-2 or higher valence electrolytes, and corrects deviations caused by electrostatic ion-pair formation in these systems. $C^{(\phi)}_{ij}$ has significance only at high ionic strength.

θ_{ij} (or θ_{ij}^*) and Ψ_{ij} (or Ψ_{ij}^*) are the mixing parameters in the case of ternary and higher electrolyte systems and their contribution is expected to be very small except for mixing of non-identical charged species. The interaction between the ions and the neutral charged species are defined with λ_{ni} (or λ_{nj}). B_{ca} and C_{ca} are calculated based on the binary parameters and Φ_{ij} are calculated based on the electrostatic unsymmetrical mixing effects depending on the charged species, total ionic strength and solvent properties. The formulism of the terms used in Pitzer equations are given in Appendix I.

1.2.3.3 Solubility and hydrolysis of Tc(IV) in the absence of complexing ligands

Previous redox studies showed that $\text{TcO}_2 \cdot x\text{H}_2\text{O}$ is the predominant Tc solid phase forming under reducing conditions. The solubility of Tc(IV) has been also investigated by a limited number of research groups, in most of the cases at low ionic strength. Meyer et al. [42] studied the solubility of Tc(IV) in the pH range 1 to 10. Two different approaches were used for the preparation of the solid phase, namely electrodeposition of an oxide solid phase and the oxide precipitation onto sand particles from reduction of Tc(VII) by hydrazine. Based on their solubility data, Meyer and co-workers proposed a chemical model with the species TcO^{2+} and $\text{TcO}(\text{OH})^+$ prevailing in acidic conditions. On the other hand, the chemical equilibrium $\text{TcO}_2 \cdot 1.6\text{H}_2\text{O} \Leftrightarrow \text{TcO}(\text{OH})_2(\text{aq}) + 0.6\text{H}_2\text{O}$ was observed to set a very low Tc(IV) solubility (10^{-8} – 10^{-9} M) within $4 \leq \text{pH} \leq 10$. Eriksen et al. [43] performed solubility experiments with electrodeposited Tc(IV) oxide as a function of pH and P_{CO_2} . Consistently with Meyer and co-workers, these authors observed a pH-independent solubility ($\sim 7 \times 10^{-9}$ M) within the pH range 6 to 9.5. The increase in solubility with slope +1 observed above pH = 9.5 was interpreted as the formation of the species $\text{TcO}(\text{OH})_3^-$ according to the chemical reaction $\text{TcO}_2 \cdot 1.6\text{H}_2\text{O}(\text{s}) + 0.4\text{H}_2\text{O}(\text{l}) \Leftrightarrow \text{TcO}(\text{OH})_3^- + \text{H}^+$ and $\log {}^*K_{\text{s},\text{TcO}(\text{OH})_3^-}^0 = -19.3 \pm 0.3$. These two studies were reviewed in the NEA Thermochemical Database Project (NEA–TDB) series and considered for the final thermodynamic data selection of Tc [14]. Recently, Warwick and co-workers investigated the solubility of Tc(IV) reduced by Sn(II) and Fe(II) within the pH range 11.8 to 14.4. In contrast to the solubility data by Eriksen and co-workers, these authors only observed a slight increase of Tc(IV) solubility above pH = 13.5. No solid phase characterization was conducted by the authors, and thus an open question remains whether a more crystalline solid phase was responsible for the control of the solubility in the later study. Hess et al. (2004) conducted solubility experiments in highly saline (up to 5.0 M NaCl) and highly acidic (up to 6.0 M HCl) solutions. The authors followed the solubility samples up to 65 days of equilibrium time and complemented the experiments with extended solid and aqueous phase characterisation including spectroscopic techniques. The significant increase in solubility observed by the authors in high NaCl concentrations was explained through ion interaction processes using the Pitzer approach. Comprehensive thermodynamic and activity models for Tc(IV) under acidic NaCl conditions were derived by the authors based on their solubility data at $t = 11$ days and speciation analysis. The chemical model reported in the study of Hess et al. is in line with current NEA–TDB data selection, although the authors reported lower $\log {}^*K_{\text{s},\text{TcO}(\text{OH})^+}^0$ for the species $\text{TcO}(\text{OH})^+$.

Besides solubility experiments, several spectroscopic studies focussed on the speciation of Tc in acidic pH region. Vichot et al. (2002) investigated polymer formation of Tc(IV) in aqueous Cl^- and SO_4^{2-} media at pH = 1.5 and $I \leq 3$ [44]. Based on the evaluation of EXAFS data, the authors suggested the formation of small size polynuclear species independently of the composition of considered solution.

The short distances observed by EXAFS for Tc-Tc interactions are attributed to polymers, whereas no Cl⁻ ions are found in the first coordination shell. In 2003, Vichot and co-workers confirmed the formation of polymeric $Tc_nO_p^{(4n-2p)+}$ species up to pH = 3 by UV-VIS spectra, instead of currently considered monomeric species TcO^{2+} and $TcO(OH)^+$ in NEA-TDB [45]. In the latter study, the authors modelled their data with the formation of the trimer $Tc_3O_4^{4+}$ at pH ≤ 3, which shows clear analogies with the cluster $Mo_3O_4 \cdot 9H_2O^{4+}$ known for Mo(IV) [54]. In 2006, Poineau and co-workers assessed this polymeric species in different aspects and reported that this $Tc_nO_p^{(4n-2p)+}$ species is stable up to pH = 3 under various conditions [21, 46, 47]. These recent spectroscopic studies show the need of an accurate understanding of the aqueous speciation of Tc as the basis to derive correct thermodynamic and activity models.

1.2.4 Sorption processes

Sorption processes occurring at solid/water interfaces represent one of the most relevant mechanisms controlling the immobilisation of radionuclides. In general, sorption processes can be categorized as outer-sphere or inner-sphere surface complexation of ionic and colloidal species, including also incorporation to the structure of sorbing material [48]. Empirically, quantitative sorption data can be expressed in terms of distribution coefficients, K_d ($L \cdot kg^{-1}$), defined as the amount of metal sorbed per unit mass of the sorbent according to Eq (1.34):

$$K_d = \frac{[M]_s}{[M]_{aq}} \cdot \frac{V}{m} \quad (L \cdot kg^{-1}) \quad (1.34)$$

$[M]_s$ and $[M]_{aq}$ are the metal concentration in solid and solution, respectively. V is the solution volume (L) and m is the mass of the sorbent (kg). The term R_d is also used for the systems where the equilibrium is not ensured. Sorption experiments are often performed as a function of metal concentration or solid-to-liquid (S:L) ratios, aiming at the determination of sorption isotherms. The use of complementary spectroscopic data can provide key structure data, thus helping in the assessment of the underlying uptake mechanism.

1.2.4.1 Sorption of Tc on Fe minerals

In the near-field of deep geological repositories, the release of Fe(II) through the anoxic corrosion of metallic iron canisters and corresponding Fe(II) minerals are of high relevance in terms of their reduction capacity and sorption properties. Three relevant corrosion products of Fe expected under repository relevant conditions are magnetite (Fe_3O_4), mackinawite (FeS) and siderite ($FeCO_3$). Among Fe phases, magnetite (Fe_3O_4) is often considered as one of the most relevant corrosion products of Fe under reducing conditions expected in the repository. Mackinawite and siderite form depending on the carbonate and sulphide content of the groundwater but are found as well in certain types [2, 16] of clay formations.

The role of Fe solid phases in the reduction of Tc(VII) has been intensively studied within the last decades. Cui et al. (1996b) [49] studied the uptake of Tc by magnetite in the presence of synthetic ground water. The authors assessed the effect of ionic strength and pH (7.8–9.5), investigated the rate of the sorption reaction, and concluded that the uptake was controlled by a ligand exchange mecha-

nism. Geraedts et al. (2002) [50] and Maes et al. (2004) [51] studied the system magnetite-Tc in the presence of natural and synthetic Gorleben groundwater. The authors concluded that $\text{TcO}_2 \cdot x\text{H}_2\text{O}(\text{s})$ formed in this system, and suggested that Tc(IV) polymers or colloids were responsible for the observed increase in solubility ($\sim 10^{-6}$ M). Wharton et al. (2000) [29] studied the coprecipitation of Tc(VII) and Tc(IV) with mackinawite (FeS) and characterized the resulting solid phases by X-ray absorption spectroscopy. Tc was immobilized as a $\text{Tc}^{\text{IV}}\text{S}_2$ -like phase regardless of the initial oxidation state of Tc. Similar observations were reported by Livens et al. (2004) [31], who investigated the interaction between Tc and mackinawite using both +VII and +IV as initial redox state of Tc. Liu et al. (2008) [30] performed comprehensive immobilization experiments with Tc in the presence of mackinawite. The authors assessed the effect of ionic strength (≤ 1.0 M NaCl) and pH (6.1–9.0) on the uptake of Tc, and observed a strong pH-dependence and the increase of the uptake rate with increasing ionic strength. In contrast to Livens and co-workers, TcO_2 -like phase were reported to form on the surface of mackinawite instead of TcS_2 -like phases. Llorens et al. (2008) [33] coprecipitated Tc(VII) with siderite, an Fe(II) solid phase forming in the presence of carbonate-rich groundwater. The reduction of Tc(VII) and incorporation of Tc(IV) into the structure of siderite were confirmed by X-ray diffraction and transmission electron microscopy. Peretyazhko et al. (2012) [52] studied the reduction of Tc by reactive ferrous iron forming in naturally anoxic, redox transition zone sediments from the Hanford site. A number of Fe(II) minerals were identified in the sediments, including Fe(II)-phyllosilicates, pyrite, magnetite and siderite. The authors observed $\text{TcO}_2 \cdot x\text{H}_2\text{O}$ -like phases regardless of Fe(II) mineralogy or reduction rate. Recently, Kobayashi and co-workers [34] investigated the reduction/sorption of Tc(VII) in the presence of Fe minerals such as magnetite, mackinawite, siderite, goethite, hematite. The reduction and also retention of Tc were only observed in the presence of magnetite, mackinawite and siderite phases. The authors reported the complete incorporation of Tc(IV) into the magnetite structure, while they observed TcS_2 -like phase in the mackinawite samples as a results of XANES spectra.

In spite of a number of publications dedicated to the study of Tc uptake by magnetite (Fe_3O_4), mackinawite (FeS) and siderite (FeCO_3), significant contradictions arise in the retention mechanism proposed according to spectroscopic evidences. The lack of comprehensive studies with systematic variation of key parameters such as [Tc], solid-to-liquid ratio (S:L) or loading and equilibration time importantly hinders a correct and complete interpretation of these mechanism. Furthermore, not a single work focussing on the Tc uptake mechanism by Fe(II) minerals in highly saline systems has been reported so far. In this framework, experimental studies combining classical wet-chemistry methods with advanced spectroscopic techniques extending from dilute to concentrated saline systems are needed to properly assess the impact of these retention processes in the safety of repositories for nuclear waste disposal.

1.3 Thermodynamics of Tc. Thermodynamic databases (TDB)

For the long-term safety assessment of nuclear waste repositories, the migration behaviour and pathways of radionuclides need to be properly assessed. Geochemical calculations and geochemical modelling represent one of the tools providing key input for performance assessment exercises. These are fed by complete and self-consistent thermodynamic databases. The national and international thermochemical databases (TDB) select a comprehensive set of thermodynamic data of radionuclides and relevant elements for the long-term performance assessment of nuclear waste repositories. The selection is based on a strict review process of the various experimental studies, following well-defined guidelines.

The thermochemical database project of the Nuclear Energy Agency (NEA-TDB) comprises the most comprehensive selection of thermodynamic data currently available for actinides and fission products. Technetium was initially reviewed in the volume 3 of the NEA-TDB series [14], although the thermodynamic selection was later revisited in the update volume by Guillaumont and co-authors [35]. The outcome is a critically reviewed selection of Tc thermodynamic data, rather complete for Tc(VII)/Tc(IV) redox reactions and Tc(IV) hydrolysis, solubility and carbonate complexation as shown in Table 1.2. The data selection is limited or non-existent for other potentially relevant ligands such as chloride, phosphate or sulphate, as well as for ternary complexes eventually forming in concentrated saline systems. No ion interaction coefficients are selected for ionic species of Tc, thus limiting the applicability of the selected thermodynamic data to very dilute systems.

NAGRA-TDB is the thermodynamic database developed by PSI-LES for the National Cooperative for the Disposal of Radioactive Waste which supports the safety assessments of all possible Swiss radioactive waste repositories. The last update of Tc database is so far based on the selected data in NEA-TDB series (see Table 1.1). NAGRA-TDB selects the specific ion interaction coefficients according to the charge-based estimations based on the PSI report [53]. The selected ion interaction coefficients are shown in Table 1.3.

ThermoChimie-TDB is the thermodynamic database developed by Amphos 21 for ANDRA (French National Radioactive Waste Management Agency) and it is, therefore closely related to the French necessities for the safety case (disposal in clay). As in the case of NAGRA-TDB, most of the selected thermodynamic data of Tc in ThermoChimie is based on NEA-TDB. Reported values are shown in Table 1.2. ThermoChimie-TDB does not select any activity model for Tc so far but the charged-based estimations are used in the thermodynamic calculations of Tc.

The Thermodynamic Reference Database (THEREDA) project is currently being developed by several German institutions (KIT-INE, GRS, HZDR, University of Freiberg, AF-Consult Switzerland). The goal of THEREDA is to provide a comprehensive selection of thermodynamic data allowing an adequate modelling of geochemical processes taking place in the near- to far-field of repository for radioactive waste disposal. THEREDA aims at covering all possible repository concepts under consideration in Germany (including disposal of in salt-rock) and focusses on Pitzer as approach for ionic strength corrections. So far, THEREDA does not select thermodynamic data for Tc. One of the

goals of this PhD thesis is to provide a comprehensive Pitzer-based Tc thermodynamic model to be included in the THEREDA database.

Table 1.2 Stability constants for the solubility, hydrolysis and redox of Tc(IV) as reported in the NEA–TDB, NAGRA–TDB and Thermochimie–TDB.

Chemical Reactions	NEA–TDB	NAGRA–TDB	Thermochimie–TDB
	$\log^* K^0$	$\log^* K^0$	$\log^* K^0$
$\text{TcO}_4^- + 4\text{H}^+ + 3\text{e}^- \Leftrightarrow \text{TcO}_2 \cdot 1.6\text{H}_2\text{O}(\text{s}) + 0.4\text{H}_2\text{O}(\text{l})$	37.8 ± 0.6	NEA–TDB	NEA–TDB
$\text{TcO}_2 \cdot 1.6\text{H}_2\text{O}(\text{s}) \Leftrightarrow \text{TcO}(\text{OH})_2 + 0.6\text{H}_2\text{O}$	-8.4 ± 0.5	NEA–TDB	NEA–TDB
$\text{TcO}(\text{OH})_2(\text{aq}) + 2\text{H}^+ \Leftrightarrow \text{TcO}^{2+} + 2\text{H}_2\text{O}(\text{l})$	<4	NEA–TDB	2.58
$\text{TcO}(\text{OH})_2(\text{aq}) + \text{H}^+ \Leftrightarrow \text{TcO}(\text{OH})^+ + \text{H}_2\text{O}(\text{l})$	2.5 ± 0.8	NEA–TDB	2.79
$\text{TcO}(\text{OH})_2(\text{aq}) + \text{H}_2\text{O} \Leftrightarrow \text{TcO}(\text{OH})_3^- + \text{H}^+$	-10.9 ± 0.4	NEA–TDB	-10.80
$\text{TcO}(\text{OH})_2(\text{aq}) + \text{CO}_2 \Leftrightarrow \text{TcCO}_3(\text{OH})_2$	1.1 ± 0.3	NEA–TDB	NEA–TDB
$\text{TcO}(\text{OH})_2(\text{aq}) + \text{CO}_2 + \text{H}_2\text{O} \Leftrightarrow \text{TcCO}_3(\text{OH})_3^- + \text{H}^+$	-7.2 ± 0.6	NEA–TDB	NEA–TDB

Table 1.3 SIT ion interaction coefficients: ε_{ij} [kg mol^{-1}] for Tc hydrolysis species reported in NAGRA–TDB.

Species		SIT ion interaction coefficients (NAGRA–TDB)		
i	j	ε_{ij}	j	ε_{ij}
TcO_4^-	Na^+	-0.05 ± 0.1		
TcO^{2+}	Cl^-	0.15 ± 0.1	ClO_4^-	0.40 ± 0.1
$\text{TcO}(\text{OH})^+$	Cl^-	0.05 ± 0.1	ClO_4^-	0.20 ± 0.1
$\text{TcO}(\text{OH})_3^-$	Na^+	-0.05 ± 0.1		
$\text{TcCO}_3(\text{OH})_3^-$	Na^+	-0.05 ± 0.1		

1.4 Aim of the present work

This PhD thesis targets three of the main processes affecting the retention and migration of technetium in the context of repositories for nuclear waste disposal, namely redox chemistry, solubility and sorption phenomena. The study aims at a comprehensive description of these processes from dilute to concentrated saline solutions, although special focus is given to the assessment of concentrated brine systems. The latter are systematically disregarded in previously reported studies, in spite of their relevance in the context of repositories in rock-salt formations. The main objectives of this work are summarized in the following:

- The redox behaviour of Tc(VII)/Tc(IV) is investigated in the presence of various reducing systems in dilute to concentrated NaCl and MgCl_2 systems. Measured E_{h} -pH values are systemized according to *Pourbaix* diagrams. The effect of different reducing systems and ionic strengths on the redox behaviour of Tc(VII)/Tc(IV) is evaluated. Available thermodynamic data reported in NEA–TDB and activity models calculated using SIT estimations and Pitzer parameters are compared with obtained experimental data. The main goals of this study in-

volve the assessment of $p_e + pH$ measurements as key input for the characterization of Tc redox distributions, and the evaluation of the reduction of Tc(VII) to Tc(IV) in concentrated brine systems relevant for waste disposal in rock-salt formations (Chapter 3).

- The solubility of Tc(IV) is investigated in dilute to concentrated NaCl, MgCl₂ and CaCl₂ systems. Measurements of pH, p_e and [Tc] are complemented with solid phase characterization (XRD, SEM-EDS, quantitative chemical analysis) and aqueous speciation (solvent extraction and EXAFS analysis). The combination of these methods is aimed at providing comprehensive chemical, thermodynamic and activity models (SIT and Pitzer) for the system Tc⁴⁺-Na⁺-Mg²⁺-Ca²⁺-H⁺-Cl⁻-OH⁻-H₂O at 25 °C (Chapter 4). In a final step after the completion of this PhD thesis, the generated thermodynamic data are expected to provide those Tc data selected for THEREDA thermodynamic database.
- The reduction and uptake of Tc by Fe(II) minerals (magnetite, mackinawite and siderite) are investigated in dilute to concentrated NaCl and MgCl₂ systems. Batch experiments are performed by adding Tc(VII) into background solutions equilibrated with Fe(II) minerals. After given equilibration time, pH, E_h and [Tc] are measured, and investigated by advanced spectroscopic techniques (XANES/EXAFS). The main goal of this study is to provide an accurate mechanistic understanding of Tc uptake processes by Fe(II) solid phases relevant in the context of nuclear waste disposal, in combination with an empirical quantification of the sorption process based on the determination of the R_d values (Chapter 5).

2 Experimental

2.1 Chemicals and analytical methods

2.1.1 Chemicals

All sample preparation and handling was performed in Ar-gloveboxes with < 1 ppm O_2 at 22 ± 2 °C. All solutions were prepared with purified water (Millipore Milli-Q Advantage A10 with Millipore Millipak® 40 0.22 μm ; 18.2 M Ω -cm at 25 °C, 4 ppb TOC) and purged with Ar for 1 hour before use to remove traces of O_2 and CO_2 .

The pH standard buffer solutions (pH = 2 to 12) (Merck) were used for the calibration of the pH electrode. Perkin Elmer Ultima Gold™ XR was used as liquid scintillation counting (LSC) cocktail. An overview of other chemicals used in this work is given in Table 2.1.

Table 2.1 Chemicals used in the present work.

Name	Chemical formula	Molar weight (g.mol ⁻¹)	Firm
2-Amino-2-(hydroxymethyl)propan-1,3-diol (TRIZMA, TRIS)	$C_4H_{11}NO_3$	121.14	Sigma-Aldrich (99.9%)
Ammonium iron(II) sulphate hexahydrate	$(NH_4)_2Fe(SO_4)_2 \cdot 6H_2O$	392.14	Sigma-Aldrich (99.8%)
Ammonium hydroxide	NH_4OH	35.05	Sigma-Aldrich (30%)
Calcium chloride -dihydrate	$CaCl_2 \cdot 2H_2O$	147.02	Merck (p.a.)
Calcium hydroxide	$Ca(OH)_2$	74.10	Merck (p.a.)
Chloroform	$CHCl_3$		Merck (p.a.)
Iron powder	Fe	55.85	Merck (p.a.)
Iron(II) chloride	$FeCl_2$	126.75	Alfa Aesar (99.5%)
Iron(III) chloride	$FeCl_3$	162.20	Alfa Aesar
Ethanol (absolute)	CH_3CH_2OH		VWR Chemicals (99.9%)
Hydrochloric acid	HCl		Merck Titrisol®
Hydroquinone	$C_6H_6O_2$	110.11	Merck (p.a.)
Magnesium chloride hexahydrate	$MgCl_2 \cdot 6H_2O$	203.30	Merck (p.a.)
Magnesium hydroxide (cr)	$Mg(OH)_2$	58.32	Merck
2-(N-morpholino)ethanesulfonic acid (MES)	$C_6H_{13}NO_4S$	195.24	Sigma-Aldrich
Nitric acid (65%)	HNO_3	63.01	Merck (suprapure)
Piperazine-1,4-bis(2-ethanesulfonic acid) disodium salt (PIPES)	$C_8H_{16}N_2Na_2O_6S_2$	514.44	Sigma-Aldrich ($\geq 99\%$)
Sodium carbonate	Na_2CO_3	105.99	Sigma-Aldrich ($\geq 99.5\%$)
Sodium chloride	NaCl	58.44	Merck (p.a.)
Sodium dithionite	$Na_2S_2O_4$	174.11	Merck ($>87\%$)
Sodium hydroxide	NaOH		Merck Titrisol®
Sodium monosulfide	Na_2S	78.04	Sigma-Aldrich
Tin(II) chloride	$SnCl_2$	189.60	Sigma-Aldrich (98%)
Tetraphenylphosphonium chloride (TPPC)	$C_{24}H_{20}PCl$	374.84	Sigma-Aldrich (98%)

2.1.2 ^{99}Tc

^{99}Tc is a β -emitting fission product with half-life $t_{1/2} = 2.13 \cdot 10^5$ a and a specific activity of $6.25 \cdot 10^8$ Bq·g⁻¹. In all experiments, the required amount of Tc was prepared from a purified and radiochemically well-characterized ^{99}Tc stock solution (1.0 M NaTcO₄). A diluted TcO₄⁻ solution with $13 \text{ mM} \leq [\text{Tc}] \leq 20 \text{ mM}$ was directly used for the redox and reduction/sorption experiments. For Tc(IV) solubility experiments, an aliquot of the colourless NaTcO₄ stock solution was electrochemically reduced to Tc(IV) and precipitated as black TcO₂·xH₂O under alkaline conditions. The protocol used is detailed in Section 2.3.1. The resulting solid phase was then used to set up a series of undersaturation solubility experiments as described in Section 2.3.2.

2.1.3 Fe minerals

Magnetite (Fe₃O₄), mackinawite (FeS) and siderite (FeCO₃) were synthesized according to the experimental conditions described in Table 2.2. The resulting solid phases were used to perform Tc reduction/sorption experiments (performed in the framework of a cooperation project with the Helmholtz-Zentrum Dresden-Rossendorf Beamline (ESRF-ROBL)). All Fe minerals were equilibrated for 4 weeks in the original synthesis solution, washed three times with the corresponding background electrolyte (0.1 M NaCl, 5.0 M NaCl and 4.5 M MgCl₂) and equilibrated in this solution for 3 weeks. Magnetite and mackinawite were characterized by high energy powder XRD (D8 ADVANCE, Bruker) before and after washing with the respective background solutions. No XRD characterization was performed for siderite due to the rapid oxidation of the dry powder during measurement. However, the characteristic light-grey colour of siderite was retained in the aqueous samples throughout the reduction/sorption experiment with Tc. Figure 2.1 shows the XRD patterns of the magnetite and mackinawite Fe minerals synthesized in this work, together with the peak positions and relative intensities reported for the corresponding reference materials (PDF 19-0629 and 24-0073).

Table 2.2 Description of the experimental conditions for the synthesis of the Fe minerals studied in this work.

Fe minerals	Recipe	[Fe] _{tot}	Particle Size	Ref.
Magnetite (Fe ₃ O ₄)	60 mL of 6 M NH ₄ OH + 50 mL of mixed Fe(II)/Fe(III) with [Fe(II)]=0.4 M and [Fe(III)]=0.8 M	0.5 M	~10 nm	[54]
Mackinawite (FeS)	100 mL of 0.6 M Fe(II) solution ((NH ₄) ₂ Fe(SO ₄) ₂ · 6H ₂ O) + 100 mL of 0.6 M Na ₂ S	0.3 M	2 to 10 nm	[55]
Siderite (FeCO ₃)	100 mL of 0.4 M Fe(II) solution + 100 mL of 0.8 M Na ₂ CO ₃	0.2 M	-	[56]

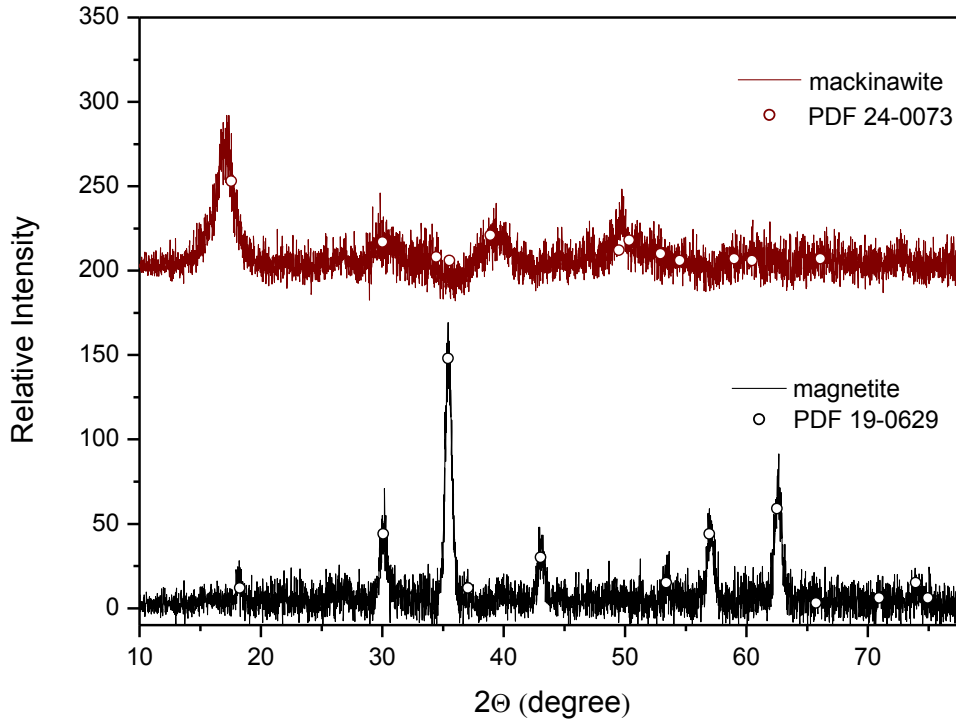


Figure 2.1 XRD patterns of the magnetite and mackinawite minerals synthesized in this work. Small circles indicate peak positions and relative intensities reported for the corresponding reference materials (PDF 19-0629 and 24-0073).

2.1.4 pH measurements

2.1.4.1 General definition

pH was first defined by Sørensen and Linderstrøm-Lang as the negative logarithm of molar hydrogen ion concentration [57]. Subsequently, it was modified to a thermodynamically more satisfactory definition as the negative logarithm of H^+ ion activity a_{H^+} [58-60];

$$pH = -\log(a_{H^+}) = \log \left[\left(\frac{m_{H^+} m_{\gamma_{H^+}}}{m^0} \right) \right] = \log \left[\left(\frac{c_{H^+} c_{\gamma_{H^+}}}{c^0} \right) \right] \quad (2.1)$$

where m_{H^+} and c_{H^+} are the molal and molar concentration of H^+ . $m_{\gamma_{H^+}}$ and $c_{\gamma_{H^+}}$ represent the molal and molar activity coefficients of H^+ . m^0 and c^0 are arbitrary constants, representing the standard amount of concentration equal to $1 \text{ mol} \cdot \text{kg}^{-1}$ and $1 \text{ mol} \cdot \text{dm}^{-3}$, respectively.

Since the activity of the H^+ ion itself cannot be experimentally measured, an internationally accepted pH scale was introduced which is a reproducible method for measuring and comparing the acidity of the solutions in dilute solutions of $I \leq 0.1 \text{ m}$ [60]. International consensus (IUPAC recommendations) suggest the primary method for the measurement of standard buffers of known pH by a H^+ sensitive electrode without junction potential, known as Harned cell:



The potential difference of this cell is given by the respective Nernst equation:

$$E = E^{\circ} - \left(\frac{RT}{F} \ln 10 \right) \log[(m_{\text{H}^+} \gamma_{\text{H}^+})(m_{\text{Cl}^-} \gamma_{\text{Cl}^-})] \quad (2.3)$$

The reference standard potential difference E° of the Ag/AgCl electrode is derived using an electrode filling solution of pure 0.01 m HCl. The activity coefficient of Cl^- is again an immeasurable value but, at $I < 0.1$ m, it can be calculated based on the Debye-Hückel theory using the Bates-Guggenheim convention ($\log \gamma_{\text{Cl}^-} = -A I^{1/2} / (1 + 1.5 I^{1/2})$). pH measurements further require operational pH standards that also account for liquid junction potential, so called secondary standards. They are generally inorganic or organic solutions with known pH which show small temperature dependence ($\pm 0.01 \text{ K}^{-1}$), low residual liquid junction potential and low ionic strength (≤ 0.1 m to remain valid according to the Bates-Guggenheim convention) [60].

2.1.4.2 pH measurements with glass electrode

Conventional determination of pH in a solution is carried out with electrochemical cells consisting of a glass electrode (GE) sensitive to hydrogen ions and a reference electrode (REF) with a salt bridge. These two electrodes are combined in a single glass body and connected to a sensitive electrometer to measure the potential between them. The measured potential can be expressed by:

$$E = E^{\circ}(\text{REF}) - E^{\circ}(\text{GE}) - E_{\text{AS}} + [RT \ln(10) / F] \cdot \log a_{\text{H}^+} + E_j \quad (2.4)$$

where $E^{\circ}(\text{REF})$ and $E^{\circ}(\text{GE})$ are the potential of the reference electrode and the glass electrode, respectively, which are dependent on temperature. E_{AS} is the asymmetry potential of the glass electrode, which depends on the internal and external hydrated ion exchange layers. E_j is the liquid junction potential at the interface between the electrolyte in the reference and the respective sample solution. The Nernst slope $RT \ln(10) / F$ in Eq (2.4) has the value of 59.16 mV at $T = 25 \text{ }^{\circ}\text{C}$. The pH of a standard buffer solution (S) and an unknown sample solution (X) are measured as electron potentials E (in mV) [61]:

$$E(\text{S}) = E(\text{REF}) - E(\text{GE}) - E_{\text{AS}} + [RT \ln(10) / F] \cdot \log a_{\text{H}^+}(\text{S}) + E_j(\text{S}) \quad (2.5)$$

$$E(\text{X}) = E(\text{REF}) - E(\text{GE}) - E_{\text{AS}} + [RT \ln(10) / F] \cdot \log a_{\text{H}^+}(\text{X}) + E_j(\text{X}) \quad (2.6)$$

The unknown pH of a given solution can be determined as the voltage difference between $E(\text{X})$ and the adjusted pH standard buffer $E(\text{S})$:

$$\text{pH}(\text{X}) = \text{pH}(\text{S}) + [E(\text{S}) - E(\text{X})] \cdot F / RT \ln(10) + [E_j(\text{X}) - E_j(\text{S})] \cdot F / RT \ln(10) \quad (2.7)$$

The terms E_{AS} , $E(\text{REF})$ and $E(\text{GE})$ remain the same in the calibration and sample measurement, and thus are cancelled by calibration of pH. The pH value of the unknown sample $\text{pH}(\text{X})$ can be calculated if the difference between $E_j(\text{X})$ and $E_j(\text{S})$ in Eq (2.7) is negligible, which requires low and similar ionic strengths in both buffer and unknown sample solution ($I \leq 0.1$ m). In the case of samples with high

acidity/alkalinity or elevated ionic strengths, the standard method for the measurement of pH is no longer valid and a modified approach needs to be considered [61].

2.1.4.3 pH measurements in saline solutions

At $I \geq 0.1$ m, ion interactions processes significantly affect the activity coefficient of H^+ (γ_{H^+}) and the liquid junction potential, and conventional pH measurements as those performed in dilute solutions are no longer valid. In such cases, the use of H^+ concentration instead of activity is favoured, the former being a well-defined parameter under all conditions [62];

$$pH_m = -\log(m_{H^+}) \text{ and } pH_c = -\log(c_{H^+}) \quad (2.8)$$

where pH_m and pH_c represent the negative logarithm of molal and molar concentration of H^+ ions, respectively. The values of pH_m and pH_c are calculated from the operational “measured” pH_{exp} using empirical correction factors (A), which include both the liquid junction potential and the activity coefficient of H^+ .

$$pH_m = pH_{exp} + A_m \text{ and } pH_c = pH_{exp} + A_c \quad (2.9)$$

with,

$$A_m = \log^m \gamma_{H^+} + \Delta E_j \frac{F}{RT} \ln 10 \quad \text{and } A_c = \log^c \gamma_{H^+} + \Delta E_j \frac{F}{RT} \ln 10 \quad (2.10)$$

A values are experimentally determined as a function of salt type and concentration by measuring a set of reference sample solutions with known proton concentrations.

2.1.4.4 pH measurements in this work

The pH measurements in the present work were performed in Ar-gloveboxes (22 ± 2 °C) using a ROSS combination pH electrode (Orion). Calibration prior to pH measurement was performed using pH standard buffer solutions (pH = 2 to 12). Whenever needed, the pH of the solutions was adjusted using HCl–NaCl–NaOH, HCl–MgCl₂ and HCl–CaCl₂ solutions of appropriate ionic strength, as well as with Mg(OH)₂(s) and Ca(OH)₂(s). A-factors used in this work for NaCl, MgCl₂ and CaCl₂ systems were previously reported by Altmaier and co-workers [63, 64] and are summarized in Table 2.3. In MgCl₂ and CaCl₂ solutions, the maximum pH is fixed by the precipitation of Mg(OH)₂(s) and Ca(OH)₂(s) (or corresponding hydroxochlorides at high CaCl₂ or MgCl₂ concentrations), which buffer pH_m at ~9 and ~12, respectively [64]. In NaCl systems with $[OH^-] > 0.03$ M, pH_m values were not measured but calculated from the known hydroxide concentration using γ_{H^+} , γ_{OH^-} (as calculated by SIT) and the activity of water (a_{H_2O}) at each ionic strength.

2 Experimental

Table 2.3 A_c and A_m values used in this study.

Background electrolyte		A_c	A_m
Molar	Molal		
0.10 M NaCl	0.10 m NaCl	-0.08	-0.08
0.50 M NaCl	0.51 m NaCl	-0.01	-0.01
1.00 M NaCl	1.02 m NaCl	0.09	0.08
3.00 M NaCl	3.20 m NaCl	0.49	0.46
5.00 M NaCl	5.60 m NaCl	0.95	0.90
0.25 M MgCl ₂	0.25 m MgCl ₂	0.03	0.03
1.00 M MgCl ₂	1.03 m MgCl ₂	0.40	0.40
2.00 M MgCl ₂	2.10 m MgCl ₂	0.97	0.95
3.00 M MgCl ₂	3.26 m MgCl ₂	1.62	1.58
4.50 M MgCl ₂	5.15 m MgCl ₂	2.77	2.71
0.25 M CaCl ₂	0.25 m CaCl ₂	0.00	-0.01
1.00 M CaCl ₂	1.02 m CaCl ₂	0.34	0.33
2.00 M CaCl ₂	2.11 m CaCl ₂	0.85	0.83
4.50 M CaCl ₂	5.25 m CaCl ₂	2.48	2.41

2.1.5 E_h measurements

Redox potentials were measured with Pt combination electrodes with Ag/AgCl reference system (Metrohm) and converted to E_h versus the standard hydrogen electrode (SHE) by correction for the potential of the Ag/AgCl reference electrode:



with

$$E = E^\circ_{\text{Ag/AgCl}} + \frac{RT \ln(10)}{F} \log a_{\text{Cl}^-} = 0.208 \text{ V} \quad (\text{at } T = 25 \text{ }^\circ\text{C} \text{ and for } 3.0 \text{ M KCl}) \quad (2.12)$$

where $E^\circ_{\text{Ag/AgCl}} = 0.2222 \text{ V}$ and $(RT \ln(10) / F) = 0.059 \text{ V}$ at $T = 25 \text{ }^\circ\text{C}$. The correct response of the electrode was checked using a standard redox buffer (+220 mV vs. Ag/AgCl, Schott Instruments), which in all cases provided readings within $\pm 10 \text{ mV}$ of the certified value.

The redox potential of a system was also used to describe the pe value in analogy with the pH as negative logarithm of the (hypothetical) electron activity. The apparent electron activity was calculated from

$$E_h = -(RT/F) \ln a_{e^-} \quad (2.13)$$

$$\text{pe} = -\log a_{e^-} = 16.9 \cdot E_h [\text{V}] \text{ at } T = 25 \text{ }^\circ\text{C}. \quad (2.14)$$

E_h measurements were carried out under continuous stirring of the sample vessel. Stable E_h readings were obtained within 10–30 minutes in most of the samples.

In analogy to pH, previous studies [65, 66] have suggested the need of (experimentally determined) correction factors for E_h measured at high ionic strengths, which should mostly account for variations in the liquid junction potential. Liquid junction potentials below 50 mV are expected in the conditions of this study [67]. These values are well within the uncertainty considered for E_h measurements, and thus the use of such corrections was disregarded in the present work.

2.1.6 Determination of total concentration and redox speciation of Tc in solution

2.1.6.1 Liquid scintillation counting (LSC)

Liquid scintillation counting (LSC) was used in the present work to quantify the total concentration of Tc in the aqueous phase. The principle of liquid scintillation counting is based on the conversion of radiation, emitted by the radionuclide, to photons. This conversion occurs due to the excitation of the scintillator molecules through radiation, which leads to the emission of light quanta when the scintillator molecules relax back to their respective ground states. These light quanta are then multiplied in a photomultiplier and subsequently detected. The detected quanta are directly proportional to the original amount of radiation emitted by the radioisotope.

For the sample preparation, 500 μL of the supernatant solution were taken and centrifuged for 5-20 minutes to separate colloids or suspended solid phase particles in Polyether – 10 kD filter (2-3 nm cut-off, Nanosep® and Mikrosep® centrifuge tubes Pall Life Sciences). Depending on the activity of the sample, between 10 μL - 400 μL of the filtrate were acidified with 1 M HCl (up to 1 mL) and 600 μL of the solution mixed with 10 mL LSC cocktail (Ultima Gold™ XR, Perkin-Elmer) in a screw-cap vessel (PP, 20 mL, Zinsser Analytic) and measured with a LKB Wallac 1220 Quantulus Liquid Scintillation Counter for 30 minutes each. No quenching effect was observed even in highly saline systems. A detection limit of $4 \cdot 10^{-10}$ M was calculated as threefold the standard deviation of five measured inactive blanks.

2.1.6.2 Solvent extraction

A solvent extraction method was used to determine the oxidation state of Tc (+IV or +VII) in the aqueous phase. The technique is based on the difference in solubility of Tc(IV) and Tc(VII) species in the organic solvent and aqueous phase.

In the present work, tetraphenylphosphonium chloride (TPPC, $(\text{C}_6\text{H}_5)_4\text{PCl}$) was used to separate Tc(VII) and Tc(IV) [68, 69]. Once TPPC is in contact with an aqueous phase, it dissociates to give $(\text{C}_6\text{H}_5)_4\text{P}^+$ and Cl^- ions [69]. The ion pair complexes between $(\text{C}_6\text{H}_5)_4\text{P}^+$ and TcO_4^- and TcCl_6^{2-} are very stable and insoluble in water. In the case of tetravalent and heptavalent Tc, TcO_4^- is extracted to the organic solvent and the activity remaining in aqueous phase is interpreted as Tc(IV).

After the ultrafiltration (10 kD) of each sample, 400 μL of the filtered solution were contacted with 400 μL chloroform (CHCl_3) containing 50 mM of TPPC. The mixture was vigorously shaken for 60 seconds and centrifuged for 5 minutes for subsequent separation of the aqueous and organic phases.

300 μL of the aqueous (inorganic) phase were then transferred into 700 μL of 1.0 M HCl. Under standard ambient temperature and pressure, 600 μL of this solution were added to 10 mL of LSC cocktail and measured for 30 minutes each. A correction for quench effects in the LSC samples containing organics was not required. An uncertainty of 10 % is assigned to the experimental results of solvent extraction in dilute systems. No data have been reported about the applicability and efficiency of this method in highly saline solutions.

2.1.7 Solid phase characterization (XRD, SEM–EDS, chemical analysis)

After reaching equilibrium conditions, the selected solid phases used in the corresponding solubility/sorption experiments were characterized using the following methods:

- X - ray diffraction (XRD),
- scanning electron microscopy energy dispersive spectroscopy (SEM – EDS),
- quantitative chemical analysis.

An aliquot of each solid phase (~1 mg) was washed under Ar-atmosphere 3-5 times with ethanol to remove the salt-containing matrix solution which would otherwise interfere with the analysis. After the last cleaning step, the solid was resuspended in ethanol, transferred to the XRD sample plate, dried under Ar-atmosphere for a few minutes and transferred outside the glovebox for the collection the XRD diffractogram. The XRD measurements were performed on a Bruker AXS D8 Advance X-ray powder diffractometer at measurement angles $2\theta = 10\text{-}78^\circ$ with incremental steps of 0.015° and a measurement time of 1.7 seconds per step. The spectra obtained were compared with the JCPDS database (Joint Committee on Powder Diffraction Standards [70]). After the measurement, the solid phase was dissolved in 1 mL of 2-3% HNO_3 and used for quantitative chemical analysis. The dissolved solid phase was analysed by LSC and ICP-OES (inductively coupled plasma – optical emission spectroscopy, Perkin-Elmer Optima 2000TM) to determine the Tc and salt-cation (Na, Mg, Ca) content, respectively. The total error for the combined determination is in the range of 10 %.

For the determination of crystallinity and morphology of the solid phase, and to further assess its chemical composition, a second fraction of the washed solid was characterized by scanning electron microscope-energy disperse spectrometry (SEM–EDS), using a FEI Quanta 650 FEG equipped with a Noran EDS unit.

2.2 Tc redox experiments in the presence of reducing chemicals

The redox chemistry of the Tc(VII)/Tc(IV) couple was investigated in NaCl (0.5 M and 5.0 M) and MgCl₂ (0.25 M, 2.0 M and 4.5 M) solutions in the presence of different reducing systems (1 mM Na₂S₂O₄, 1 mM SnCl₂, 3 mM hydroquinone, 1 mM/0.1 mM Fe(II)/Fe(III), 1 mg/ 15 mL Fe powder). In some of these systems, the formation of a solid phase occurred at near-neutral to alkaline pH conditions (SnCl₂, Fe(II)/Fe(III) and Fe powder). In each experimental series, pH_c values were adjusted with 1.0 M HCl, NaCl–NaOH (of appropriate ionic strength) or Mg(OH)₂(s). For the samples in the near-neutral pH-range, the pH was buffered with 10 mM solutions of MES (pH_c = 5–7) and PIPES (pH_c = 7–9). The resulting matrix solutions were equilibrated until attaining stable pH and *E*_h readings (~2 weeks). The initial Tc(VII) concentration was set to 1·10⁻⁵ M by adding 11.5 μL of 13 mM NaTcO₄ stock solution into the 15 mL pre-equilibrated system in a screw-cap vessel (PP, 20 mL, Zinsser Analytic). pH_c, *E*_h and Tc concentration were measured at regular time intervals for up to 395 days. After attaining equilibrium conditions (assumed after stable pH_c and [Tc] measurements), the content of Tc(IV) in the aqueous phase of selected samples was determined by solvent extraction. The experimental conditions in NaCl and MgCl₂ systems before the addition of TcO₄⁻ are summarized in Table 2.4 and Table 2.5, respectively.

2 Experimental

Table 2.4 Initial pH_c and E_h values of Tc redox experiments in NaCl systems and presence of different reducing chemicals.

Background Electrolyte	0.5 M NaCl		5.0 M NaCl	
Reducing chemicals	pH_c^a	E_h (mV) ^b	pH_c^a	E_h (mV) ^b
Na ₂ S ₂ O ₄	7.9	-429	8.7	-379
Na ₂ S ₂ O ₄	7.2	-396	7.6	-393
Na ₂ S ₂ O ₄	9.9	-441	10.6	-457
Na ₂ S ₂ O ₄	11.0	-457	11.6	-470
Na ₂ S ₂ O ₄	12.1	-489	12.6	-487
Na ₂ S ₂ O ₄	13.6	-577	13.6	-635
Sn(II)	1.7	116	2.8	-30
Sn(II)	3.4	44	4.8	-119
Sn(II)	5.7	-26	6.7	-233
Sn(II)	7.9	-124	8.9	-410
Sn(II)	9.9	-322	11.0	-531
Sn(II)	13.6	-745	14.1	-744
Hydroquinone	1.6	193	2.9	232
Hydroquinone	3.9	180	4.9	217
Hydroquinone	5.9	201	7.0	184
Hydroquinone	8.1	94	9.1	69
Hydroquinone	10.1	-55	10.0	-71
Hydroquinone	12.3	-153	12.9	-157
Fe(II)/Fe(III)	2.0	475	3.0	600
Fe(II)/Fe(III)	3.9	-46	4.7	-13
Fe(II)/Fe(III)	5.8	-132	6.9	-88
Fe(II)/Fe(III)	7.9	-304	8.9	-261
Fe(II)/Fe(III)	9.6	-425	10.9	-232
Fe(II)/Fe(III)	11.9	-317	13.1	-186
Fe Powder	6.4	52	7.2	89
Fe Powder	8.5	-283	9.0	-130
Fe Powder	10.0	-320	10.9	-130
Fe Powder	11.0	-319	12.1	-130
Fe Powder	12.0	-321	13.2	-138

a: ± 0.05 ; **b:** ± 30 mV

Table 2.5 Initial pH_c and E_h values of Tc redox experiments in MgCl_2 system and presence of different reducing chemicals.

Background Electrolyte	0.25 M MgCl_2		2.0 M MgCl_2		4.5 M MgCl_2	
	pH_c^a	E_h (mV) ^b	pH_c^a	E_h (mV) ^b	pH_c^a	E_h (mV) ^b
$\text{Na}_2\text{S}_2\text{O}_4$	4.1	89	4.1	-101	4.8	160
$\text{Na}_2\text{S}_2\text{O}_4$	7.3	-419	7.1	-369	6.6	4
$\text{Na}_2\text{S}_2\text{O}_4$	9.2	-470	9.2	-428	9.3	-170
Sn(II)	3.4	-54	3.6	-42	4.0	53
Sn(II)	6.9	-199	6.5	-175	6.7	-49
Sn(II)	9.1	-403	9.1	-383	9.3	-204
Hydroquinone	4.2	-33	4.4	90	4.4	63
Hydroquinone	7.4	16	7.3	218	6.8	45
Hydroquinone	9.2	-27	9.1	61	9.3	-36
Fe(II)/Fe(III)	3.3	448	3.7	604	4.2	609
Fe(II)/Fe(III)	7.2	-83	7.2	-170	6.5	42
Fe(II)/Fe(III)	8.8	-465	9.0	-484	9.3	-131
Fe Powder	4.2	-337	4.3	-215	4.0	-46
Fe Powder	7.7	-406	7.6	-247	7.8	-247
Fe Powder	9.1	-312	9.1	-249	9.2	-306

a: ± 0.05 ; **b:** ± 30 mV

2.3 Tc(IV) solubility experiments

2.3.1 Tc(IV) solid phase preparation

A TcO_4^- stock solution was electrochemically reduced to Tc(IV) in an Ar-atmosphere as follows: 200 μL of 1.0 M NaTcO_4 stock solution was added to 20 mL of 1.0 M HCl, and the resulting solution transferred to a glass vessel with a magnetic stirring bar. Pt-working electrode and two galvanic cells (filled with 1.0 M HCl) were placed into the glass vessel with the TcO_4^- solution. Pt-counter electrode (Metrohm) and Ag/AgCl reference electrode (Metrohm; filled with 3.0 M KCl) were inserted into the galvanic cells as shown in Figure 2.2a. A Potentiostat Princeton Applied Research (Model 362) was used to adjust the electron potential as -250 mV vs. Ag/AgCl electrode (-42 mV vs. SHE). The surface of the Pt electrode became black as soon as electrolysis was started. In few minutes, the solution became completely brownish as shown in Figure 2.2b. The complete reduction of Tc(VII) to Tc(IV) was confirmed by solvent extraction and UV-VIS/NIR after 5 hours of reduction. The resulting suspension was transferred to a 50 mL PP vial (Sarstedt), and the pH of suspension shifted to $\text{pH} \sim 3$ by slow addition of 2-3 mL of 10 M NaOH. 40 mL of a 5 mM $\text{Na}_2\text{S}_2\text{O}_4$ solution at $\text{pH} \sim 12.5$ were prepared in a 100 mL Polyethylene vial (Kautex), and the Tc(IV) suspension was added drop by drop accompanied by a gentle agitation of the flask. The use of $\text{Na}_2\text{S}_2\text{O}_4$ solutions with $\text{pH} < 12.5$ led to an undesired pH-shift in the final solution towards near-neutral conditions ($\text{pH} \sim 6$).

After eight consecutive reduction steps, a total of 160 mg of Tc(IV) solid phase were collected in a 500 mL Kautex bottle and left aging for two months to allow for an appropriate equilibration of the system. pH, E_h and [Tc] were monitored during this time. pH and E_h readings (12.3 and -500 mV) indicated in all cases the expected predominance of Tc(IV) according with thermodynamic calculations (see *Pourbaix* diagram in Figure 1.1). Tc concentration after reaching equilibrium conditions ($3.6 \cdot 10^{-7}$ M) agrees well with the solubility of $\text{TcO}_2 \cdot 1.6\text{H}_2\text{O}(\text{s})$ calculated for this pH (pH = 12.3 at $I = 0$) using the NEA–TDB thermodynamic data selection. The characterization of this solid phase by XRD revealed its amorphous character, whereas quantitative chemical analysis and SEM–EDS showed no presence of any stoichiometric alkali or alkali-earth metals in the solid phase.

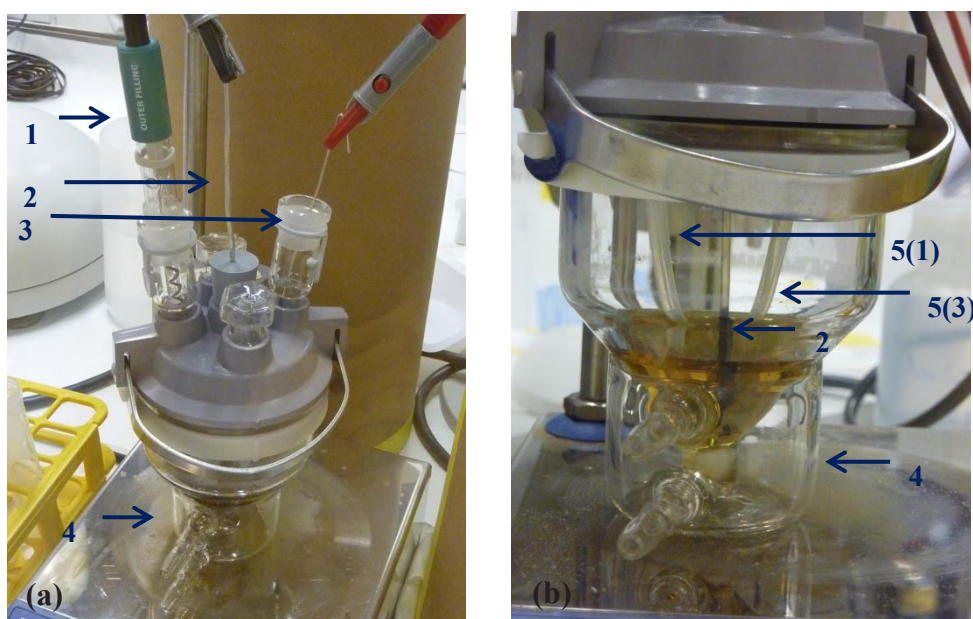


Figure 2.2 Electrochemical reduction system in Ar-glovebox. 1. Ag/AgCl reference electrode; 2. Pt-working electrode; 3. Pt-counter electrode; 4. glass vessel with magnetic stirring bar; 5. Galvanic cells.

2.3.2 Sample preparation

The solubility of Tc(IV) was studied in 0.1–5.0 M NaCl, 0.25–4.5 M MgCl_2 and 0.25–4.5 M CaCl_2 solutions at undersaturation in Ar atmosphere at 22 ± 2 °C. The pH values were adjusted at $1.5 \leq \text{pH}_m \leq 14.5$ by using HCl–NaCl–NaOH, HCl– MgCl_2 and HCl– CaCl_2 of appropriate ionic strength, as well as $\text{Mg}(\text{OH})_2(\text{s})$ and $\text{Ca}(\text{OH})_2(\text{s})$. 0.5 M PIPES and 1.0 M TRIS stock solutions were used for buffering of solubility samples at $\text{pH}_m = 7$ and $\text{pH}_m = 8$, respectively. In both cases, the final buffer concentration was 12 mM. To maintain reducing conditions, different reducing chemicals such as $\text{Na}_2\text{S}_2\text{O}_4$, SnCl_2 or Fe powder were used depending upon target pH values and according to the Tc redox studies described in Chapter 3. Background electrolyte solutions with adjusted pH_m and E_h conditions were equilibrated for two weeks. Table 2.6, Table 2.7 and Table 2.8 show the starting composition of background matrix solutions and adjusted pH_m values in NaCl, MgCl_2 and CaCl_2 systems, respectively. About 5 mg of Tc(IV) solid phase prepared according to the description in section 2.3.1 was washed three times with 1 mL of the respective pre-equilibrated matrix solution and

then added to 20 mL of the same matrix solution in 50 mL screw cap centrifuge vials (Nalgene™, Thermo Scientific). pH_m and Tc concentrations in the solubility samples were repeatedly measured at regular time intervals, usually from 3 to 600 days. After reaching equilibrium conditions (stable pH_m and [Tc] readings), pH conditions in some samples were slightly shifted by addition of acidic or basic solutions of the same ionic strength to obtain additional data points in the solubility curve. After reaching equilibrium conditions, selected solid and aqueous phases from batch experiments were characterized using several techniques, as described in sections 2.1.6 and 2.1.7.

Table 2.6 Composition of background matrix of Tc(IV) solubility experiments in NaCl systems.

Background matrix composition	pH_m
600 μ L 0.1 M Sn(II) + 24.6 mL 0.1 M NaCl + 320 μ L 1.0 M HCl	2.0
600 μ L 0.1 M Sn(II) + 24.6 mL 0.1 M NaCl	2.8
600 μ L 0.1 M Sn(II) + 24.6 mL 0.1 M NaCl + 1.58 mL 0.1 M NaOH	10.6
600 μ L 0.1 M Sn(II) + 24.6 mL 0.1 M NaOH	12.8
500 μ L 0.1 M Sn(II) + 24.5 mL 0.5 M NaCl	4.1
500 μ L 0.1 M Sn(II) + 24.2 mL 0.5 M NaCl + 300 μ L 0.5 M PIPES in 0.5 M NaCl	8.0
800 μ L 0.1 M Sn(II) + 39.2 mL 0.5 M NaCl + 3 μ L 10 M NaOH	11.1
500 μ L 0.1 M Na ₂ S ₂ O ₄ + 24.5 mL 0.5 M NaCl + 45 μ L 10 M NaOH	11.9
500 μ L 0.1 M Na ₂ S ₂ O ₄ + 15.5 mL 0.5 M NaCl + 450 μ L 10 M NaOH + 8.55 mL H ₂ O	13.0
600 μ L 0.1 M Sn(II) + 24.4 mL 0.5 M NaCl	3.3
600 μ L 0.1 M Sn(II) + 24.6 mL 1.0 M NaCl + 275 μ L 1.0 M HCl	2.0
600 μ L 0.1 M Sn(II) + 24.6 mL 1.0 M NaCl	2.8
600 μ L 0.1 M Sn(II) + 28.92 mL 3.0 M NaCl + 480 μ L 2.0 M NaCl/1.0 M NaOH	13.0
600 μ L 0.1 M Sn(II) + 29.4 mL 3.0 M NaCl + 120 μ L 1.0 M HCl	2.4
600 μ L 0.1 M Sn(II) + 29.4 mL 3.0 M NaCl + 10 μ L 2.0 M NaCl/1.0 M NaOH	4.27
600 μ L 0.1 M Sn(II) + 29.4 mL 3.0 M NaCl + 300 μ L 1.0 M HEPES	7.34
600 μ L 0.1 M Sn(II) + 29.4 mL 3.0 M NaCl + 250 μ L 2.0 M NaCl/1.0 M NaOH	12.0
500 μ L 0.1 M Sn(II) + 24.5 mL 5.0 M NaCl	4.1
500 μ L 0.1 M Sn(II) + 24.2 mL 5.0 M NaCl + 300 μ L 0.5 M PIPES in 5.0 M NaCl	8.0
800 μ L 0.1 M Sn(II) + 39.2 mL 5.0 M NaCl + 4 μ L 10 M NaOH	11.5
500 μ L 0.1 M Na ₂ S ₂ O ₄ + 24.5 mL 5.0 M NaCl + 6 μ L 10 M NaOH	11.9
500 μ L 0.1 M Na ₂ S ₂ O ₄ + 24.433 mL 5.0 M NaCl + 67.5 μ L 10 M NaOH	13.0
800 μ L 0.1 M Na ₂ S ₂ O ₄ + 37.04 mL 5.0 M NaCl + 1.08 mL 10 M NaOH + 1.08 mL H ₂ O	14.0
600 μ L 0.1 M Na ₂ S ₂ O ₄ + 23.52 mL 5.0 M NaCl + 5.88 mL 5.0 M NaOH	14.6
600 μ L 0.1 M Sn(II) + 24.4 mL 5.0 M NaCl	5.2

2 Experimental

Table 2.7 Composition of background matrix of Tc(IV) solubility experiments in MgCl₂ systems.

Background matrix composition	pH _m
600 μL 0.1 M Sn(II) + 29.4 mL 0.25 M MgCl ₂	3.3
600 μL 0.1 M Sn(II) + 28.8 mL 0.25 M MgCl ₂ + 600 μL 0.5 M PIPES in 0.25 M MgCl ₂	6.7
600 μL 0.1 M Sn(II) + 29.4 mL 0.25 M MgCl ₂ + 300 μL 1.0 M TRIS in 0.25 M MgCl ₂	7.6
600 μL 0.1 M Sn(II) + 29.4 mL 0.25 M MgCl ₂ /Mg(OH) ₂ (s)	8.9
400 μL Fe Powder (1 mg/15mL) + 29.5 mL 0.25 M MgCl ₂ + 300 μL 1.0 M TRIS in 0.25 M MgCl ₂	8.3
600 μL 0.1 M Sn(II) + 29.4 mL 0.25 M MgCl ₂	1.1
600 μL 0.1 M Sn(II) + 29.4 mL 1.0 M MgCl ₂	3.9
600 μL 0.1 M Sn(II) + 29.4 mL 2.0 M MgCl ₂	4.3
600 μL 0.1 M Sn(II) + 29.4 mL 3.0 M MgCl ₂	4.8
600 μL 0.1 M Sn(II) + 29.4 mL 4.5 M MgCl ₂	5.9
600 μL 0.1 M Sn(II) + 28.8 mL 4.5 M MgCl ₂ + 600 μL 0.5 M PIPES in 4.5 M MgCl ₂	7.4
600 μL 0.1 M Sn(II) + 29.4 mL 4.5 M MgCl ₂ + 300 μL 1.0 M TRIS in 4.5 M MgCl ₂	8.1
600 μL 0.1 M Sn(II) + 29.4 mL 4.5 M MgCl ₂ /Mg(OH) ₂ (s)	8.8
400 μL Fe Powder (1 mg/15mL) + 29.5 mL 4.5 M MgCl ₂ + 300 μL 1.0 M TRIS	8.9
400 μL 0.1 M Sn(II) + 20 mL 4.5 M MgCl ₂ + 100 μL 1.0 M HCl	2.8
400 μL 0.1 M Sn(II) + 20 mL 4.5 M MgCl ₂ + 60 μL 1.0 M HCl	3.5

Table 2.8 Composition of background matrix of Tc(IV) solubility experiments in CaCl₂ systems.

Background matrix composition	pH _m
600 μL 0.1 M Sn(II) + 23 mL 0.25 M CaCl ₂ + 4.2 mL 0.25 M CaCl ₂ /Ca(OH) ₂ (s)	10.5
600 μL 0.1 M Sn(II) + 23 mL 1.0 M CaCl ₂ + 4.0 mL 1.0 M CaCl ₂ /Ca(OH) ₂ (s)	10.5
800 μL 0.1 M Sn(II) + 35 mL 2.0 M CaCl ₂ + 10 mL 2.0 M CaCl ₂ /Ca(OH) ₂ (s)	11.2
800 μL 0.1 M Na ₂ S ₂ O ₄ + 39.2 mL 2.0 M CaCl ₂ /Ca(OH) ₂ (s)	12.0
600 μL 0.1 M Sn(II) + 35 mL 2.0 M CaCl ₂ + 5.4 mL 2.0 M CaCl ₂ /Ca(OH) ₂ (s)	7.2
800 μL 0.1 M Sn(II) + 27 mL 4.5 M CaCl ₂ + 13 mL 4.5 M CaCl ₂ /Ca(OH) ₂ (s)	11.1
800 μL 0.1 M Na ₂ S ₂ O ₄ + 39.2 mL 4.5 M CaCl ₂ /Ca(OH) ₂ (s)	11.8
600 μL 0.1 M Sn(II) + 29.4 mL 4.5 M CaCl ₂ /Ca(OH) ₂ (s)	11.4
600 μL 0.1 M Sn(II) + 24 mL 4.5 M CaCl ₂ + 8 mL 4.5 M CaCl ₂ /Ca(OH) ₂ (s)	10.2
0.047 g Sn(II) + 5 mL 4.5 M CaCl ₂ + 70 μL 30% supra pure HCl	1.8
600 μL 0.1 M Sn(II) + 25 mL 4.5 M CaCl ₂ + 5.7 mL 4.5 M CaCl ₂ /Ca(OH) ₂ (s)	9.5

2.4 Reduction and uptake of Tc by Fe(II) minerals

Tc reduction/sorption behaviour was investigated in 0.1 M NaCl, 5.0 M NaCl and 4.5 M MgCl₂ in the presence of the Fe minerals magnetite (Fe₃O₄), mackinawite (FeS) and siderite (FeCO₃). In a first experimental series, the retention of Tc was investigated in the presence of magnetite and mackinawite suspensions after 3 weeks of pre-equilibration in 0.1 M NaCl, as a function of initial TcO₄⁻

concentration ($2 \cdot 10^{-4}$ M and $2 \cdot 10^{-5}$ M) and Tc loading on Fe minerals (400 ppm, 600 ppm and 900 ppm, resulting from decreasing solid-to-liquid ratios). Experimental conditions including pH_c and E_h measurements before adding Tc are shown in Table 2.9. After the addition of Tc, samples were equilibrated for 6 weeks and pH_c , E_h and $[\text{Tc}]$ (after 10 kD ultrafiltration) were measured. Magnetite and mackinawite samples with the highest amount of Tc ($[\text{TcO}_4^-]_{\text{in}} = 2 \cdot 10^{-4}$ M and 900 ppm loading) (~ 0.5 mg each) were analysed by SEM to assess the morphology of the Fe phases responsible for Tc retention.

In a second experimental series, magnetite, mackinawite and siderite were pre-equilibrated in 5.0 M NaCl and 4.5 M MgCl_2 solutions for 3 weeks. Initial Tc concentration and Tc loading on Fe minerals were set to $2 \cdot 10^{-4}$ M and 1000 ppm for each sample, respectively. Experimental conditions considered for this system are shown in Table 2.10. As in the first experimental series, pH_c , E_h and $[\text{Tc}]$ (after 10 kD ultrafiltration) values were measured after an equilibration time of 4 weeks in the presence of Tc.

In both experimental series, solid phases were centrifuged at 4020 g after the corresponding equilibration time. The wet paste resulting after phase separation was placed into double confined sample holders, heat-sealed inside the Ar-glovebox and stored in a liquid N_2 Dewar (Voyager 12, Air Liquide – DMC, France) until the collection of EXAFS/XANES spectra in ESRF–ROBL (France). This approach has been previously shown to prevent the oxidation of redox sensitive samples (Np(IV), Pu(III/V), Tc(IV)) [71-73].

Table 2.9 Experimental conditions of Tc reduction/sorption experiments on magnetite and mackinawite in 0.1 M NaCl systems (before addition of Tc).

Fe minerals	Background electrolyte	pH_c^a	E_h (mV) ^b	$[\text{TcO}_4^-]_0$	solid/liquid ratio (g/L)	loading (ppm)
Magnetite	0.1 M NaCl	9.27	31	$2 \cdot 10^{-4}$	50	400
Magnetite	0.1 M NaCl	9.20	-50	$2 \cdot 10^{-4}$	33	600
Magnetite	0.1 M NaCl	9.18	-57	$2 \cdot 10^{-4}$	22	900
Magnetite	0.1 M NaCl	9.15	-67	$2 \cdot 10^{-5}$	5	400
Magnetite	0.1 M NaCl	8.90	-57	$2 \cdot 10^{-5}$	3	600
Magnetite	0.1 M NaCl	8.71	-69	$2 \cdot 10^{-5}$	2	900
Mackinawite	0.1 M NaCl	9.07	-300	$2 \cdot 10^{-4}$	50	400
Mackinawite	0.1 M NaCl	9.13	-308	$2 \cdot 10^{-4}$	33	600
Mackinawite	0.1 M NaCl	8.99	-293	$2 \cdot 10^{-4}$	22	900
Mackinawite	0.1 M NaCl	8.97	-288	$2 \cdot 10^{-5}$	5	400
Mackinawite	0.1 M NaCl	8.88	-283	$2 \cdot 10^{-5}$	3	600
Mackinawite	0.1 M NaCl	8.78	-278	$2 \cdot 10^{-5}$	2	900

a: ± 0.05 ; **b:** ± 30 mV

2 Experimental

Table 2.10 Experimental conditions of Tc reduction and sorption experiments on Fe minerals in 5.0 M NaCl and 4.5 M MgCl₂ systems (before addition of Tc).

Fe minerals	Background electrolyte	pH _c ^a	E _h (mV) ^b	[TcO ₄] ₀	solid/liquid ratio (g/L)	loading (ppm)
Magnetite	5.0 M NaCl	9.6	-140	2·10 ⁻⁴	21	989
Magnetite	4.5 M MgCl ₂	8.7	10	2·10 ⁻⁴	21	939
Mackinawite	5.0 M NaCl	8.7	-290	2·10 ⁻⁴	30	990
Mackinawite	4.5 M MgCl ₂	8.3	-150	2·10 ⁻⁴	30	986
Siderite	5.0 M NaCl	8.7	-175	2·10 ⁻⁴	20	990
Siderite	4.5 M MgCl ₂	8.3	-25	2·10 ⁻⁴	20	983

a: ± 0.05; b: ± 30 mV

2.5 EXAFS/XANES

EXAFS/XANES measurements were performed at ANKA (INE-beamline for Actinide Research, Karlsruhe, Germany) and ESRF (ROBL beamline, Grenoble, France) synchrotron facilities. In both cases, measurements and data interpretation were performed in cooperation with the respective beamline scientists.

2.5.1 ANKA, INE-beamline

2.5.1.1 Sample Preparation

After attaining equilibrium conditions, the sample in 4.5 M MgCl₂ at pH_m = 2.0 ([Tc] ~3 mM) was prepared for XAFS analysis to confirm the Tc redox state and assess the stoichiometry of the complex prevailing in solution. Approximately 300 µL of the supernatant solution of this sample was directly transferred to the 400 µL polyethylene vial under Ar atmosphere. This vial was mounted in a gas-tight cell with windows of Kapton® film (polyimide) inside the Ar-glovebox and transported to the INE-Beamline. The samples were measured under continuous Ar-flow within few hours after preparation for XAFS measurements.

2.5.1.2 XAFS measurements

Tc-K edge (21044 eV) XAFS spectra (3–4 replicates per sample) were collected under continuous flow of Ar. Tc spectra were energy calibrated with respect to the first inflection point in the XANES spectra of a Mo metal foil (20000 eV), which was measured simultaneously. The XAFS signal was recorded at room temperature in fluorescence mode using a vortex Si-drift detector. Si(111) crystals were used in the double crystals monochromator, operating in fixed-exit mode. The parallel alignment of the crystal faces was detuned to ~ 70% of the maximum beam intensity at the beginning of each scan. The incident intensity was held constant by means of a piezo-driven feedback system to the second crystal.

2.5.1.3 Data evaluation

XANES/EXAFS data reduction and analysis were performed with the ATHENA/ARTEMIS package following standard procedures [74]. Structural information was obtained by following a multi-shell approach for EXAFS data fitting. The fit included neighbouring atomic distances (R), EXAFS Debye-Waller factors (σ^2), coordination numbers (N) and relative shift in ionization energy E_0 (ΔE_0). EXAFS spectra were Fourier transformed (FT) in the k -range between 2–8.5 \AA^{-1} using symmetric square windows. Fit is performed using paths file calculated with Feff8.4 based on the TcO_2 crystal structure ICSD database record number 17-3151, where one of the O-atoms was replaced by Cl. Coordination numbers for O- and Cl-shells are kept free in the fit, although the overall sum is constrained to 6. Overall amplitude factor S_0^2 is fixed to 0.6 to get a coordination number of 6 for ref/liquid sample.

2.5.2 ESRF, ROBL-beamline

2.5.2.1 Sample Preparation

After adequate equilibration time, magnetite, mackinawite and siderite reacted with Tc were centrifuged at 4020 g for 10 min and the supernatant removed. Since both Tc(IV) and Fe(II) minerals are very sensitive to oxygen, all preparation steps were performed with special precautions to avoid/minimize the access of air to the samples. The wet paste material resulting from phase separation was placed in a polyethylene (PE) double confined sample holder and heat-sealed inside the Ar-glovebox. Sealed PE sample holders were taken out of the glovebox, immersed in dry ice ($-78\text{ }^\circ\text{C}$) to minimize the diffusion of O_2 into the samples, and immediately measured for gamma activity for 30 minutes (mandatory according to European transport regulations). Directly after gamma measurements, the samples were transferred to a liquid N_2 -filled Dewar (Voyager 12, Air Liquide - DMC, France). The latter was used to transport the samples to the synchrotron facility and to store these until the start of the measurements. The samples were measured within 20-30 days after preparation for XAFS measurements. Previous studies with redox sensitive elements (Pu, Np, Tc) have shown that storage under liquid nitrogen condition avoids oxidation process (or significantly longer time periods) [71, 73, 75].

2.5.2.2 XAFS measurements

Spectra were acquired in fluorescence mode at the Tc-K edge (21044 eV). The energy of the Si(111) double-crystal monochromator was calibrated using a Mo foil (edge energy 20000 eV). Two Rh-coated mirrors were used to collimate the beam into the monochromator crystal and to reject higher-order harmonics. Fluorescence spectra were collected using a 13-element, high-purity, solid-state Ge detector (Canberra) with digital spectrometer (XIA XMAP). During the measurement, the samples were kept at 15 K with liquid He to avoid changes of oxidation state and to reduce thermal disorder [75].

2.5.2.3 Data evaluation

EXAFS data reduction and analysis were performed using the SIXPACK/IFEFFIT software following standard procedures. The SAMVIEW program was used for dead-time corrections and to average the raw spectra. After background subtraction, the energy was converted to photoelectron wave vector units (\AA^{-1}) by assigning the ionization energy of the Tc-K edge (21044 eV), E_0 , to the first inflection point of the absorption edge. Radial structure functions (RSFs) were obtained by Fourier transforming k^3 -weighted $\chi(k)$ functions between 2.0 and 14.5 \AA^{-1} using a Kaiser-Bessel window function.

The XANES spectra were compared with a reference spectra of Tc(VII)O_4^- [76]. The EXAFS spectra were analysed in a two-step approach. The first step consisted of a statistical analysis of the data based on principal component analysis (PCA) and iterative target-transformation factor analysis (ITFA). The factor analysis code developed by A. Rossberg [77] was used for the statistical analysis. The calculation of the IND factor was performed in $k^3\chi(k)$ spaces for $2 \leq k [\text{\AA}^{-1}] \leq 12$.

The EXAFS data were fitted with WinXAS [78] using theoretical backscattering amplitudes and phase shifts calculated with FEFF 8.2 [74]. Tc-O, Tc-Fe, Tc-Tc and Tc-S theoretical scattering paths for the fit approach were calculated using ARTEMIS by replacing Fe atoms with Tc in octahedral coordinated magnetite and mackinawite structures. The amplitude reduction factor, S_0^2 , was fixed to 0.9 for all fits. Uncertainties associated with the structural parameters were kept as $\sigma^2 \leq 0.01$ and were directly calculated using ARTEMIS along with the R-factor, which is an indicator of the quality of the fit.

3 Redox behaviour of Tc(VII)/Tc(IV) in dilute to concentrated NaCl and MgCl₂ solutions

3.1 Tc(VII)/Tc(IV) redox border: thermodynamic and activity models in NaCl and MgCl₂

Tc(VII)/Tc(IV) redox transformations were investigated in the presence of different reducing chemicals in dilute to concentrated NaCl and MgCl₂ solutions. Provided the very low solubility of Tc(IV), the main redox reaction/borderline between Tc(VII) and Tc(IV) is defined as:



where $\log^* K_{\text{VII-IVs}}^o$ is the equilibrium constant for the reduction of TcO_4^- to $\text{TcO}_2 \cdot 1.6\text{H}_2\text{O}(\text{s})$ at $I = 0$ with a selected value of 37.8 ± 0.6 in the last NEA–TDB update book [35]. At $I \neq 0$, chemical equilibria are affected by ion interaction processes and activity coefficients need to be taken into account. Because of the high ionic strength in the experiments described in this work (up to $I = 5.0$ M in NaCl and $I = 13.5$ M in MgCl₂ systems), SIT and Pitzer approaches (see details in Section 1.2.3.2) were used to calculate $\gamma_{\text{TcO}_4^-}$ and γ_{H^+} and thus determine $\log^* K'_{\text{VII-IVs}}$ for each ionic strength according to equations (3.2) – (3.3).

$$\begin{aligned} \log^* K_{\text{VII-IVs}}^o &= -\log([\text{TcO}_4^-] \cdot \gamma_{\text{TcO}_4^-}) - 4 \log([\text{H}^+] \cdot \gamma_{\text{H}^+}) \\ &+ 3 \text{pe} + 0.4 \log a_w \end{aligned} \quad (3.2)$$

$$\log^* K'_{\text{VII-IVs}} = \log^* K_{\text{VII-IVs}}^o + \log \gamma_{\text{TcO}_4^-} + 4 \log \gamma_{\text{H}^+} - 0.4 \log a_w \quad (3.3)$$

SIT model

The specific ion interaction theory (SIT approach) (see Section 1.2.3.2) is the method adopted by NEA–TDB [35] for the treatment of ion interaction processes and ionic strength effects. However, no SIT ion interaction coefficients are currently selected for TcO_4^- in the NEA–TDB. The chemical analogy of TcO_4^- with ClO_4^- is therefore considered in this work to estimate the corresponding SIT coefficients with Na^+ and Mg^{2+} , yielding $\varepsilon(\text{TcO}_4^-, \text{Na}^+) \cong \varepsilon(\text{ClO}_4^-, \text{Na}^+) = 0.01 \pm 0.01 \text{ kg} \cdot \text{mol}^{-1}$ and $\varepsilon(\text{TcO}_4^-, \text{Mg}^{2+}) \cong \varepsilon(\text{ClO}_4^-, \text{Mg}^{2+}) = 0.33 \pm 0.03 \text{ kg} \cdot \text{mol}^{-1}$ [35]. The activity of water in dilute to concentrated NaCl and MgCl₂ solutions, as well as $\varepsilon(\text{H}^+, \text{Cl}^-) = 0.12 \pm 0.01 \text{ kg} \cdot \text{mol}^{-1}$ were taken directly from the NEA–TDB [35].

Pitzer model

Due to the known limitations of the SIT approach at high ionic strengths, the use of the Pitzer formalism (see Section 1.2.3.2) is required for thermodynamic calculations and geochemical modelling in concentrated salt brine solutions [41]. The values of $\log \gamma_{H^+}$ and a_w in equation (3.2) used in this study are calculated from the parameters reported by Harvie et al. [79]. Binary parameters for (TcO₄⁻, Na⁺) and (TcO₄⁻, Mg²⁺), mixing parameter for (TcO₄⁻, Cl⁻) and ternary parameters for (TcO₄⁻, Cl⁻, Na⁺) and (TcO₄⁻, Cl⁻, Mg²⁺) were taken from Könnecke et al. [80] and Neck et al. [81] as summarized in Table 3.1.

Table 3.1 Pitzer ion interaction coefficients for TcO₄⁻ in NaCl and MgCl₂ media at 25 °C: $\beta^{(0)}$, $\beta^{(1)}$ and $\theta_{i'}$ in [kg·mol⁻¹]; $C^{(\phi)}$ and Ψ_{ij} in [kg²·mol⁻²].

i	j	Binary Pitzer parameters			Ternary Pitzer parameters			Ref.
		$\beta^{(0)}$	$\beta^{(1)}$	$C^{(\phi)}$	i'	$\theta_{i'}$	Ψ_{ij}	
TcO ₄ ⁻	Na ⁺	0.01111	0.1595	0.00236	Cl ⁻	0.067	-0.0085	[80]
TcO ₄ ⁻	Mg ²⁺	0.3138	1.84	0.0114	Cl ⁻	0.067	-0.0115	[81]

Table 3.2 summarizes the values of $\log \gamma_{TcO_4^-}$, $\log \gamma_{H^+}$ and $\log^* K'_{VII-IVs}$ in NaCl (0.5 M and 5.0 M) and MgCl₂ (0.25 M, 2.0 M and 4.5 M) calculated by SIT and Pitzer models as described above. Tc(VII)/Tc(IV) redox borderlines calculated for NaCl and MgCl₂ solutions using $\log^* K'_{VII-IVs}$ are compared in the following sections with Tc redox distribution determined experimentally for each independent reducing system.

Table 3.2 Activity coefficients of TcO₄⁻ and H⁺ in (0.5 and 5.0 M) NaCl and (0.25, 2.0 and 4.5 M) MgCl₂ solutions derived from SIT and Pitzer approaches. Conditional equilibrium constants ($\log^* K'_{VII-IVs}$) for reaction (3.1) are calculated for the corresponding ionic strength conditions according to equation (3.3).

Background electrolyte	$\log \gamma_{H^+}$		$\log \gamma_{TcO_4^-}$		$\log^* K'_{VII-IVs}$	
	SIT	Pitzer	SIT	Pitzer	SIT	Pitzer
0.5 M NaCl	-0.114	-0.104	-0.170	-0.188	37.2	37.2
5.0 M NaCl	0.408	0.590	-0.209	-0.165	39.3	40.1
0.25 M MgCl ₂	-0.131	-0.188	-0.109	-0.060	37.2	37.0
2.0 M MgCl ₂	0.237	0.206	0.427	0.497	39.2	39.2
4.5 M MgCl ₂	0.946	1.060	1.409	1.508	43.2	43.7

Figure 3.1 shows the *Pourbaix* diagram of Tc within $0 \leq \text{pH}_c \leq 14.5$ and $-14 \leq \text{pe} \leq 14.5$ as calculated with the current NEA–TDB data selection. The blue solid line (A) in Figure 3.1 corresponds to the thermodynamic borderline for Tc(VII)/Tc(IV) calculated at $I = 0$ according to reaction (3.1) and

represents 50% Tc(VII) and 50% Tc(IV) redox state distribution. Note that this borderline depends both upon ionic strength and total Tc concentration, the latter held constant at $[Tc]_0 = 1 \cdot 10^{-5}$ M in the calculations consistently with the experimental conditions selected in this study. Borderlines for Tc(VII)/Tc(IV) reduction calculated for 5.0 M NaCl and 4.5 M MgCl₂ are also included in Figure 3.1. The comparison of thermodynamic calculations for $I = 0$ (solid blue line (A)), $I = 5.0$ M (green lines (B), 5.0 M NaCl) and $I = 13.5$ M (red lines (C), 4.5 M MgCl₂) clearly indicates that a stabilization of Tc(IV) relative to Tc(VII) is expected with increasing ionic strength. Only minor differences (≤ 0.3 pe-units) are observed between Tc(VII)/Tc(IV) borderlines calculated by SIT and Pitzer, indicating the validity of the SIT also in the extremely high saline conditions evaluated in this study.

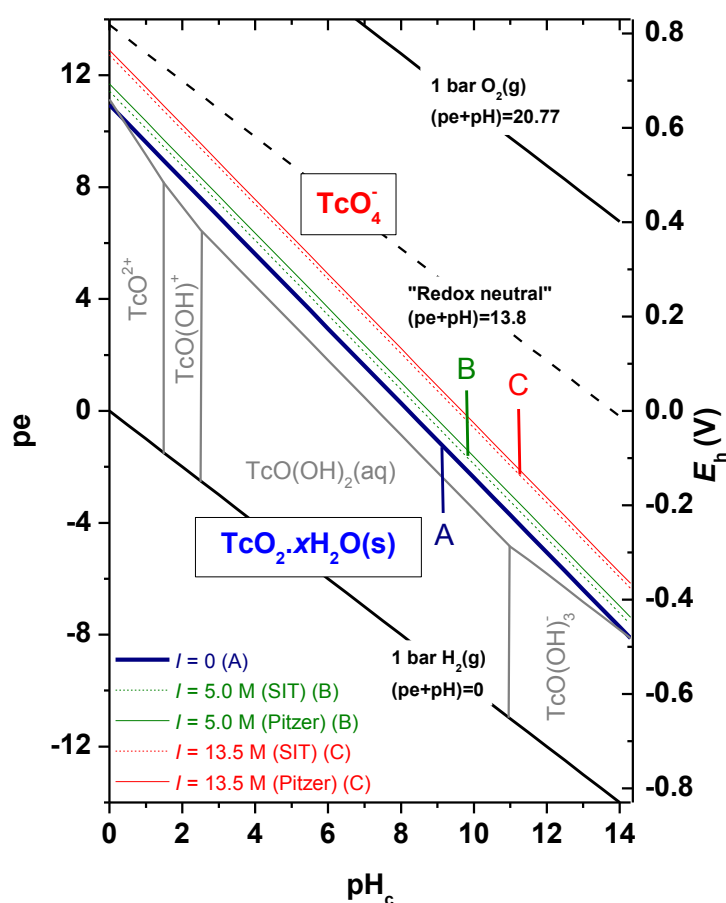


Figure 3.1 Pourbaix diagram of Tc calculated for $I = 0$ with thermodynamic data selected in NEA–TDB [35]. Thin dark grey lines correspond to 50:50 distribution borderlines between aqueous Tc species at $I = 0$. Black lines indicate upper and lower decomposition lines of water and “redox neutral” ($pe + pH = 13.8$) conditions. Coloured lines (A, B, C) correspond to Tc(VII)/Tc(IV) borderlines considering reaction (3.1), calculated for (A) $I = 0$ (blue line), (B) $I = 5.0$ M (green dashed line: SIT, green solid line: Pitzer; 5.0 M NaCl) and (C) $I = 13.5$ M (red dashed line: SIT, red solid line: Pitzer; 4.5 M MgCl₂). All calculations performed at $[Tc]_{tot} = 10^{-5}$ M. Ionic strength corrections performed by SIT and Pitzer approaches as described in Sections 1.2.3.2.

3.2 Redox behaviour of Tc(VII)/Tc(IV) in dilute to concentrated NaCl and MgCl₂ solutions: comparison of experimental pH_c, E_h and [Tc]_{aq} with thermodynamic calculations

Experimental E_h and pH_c values measured in NaCl and MgCl₂ solutions in the presence of reducing chemicals are summarized in the E_h-pH diagrams in Figures 3.2–3.6. Coloured dashed and solid lines in the figures represent the thermodynamic equilibrium between Tc(VII) and Tc(IV) (50:50 distribution borderline) calculated for reaction (3.1) by SIT and Pitzer approaches, respectively. These calculations were performed assuming a content of 1.6 H₂O molecules in hydrated TcO₂·xH₂O(s) according to literature [82]. The samples were regularly monitored for pH_c, E_h and [Tc] for up to 395 d. In order to facilitate the interpretation of the figures, only average values are plotted for samples where stable readings indicate that equilibrium has been reached. Tc concentration as a function of pH_c for each reducing system is provided besides the corresponding E_h-pH diagram. The decrease of the Tc concentration in the aqueous phase is interpreted as the reduction of Tc(VII) and consequent formation of the sparingly soluble TcO₂·1.6H₂O(s) phase. The figures also highlight those systems especially affected by kinetics. Table 3.3 summarizes the redox distribution of Tc in the aqueous phase of selected samples as quantified by solvent extraction.

3.2.1 Na₂S₂O₄ systems

E_h-pH diagrams of Tc in 1 mM Na₂S₂O₄ are shown in Figures 3.2a (NaCl) and 3.2c (MgCl₂). In all samples, measured E_h values are below the thermodynamically expected Tc(VII)/Tc(IV) borderline. E_h values with large uncertainties (up to +/- 100 mV) are observed in near-neutral to slightly alkaline pH conditions. This observation is likely related with the known degradation of Na₂S₂O₄ under less alkaline to acidic pH conditions [83, 84]. No significant differences were observed between the E_h values measured in dilute and concentrated NaCl solutions. On the contrary, large differences (up to 5 pe-units) arise between E_h values measured in dilute and concentrated MgCl₂ solutions, hence hinting towards a strong impact of ionic strength, [Cl⁻] and/or [Mg²⁺] on the redox couple controlling the E_h in this system.

A significant decrease of Tc concentration indicating the reduction of Tc(VII) to Tc(IV) is observed in all systems with Na₂S₂O₄ (Figures 3.2b and 3.2d). The predominance of Tc(IV) in the aqueous phase is confirmed for selected samples by solvent extraction (Table 3.3). This is in very good agreement with thermodynamic calculations performed using NEA-TDB and SIT/Pitzer ionic strength corrections as summarized in Table 3.2. Higher concentrations of Tc(IV) are retained in the aqueous phase in NaCl solutions at pH_c > 12. This is consistent with the expected formation of an anionic hydrolysis species (*e.g.* TcO(OH)₃⁻), which increases the solubility of TcO₂·1.6H₂O(s) in the strongly alkaline pH region. Similar to previous observations by Kobayashi and co-workers in diluted NaCl solutions and Na₂S₂O₄ [34], ~10⁻⁷ M Tc(IV) concentrations are observed in 0.5 M and 5.0 M NaCl solutions under near-neutral pH conditions. A concentration level of 10⁻⁸–10⁻⁹ M is expected for Tc(IV) solubility under these conditions according to the equilibrium reaction

$\text{TcO}_2 \cdot 1.6\text{H}_2\text{O}(\text{s}) \Leftrightarrow \text{TcO}(\text{OH})_2(\text{aq}) + 0.6 \text{H}_2\text{O}$ [35]. This observation is also in disagreement with data obtained in the present work in Sn(II) systems (see Figure 3.3b), thus indicating a possible impact of Na₂S₂O₄ degradation on the behaviour of Tc(IV). Note that the formation of very stable colloidal Tc-S species has been previously reported in the literature [85].

Very high [Tc(IV)] (up to 10^{-5.5} M) is observed in solution in concentrated MgCl₂ systems, even in the slightly alkaline pH conditions buffered by the precipitation of Mg(OH)₂(cr) or Mg₂(OH)₃Cl·4H₂O(cr) at pH_c~8.5. The comparison of these results with Sn(II) and Fe(II)/Fe(III) systems suggests that [Tc(IV)] in equilibrium with TcO₂·1.6H₂O(s) in the presence of Na₂S₂O₄ can be overestimated, especially at near-neutral conditions.

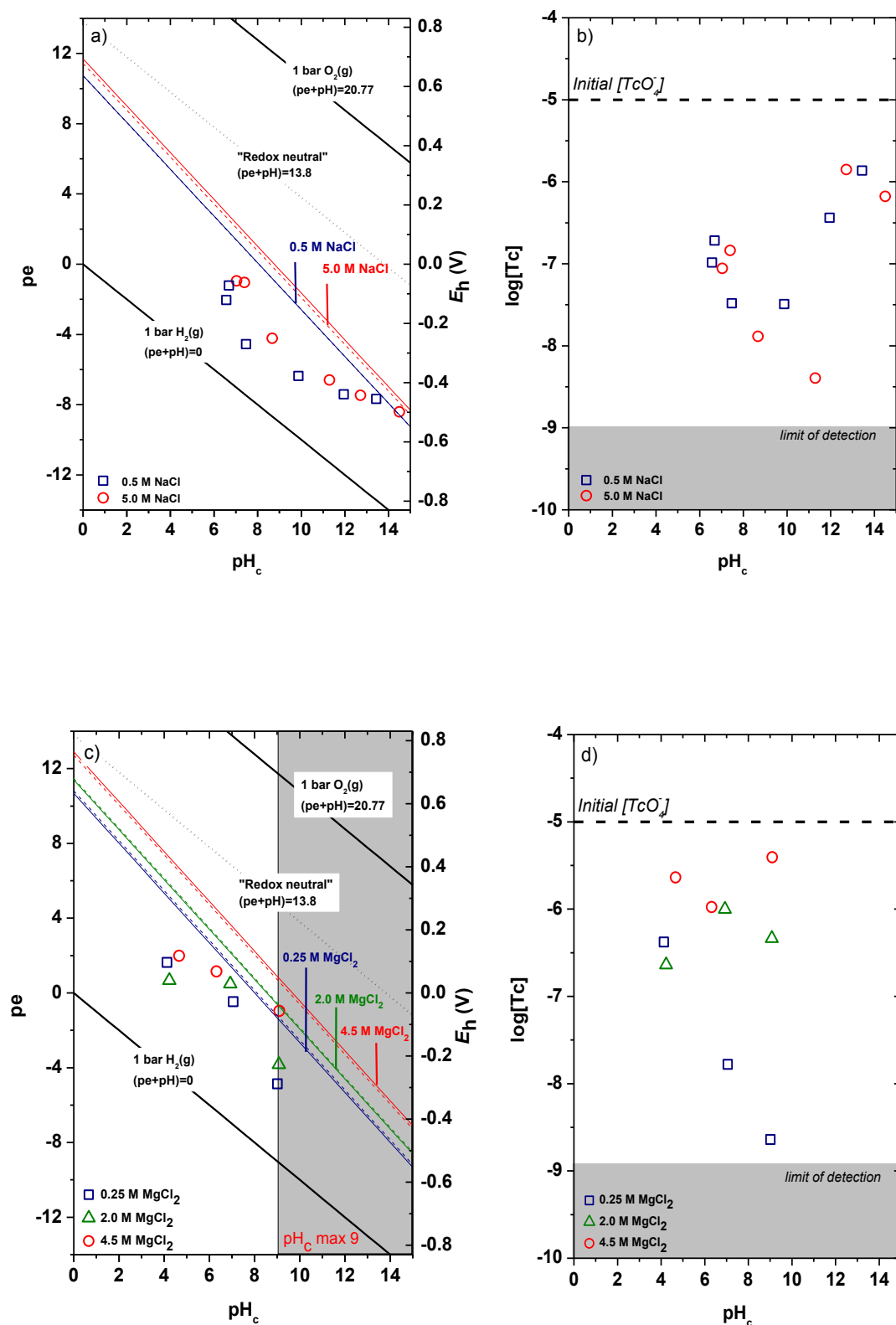


Figure 3.2 Tc(VII)/Tc(IV) redox behaviour in the presence of 1 mM Na₂S₂O₄. NaCl solutions: (a) E_h -pH diagram, (b) aqueous concentration of Tc. MgCl₂ solutions: (c) E_h -pH diagram, (d) aqueous concentration of Tc. Dashed and solid lines corresponding to the Tc(VII)/Tc(IV) redox borderline calculated for reaction (3.1) using NEA-TDB with SIT and Pitzer ionic strength corrections, respectively.

Table 3.3 Tc redox distribution of aqueous phase quantified by solvent extraction in selected samples in NaCl and MgCl₂ solutions.

Reducing system	Background electrolyte	pH _c ^a	E _h (mV) ^b	%Tc (IV) ^c
Na ₂ S ₂ O ₄	0.5 M NaCl	7.5	-270	98
Na ₂ S ₂ O ₄	0.5 M NaCl	6.6	-120	99
Na ₂ S ₂ O ₄	0.5 M NaCl	12.0	-435	92
Na ₂ S ₂ O ₄	5.0 M NaCl	12.7	-445	99
Sn(II)	0.5 M NaCl	1.9	30	98
Sn(II)	0.5 M NaCl	13.7	-760	99
Sn(II)	5.0 M NaCl	2.9	80	92
Sn(II)	5.0 M NaCl	14.5	-760	99
HQ	0.5 M NaCl	1.8	396	1.4
HQ	5.0 M NaCl	2.9	398	0.8
Fe(II)/Fe(III)	0.5 M NaCl	2.0	645	0.4
Fe(II)/Fe(III)	5.0 M NaCl	2.8	400	0.1
Fe(II)/Fe(III)	5.0 M NaCl	4.5	635	0.4
Na ₂ S ₂ O ₄	2.0 M MgCl ₂	7.0	30	99
Na ₂ S ₂ O ₄	4.5 M MgCl ₂	9.0	-55	99
Sn(II)	2.0 M MgCl ₂	3.7	5	73
Sn(II)	4.5 M MgCl ₂	4.0	140	62
Sn(II)	4.5 M MgCl ₂	6.4	-10	85
Sn(II)	4.5 M MgCl ₂	9.0	-215	99
Fe(II)/Fe(III)	0.25 M MgCl ₂	3.4	205	0.1
Fe(II)/Fe(III)	2.0 M MgCl ₂	3.8	485	0.2
Fe(II)/Fe(III)	4.5 M MgCl ₂	4.2	610	0.3
Fe(II)/Fe(III)	4.5 M MgCl ₂	6.4	365	0.6
Fe Powder	4.5 M MgCl ₂	9.0	-195	99
Fe Powder	4.5 M MgCl ₂	8.9	-125	99

a: ± 0.05; **b:** ± 50 mV; **c:** ± 10%

3.2.2 Sn(II) systems

Tin(II) is a very strong reducing agent which keeps stable E_h values slightly above the border of water reduction (Figures 3.3a and 3.3c). The redox couple Sn(II)/Sn(IV) controlling the E_h in this system is strongly impacted by ionic strength, $[Cl^-]$ and/or $[Mg^{2+}]$, with $pe + pH_c$ values ranging from 2 ± 1 to 7 ± 1 in 0.5 M NaCl and 4.5 M MgCl₂, respectively. Very similar $pe + pH_c$ values like in 0.5 M NaCl were recently reported for Sn(II) solutions in 0.1 M NaCl ($pe + pH_c = 2 \pm 1$) [34]. The very reducing E_h values fixed by Sn(II) promote a fast ($t_{1/2} = 7$ days) and complete reduction of Tc(VII) to Tc(IV) in NaCl solutions (Figure 3.3b). This observation is confirmed by solvent extraction, which indicates the predominance of Tc(IV) ($\geq 92\%$) in all NaCl samples analysed (Table 3.3). Tc concentrations

determined in the entire pH range are also in very good agreement with the undersaturation solubility data reported in this study (see Chapter 4), confirming that the same solid phase has been obtained from oversaturation and undersaturation conditions. These data also confirm the strong effect of ionic strength on Tc(IV) solubility under acidic conditions, where [Tc] in equilibrium with TcO₂·1.6H₂O(s) increases by 1.5–2 log-units between 0.5 M and 5.0 M NaCl.

Very low [Tc] are observed in 0.25 M MgCl₂ at $3.5 \leq \text{pH}_c \leq 9$ (Figure 3.3d), in good agreement with data in 0.5 M NaCl. Significantly higher [Tc] are observed in 2.0 M and 4.5 M MgCl₂. Both systems are affected by strong kinetics (especially for $\text{pH}_c = \text{pH}_{\text{max}} \sim 9$), which likely hinders thermodynamic equilibrium even after 395 days. This hypothesis is confirmed by comparison of these data with the results obtained from undersaturation solubility experiments (symbol ⊕ in Figure 3.3d, see also Section 4.1), which clearly lead to lower [Tc] than those determined in this part of the study from oversaturation conditions. Solvent extraction analysis of the supernatant solution in 2.0 M and 4.5 M MgCl₂ indicates 62–99% content in Tc(IV) for both oversaturation (Table 3.3) and undersaturation conditions (Table 4.1 in Section 4.2). Note however, that XANES analysis confirmed the predominance of Tc(IV) in solution for undersaturation experiments. This effect is discussed in more detailed in Section 4.2.1.2.

3.2.3 Hydroquinone

Figure 3.4a and Figure 3.4c show the E_h -pH diagrams of the Tc(VII)/Tc(IV) redox couple in 3 mM Hydroquinone (HQ) system in NaCl (0.5 M and 5.0 M) and MgCl₂ (0.25 M, 2.0 M and 4.5 M) solutions, respectively. Experimental E_h values in NaCl systems lie above the Tc(VII)/Tc(IV) borderline throughout the entire pH region, whereas in MgCl₂ solutions the E_h values scatter around the thermodynamically calculated transformation borderline. For both systems, Tc concentrations remain at initial level ($[\text{Tc}] = [\text{Tc}]_0 = 10^{-5}$ M) in all samples over the entire equilibration time (up to one year). Predominance of (99%) Tc(VII) determined by solvent extraction confirm that no reduction occurred in this system (Table 3.3). Note that similar observations were reported by Kobayashi et al. (2013) in diluted NaCl systems. No definitive explanation is available so far, although it can be speculated on the incapacity of (the oxidized form of) hydroquinone to provide the 3 e⁻ needed for the reduction of Tc(VII) to Tc(IV).

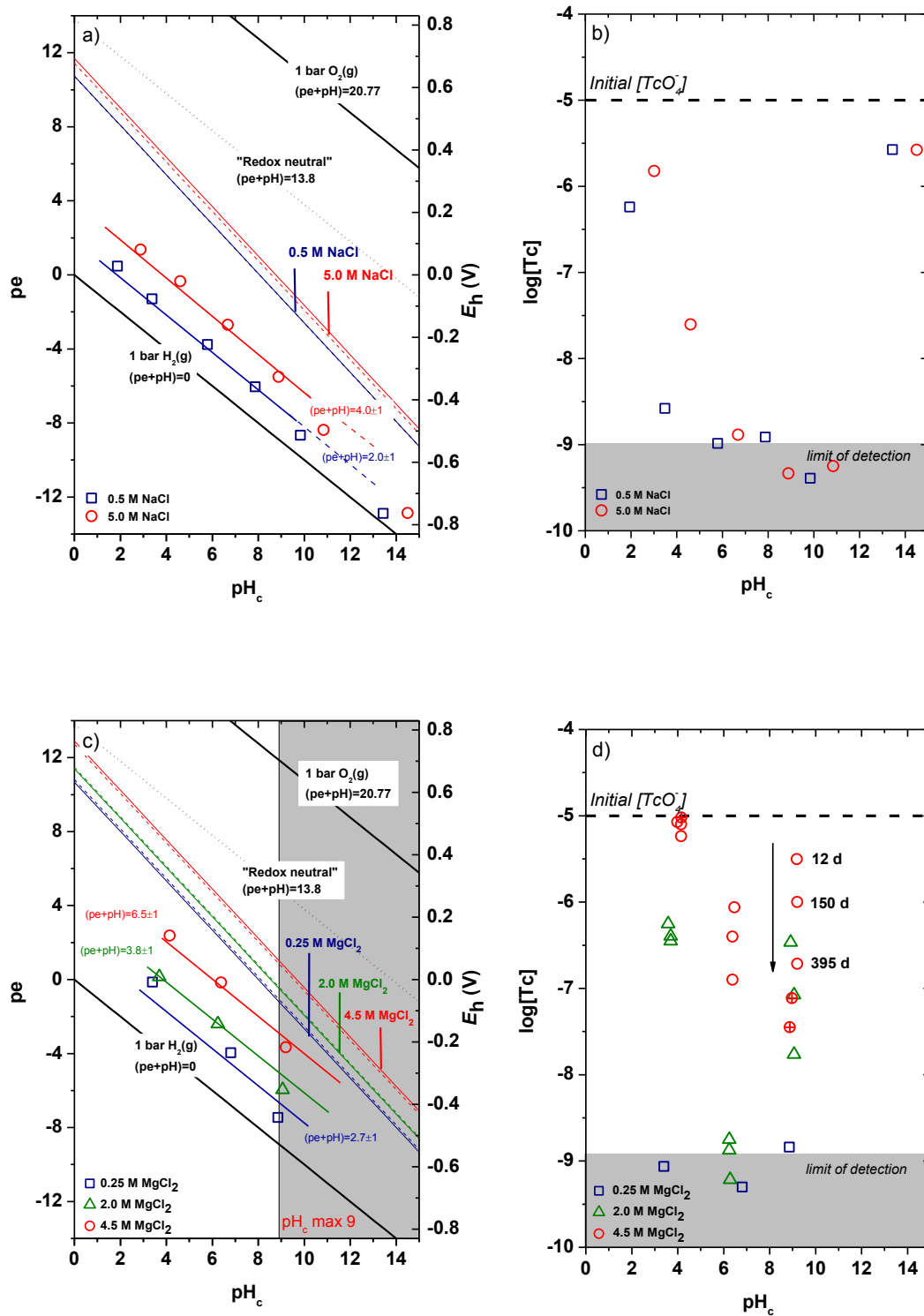


Figure 3.3 Tc(VII)/Tc(IV) redox behaviour in the presence of 1 mM Sn(II): NaCl solutions: (a) E_h -pH diagram, (b) aqueous concentration of Tc. MgCl₂ solutions: (c) E_h -pH diagram, (d) aqueous concentration of Tc. Dashed and solid lines corresponding to the Tc(VII)/Tc(IV) redox borderline calculated for reaction (3.1) using NEA-TDB data with SIT and Pitzer ionic strength corrections, respectively. Symbol \oplus in (d) indicates $[Tc(IV)]$ in 4.5 M MgCl₂ measured from undersaturation conditions (see text).

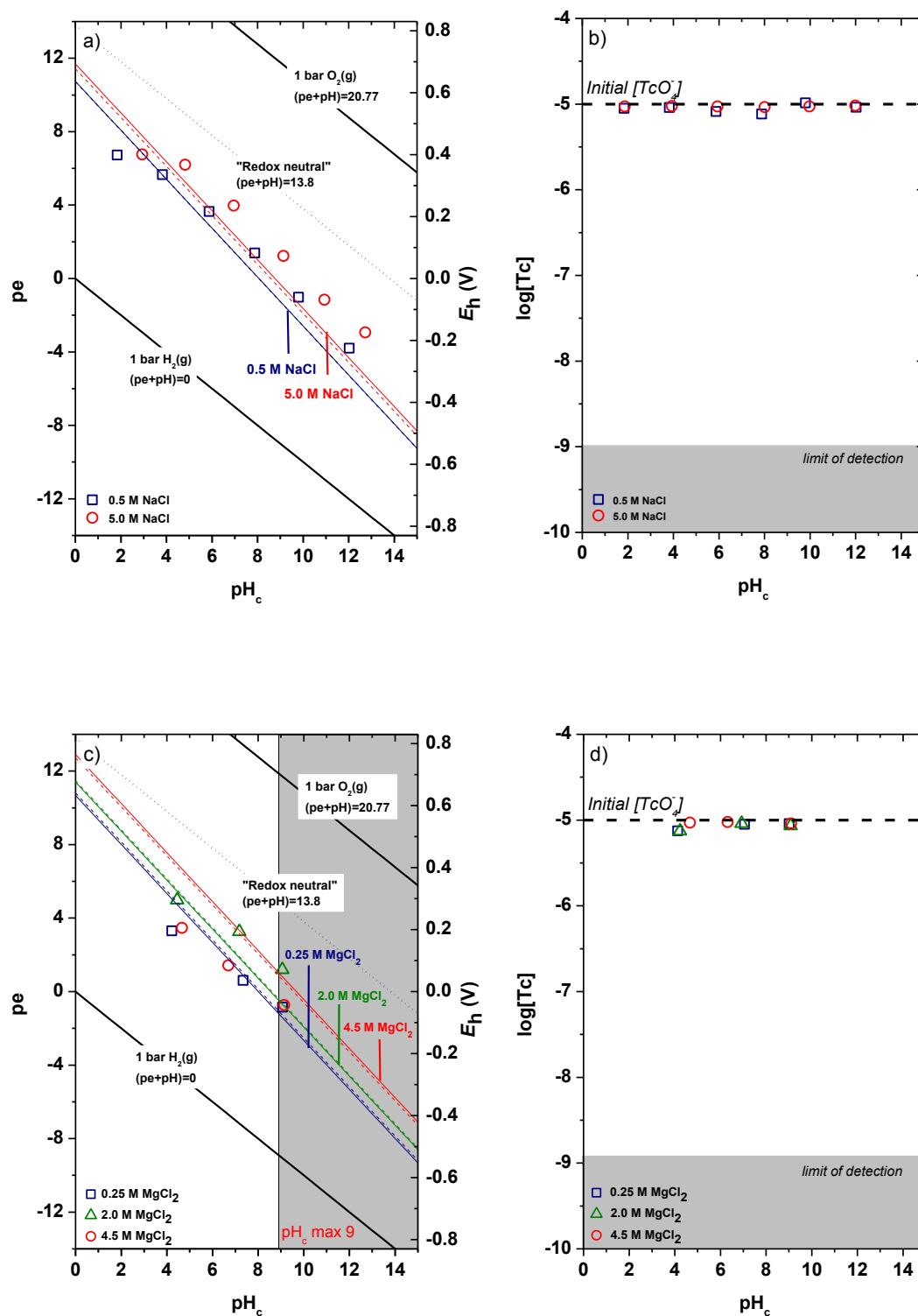


Figure 3.4 Tc(VII)/Tc(IV) redox behaviour in the presence of 3 mM HQ: NaCl solutions: (a) E_h -pH diagram, (b) aqueous concentration of Tc. MgCl₂ solutions: (c) E_h -pH diagram, (d) aqueous concentration of Tc. Dashed and solid lines corresponding to the Tc(VII)/Tc(IV) redox borderline calculated for reaction (3.1) using NEA-TDB data with SIT and Pitzer ionic strength corrections, respectively.

3.2.4 Fe(II)/Fe(III) systems

Figure 3.5 shows the redox behaviour of Tc(VII)/Tc(IV) in the presence of Fe(II)/Fe(III) in dilute to concentrated NaCl and MgCl₂ solutions. In analogy to the Na₂S₂O₄ systems, the increase of ionic strength induces only a minor effect on the E_h values measured in NaCl solutions. For this background electrolyte system, the Fe(II)/Fe(III) redox pair defines E_h values above the calculated Tc(VII)/Tc(IV) borderline under acidic pH conditions. At $\text{pH}_c = 2\text{--}3$, most of the initial $\text{Fe(II)}_{\text{aq}}$ and $\text{Fe(III)}_{\text{aq}}$ are retained in solution. For these conditions, E_h values can be thermodynamically calculated considering the chemical reaction $\text{Fe}^{2+} \leftrightarrow \text{Fe}^{3+} + \text{e}^-$. Assuming $[\text{Fe(II)}]_0 = [\text{Fe(II)}]_{\text{aq}}$ and $[\text{Fe(III)}]_0 = [\text{Fe(III)}]_{\text{aq}}$, and considering $[\text{Fe(II)}]_{\text{aq}} = [\text{Fe}^{2+}]$ and $[\text{Fe(III)}]_{\text{aq}} = [\text{Fe}^{3+}] + \Sigma[\text{FeCl}_n^{3-n}] + \Sigma[\text{Fe(OH)}_n^{3-n}]$ at $\text{pH}_c = 2$ in 0.5 M NaCl, an E_h^{therm} value of 0.63 V can be calculated based on equation (3.4) and using $\log^* K^\circ$ and SIT ion interaction parameters summarized in tables A1 and A2 in the Appendix.

$$\begin{aligned} \text{pe} = & \log(\text{Fe(III)}_{\text{tot}} \cdot \gamma_{\text{Fe}^{3+}}) - \log(\text{Fe(II)}_{\text{tot}} \cdot \gamma_{\text{Fe}^{2+}}) - \log K_{\text{Fe}^{2+}\text{Fe}^{3+}}^{\circ} \\ & - \log(1 + \Sigma \beta_{1,n,m}^* \cdot [\text{Cl}^-]^n \cdot [\text{H}^+]^{-m}) \end{aligned} \quad (3.4)$$

where $\beta_{1,n,m}^*$ are the conditional equilibrium constants for the formation of Fe(III) hydroxo and chloro complexes under given pH_c and $[\text{Cl}^-]$ conditions. This value is in excellent agreement with the measured redox potential (0.64 ± 0.05 V), thus supporting the validity of the E_h values experimentally determined in the Fe systems. E_h values below the calculated Tc(VII)/Tc(IV) borderline are measured in the near-neutral and alkaline pH regions. Under these conditions, the formation of a black Fe precipitate (likely magnetite) occurs. Thermodynamic calculations considering the formation of this solid phase predict the decrease of E_h towards more reducing conditions, although the exact redox potential is strongly dependent on the particle size of the solid forming (and thus on the selected $\log^* K_{s,0}^\circ$).

A clear decrease of Tc concentration occurs under near-neutral to hyperalkaline pH conditions indicating the reduction of Tc(VII), whereas $[\text{Tc}]$ remains $\sim 10^{-5}$ M in the acidic pH region (Figure 3.5b). This is in good agreement with the thermodynamic borderline for 50:50% Tc(VII)/Tc(IV) redox distribution calculated with NEA–TDB data and SIT/Pitzer ionic strength corrections as described in Section 1.3.2. These observations are also in line with data reported by Zachara and co-workers, who observed a rapid reduction of Tc(VII) in the presence of Fe(II) at $\text{pH} > 6.8$ [26]. In contrast to this, Cui et al. [25] reported the absence of Tc(VII) reduction in Fe(II) systems with $\text{pH} \leq 7.5$.

In contrast to the investigated NaCl systems, a significant increase of experimental E_h is observed with increasing MgCl₂ concentration (Figure 3.5c). As occurring for Sn(II) systems, this observation indicates that the Fe(II)/Fe(III) redox couple is significantly influenced by ionic strength, $[\text{Cl}^-]$ and/or $[\text{Mg}^{2+}]$. Concentration of Tc in solution remains unaffected for samples in the acidic pH region with E_h values above the calculated Tc(VII)/Tc(IV) borderline (Figure 3.5d), thus indicating the predominance of Tc(VII). These observations are further confirmed by solvent extraction analysis as summarized in Table 3.3. The sample at $\text{pH}_c \sim 3.5$ and $E_h = 0.2$ V in 0.25 M MgCl₂ is the only sample in this pH region below the Tc(VII)/Tc(IV) borderline for which unexpectedly no decrease of $[\text{Tc}]$ is observed

within 395 days. In general, a very good agreement between experimental data and thermodynamic calculations is observed for MgCl₂ solutions under near-neutral to alkaline pH conditions ($6 \leq \text{pH}_c \leq 9$). All samples in this pH region with E_h values below the Tc(VII)/Tc(IV) borderline show a clear decrease of [Tc] in solution and consequent reduction to Tc(IV). As in the case of Sn(II) systems, slow kinetics are observed in 4.5 M MgCl₂ at $\text{pH}_c = \text{pH}_{\text{max}}$, where [Tc]_{aq} decreases from $\sim 10^{-7.3}$ M to $\sim 10^{-8.3}$ M within 395 days. The very low concentration of Tc reached in these conditions compared to Sn(II) systems and undersaturation solubility experiments (see Figure 3.3) indicate that sorption of Tc(IV) on the forming magnetite may have occurred.

3.2.5 Corroding Fe powder systems

Very reducing E_h values are measured in the presence of corroding Fe powder in diluted NaCl and MgCl₂ systems at $\text{pH}_c \leq 9$ (Figures 3.6a and 3.6c). These values are in good agreement with previous studies under analogous experimental conditions at $\text{pe} + \text{pH} = 2 \pm 1$ [86]. A fast reduction of Tc(VII) to Tc(IV) is observed for all samples at $\text{pH}_c \leq 9$, as indicated by the decrease of [Tc] (Figure 3.6b) and confirmed by solvent extraction (Table 3.3). Above $\text{pH}_c \sim 10$, the reducing capacity of Fe powder is retained only for ~ 60 days, possibly indicating the formation of a protecting layer affecting Fe-corrosion. A similar behaviour of Fe powder in 0.1 M NaCl solutions was recently reported by Kobayashi et al. (2013) [34]. E_h values measured after this time are located above the Tc(VII)/Tc(IV) redox borderline, corresponding to the predominance of Tc(VII) in solution with [Tc] $\sim 10^{-5}$ M. These results again show that meaningful E_h values can be measured in Fe redox-buffered systems (also at high I). They also indicate that the NEA–TDB selection of thermodynamic data in combination with SIT or Pitzer ion interaction parameters reported in the present study (see section 3.1) offer an accurate tool to predict Tc redox behaviour in dilute to concentrated brine solutions.

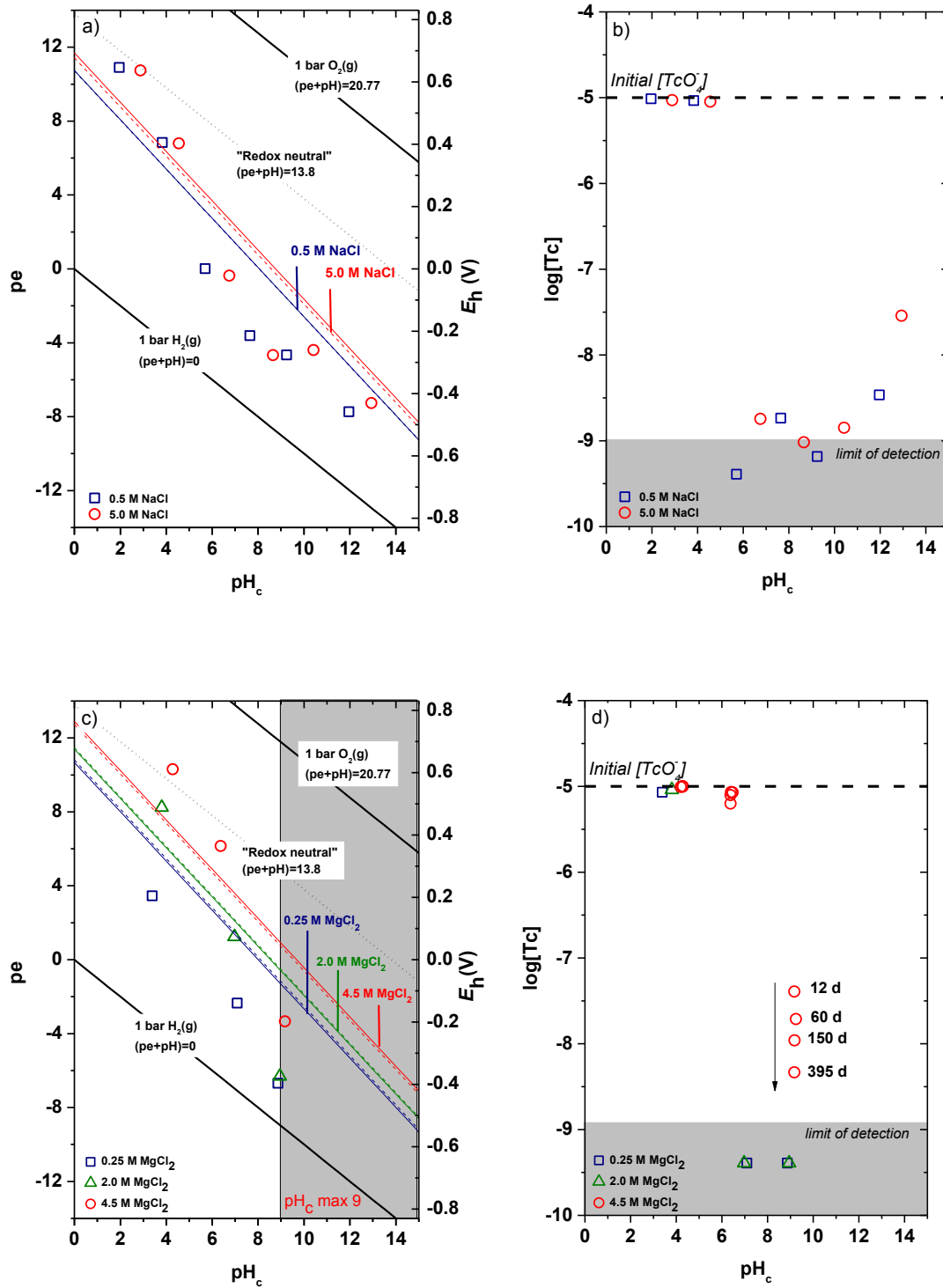


Figure 3.5 Tc(VII)/Tc(IV) redox behaviour in the presence of Fe(II)/Fe(III): NaCl solutions: (a) E_h -pH diagram, (b) aqueous concentration of Tc. MgCl₂ solutions: (c) E_h -pH diagram, (d) aqueous concentration of Tc. Dashed and solid lines corresponding to the Tc(VII)/Tc(IV) redox borderline calculated for reaction (3.1) using NEA-TDB data with SIT and Pitzer ionic strength corrections, respectively.

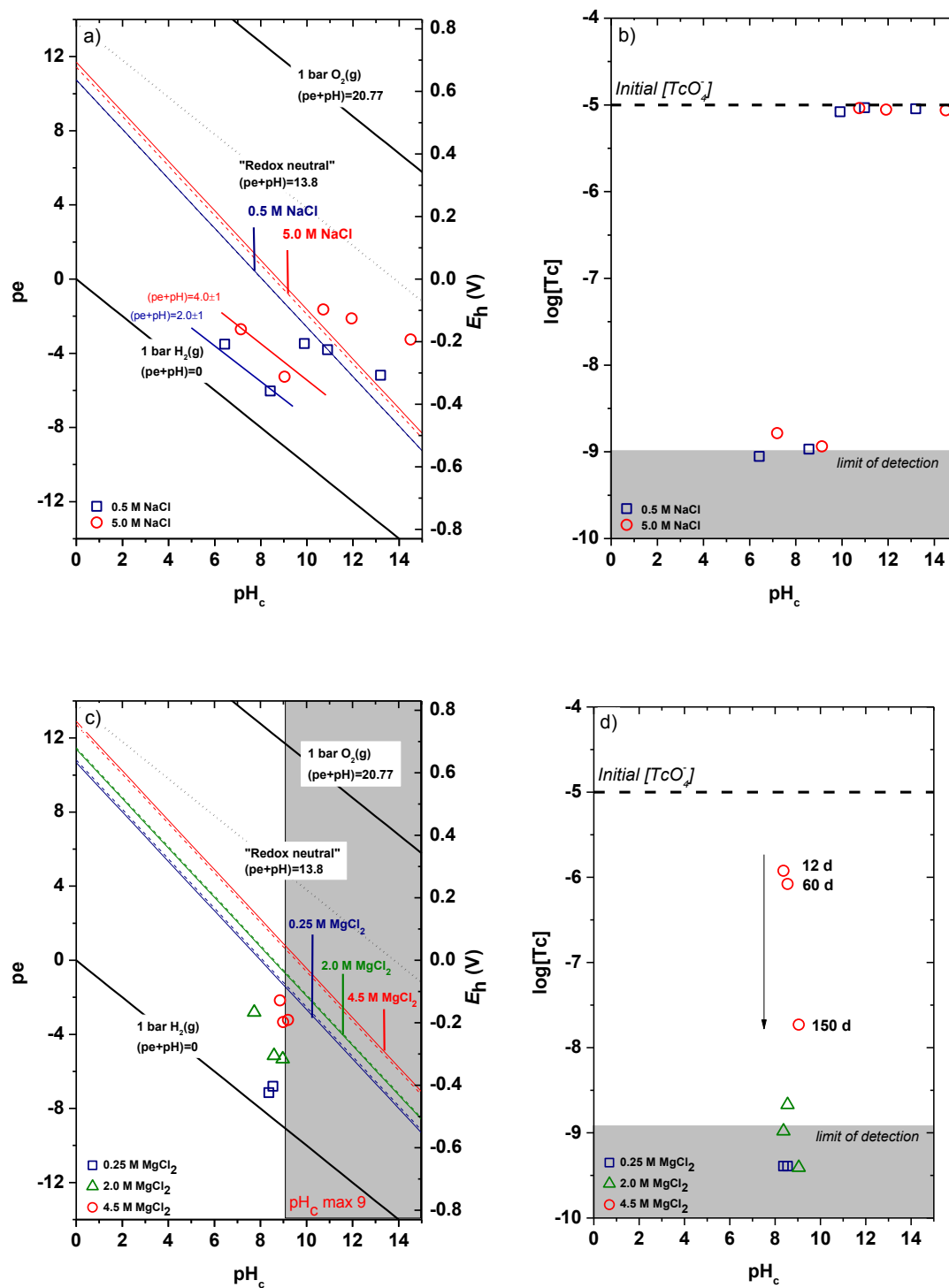


Figure 3.6 Tc(VII)/Tc(IV) redox behaviour in the presence of Fe powder: NaCl solutions: (a) E_h -pH diagram, (b) aqueous concentration of Tc. MgCl₂ solutions: (c) E_h -pH diagram, (d) aqueous concentration of Tc. Dashed and solid lines corresponding to the Tc(VII)/Tc(IV) redox borderline calculated for reaction (3.1) using NEA-TDB data with SIT and Pitzer ionic strength corrections, respectively.

3.3 Conclusions on Tc(VII)/Tc(IV) redox processes

Tc(VII)/Tc(IV) redox behaviour was systematically investigated in dilute to concentrated NaCl and MgCl₂ solutions. In the considered redox-buffered systems, the assessment of experimental pH and E_h values by thermodynamic calculations using NEA–TDB data provides an adequate tool to predict the redox distribution of Tc in aqueous solutions. The use of SIT or Pitzer ion interaction coefficients proposed in this work allows extending the predictions to concentrated NaCl and MgCl₂ brine systems. A systematic increase of experimental E_h values is related to increasing ionic strength, especially in concentrated MgCl₂ brines. This observation reflects the impact of ionic strength, chloride- and/or magnesium concentration on the redox couple controlling the redox potential of the solution. In redox-buffered systems where the two members of the redox couple (and corresponding thermodynamics) are known (i.e. Fe(II)/Fe(III) under acidic conditions), measured and thermodynamically calculated E_h values show a very good agreement.

The solubility of Tc(IV) in concentrated NaCl (5.0 M) and MgCl₂ solutions (2.0 M and 4.5 M) is significantly enhanced compared to dilute NaCl and MgCl₂ systems. This can be explained by the stabilization of charged hydrolysis species at elevated ionic strengths. Kinetics have been shown to play a relevant role when approaching the Tc reduction/solubility from oversaturation, especially in the case of MgCl₂ brines in alkaline conditions. The outcome of the studies described in this chapter is also relevant for the systematic undersaturation solubility experiments and comprehensive chemical and thermodynamic models reported in Chapter 4.

4 Solubility and hydrolysis of Tc(IV) in dilute to concentrated NaCl, MgCl₂ and CaCl₂ solutions

The solubility and hydrolysis of Tc(IV) was investigated from undersaturation with a specific well characterized solid phase in three salt systems; 0.1 M, 0.5 M, 1.0 M, 3.0 M and 5.0 M NaCl solutions with $2 \leq \text{pH}_m \leq 14.5$; 0.25 M, 1.0 M, 2.0 M, 3.0 M and 4.5 M MgCl₂ solutions with $2 \leq \text{pH}_m \leq 9$ and 0.25 M, 1.0 M, 2.0 M and 4.5 M CaCl₂ solutions with $7 \leq \text{pH}_m \leq 12$. The samples were regularly monitored for pH_m and [Tc] for up to 600 days. Equilibrium conditions were typically attained within 2-3 months in dilute systems, while strong kinetic processes are observed in some highly saline solutions. These cases are specifically depicted with arrows in the related figures. Preliminary studies undertaken in KIT-INE have shown the absence of colloidal formation under near-neutral pH conditions, and thus the assessment of this effect was not targeted within this PhD thesis. A representative selection of solid phases from equilibrated samples were characterised by XRD, SEM-EDS and quantitative chemical analysis. Redox distribution of Tc in the aqueous phase was again determined by the solvent extraction method. For the sample with highest [Tc] at $\text{pH}_m = 2$ in 4.5 M MgCl₂ system, XAFS analysis was performed at the INE Beamline for Actinide Research at ANKA. Chemical, thermodynamic and activity models were derived for the system $\text{Tc}^{4+}-\text{Na}^+-\text{Mg}^{2+}-\text{Ca}^{2+}-\text{H}^+-\text{Cl}^- - \text{OH}^- - \text{H}_2\text{O}$ using SIT and Pitzer approaches based on the newly generated solubility data. The solubility behaviour of Tc(IV) in dilute to concentrated NaCl, MgCl₂ and CaCl₂ solutions as well as thermodynamic data and model calculations are separately discussed in the following sections.

4.1 Solubility data of Tc(IV) in dilute to concentrated NaCl, MgCl₂ and CaCl₂ solutions

4.1.1 Solubility data of Tc(IV) in dilute to concentrated NaCl solutions

4.1.1.1 Acidic to weakly alkaline pH ($1.5 \leq \text{pH}_m \leq 9$)

Figure 4.1 shows the experimental solubility data obtained in the present work in dilute to concentrated NaCl systems in comparison with the solubility data reported in the literature (Meyer et al., 1991; Eriksen et al., 1992; Hess et al., 2004). Experimental data in 0.1 M NaCl agree well with previous solubility data in dilute systems reported by Meyer et al. (1991) [42]. The solubility of Tc(IV) at pH_m 1-4 increases up to 3 orders of magnitude with increasing ionic strength. This trend is qualitatively agreeing with previous experimental evidence reported by Hess et al. (2004) (see also Figure 4.1). Strong kinetics are observed for the sample at $\text{pH}_m \sim 2$ in 5.0 M NaCl, for which equilibrium is not attained even after 600 days of contact time. All investigated NaCl systems follow a well-defined slope of -2 (dashed lines in Figure 4.1) within the pH-range 1.5 to 4, which indicates that 2H^+ are consumed in the chemical reaction controlling the solubility of Tc(IV) in this pH range.

Solubility data in 0.1 M NaCl are also in good agreement with thermodynamic calculations performed for $I = 0$ using the NEA–TDB data selection [35]. With the same solid phase (TcO₂·1.6H₂O) expected to be controlling the solubility in this study, the monomeric aqueous species TcO²⁺ reported in NEA–TDB may be considered to prevail in the aqueous phase according to Eq (4.1) in the conditions of this study.



On the other hand, later spectroscopic studies in the acidic pH-range as well as experimental evidences gained in this work clearly hint towards the formation/predominance of polymeric species. A detailed discussion on this topic is provided in Section 4.3.

At $4 \leq \text{pH}_m \leq 9$, a pH-independent solubility behaviour is observed in dilute to concentrated NaCl solutions, indicating that no protons are exchanged in the chemical reaction controlling the solubility in this pH-region. Tc(IV) concentration is not affected by ionic strength, and thus data in 0.1 M and 5.0 M NaCl show similar solubility. The solubility data in this pH region scatter by 1-1.5 log-units. This behaviour is likely related with the very low solubility (close to detection limit) and the predominance of neutral species in solution, which are very prone to form polymeric species and strongly sorb on surfaces (filter, vessel walls, solid phases, etc.). A similar behaviour has been previously reported for An(III)/Ln(III) and An(IV) [38, 87]. Meyer and co-workers reported very similar observations, i.e. pH- and ionic strength independent behaviour and large scatter of the solubility data. Note that very stable Tc concentration measurements obtained at $6 \leq \text{pH} \leq 9$ in the study of Eriksen et al. (1992) [43] likely due to the detection limit of the method.

In the present work, the solubility of Tc(IV) has been found to agree well with thermodynamic calculations using the NEA–TDB. The experimental solubility limit is found to be slightly lower, most likely caused by slightly varying crystallinity effects on solid phases and/or the detection limit of different experimental measurements. According to the two studies mentioned above, NEA–TDB defines Eq (4.2) controlling the solubility in this pH region.



4.1.1.2 Alkaline pH ($\text{pH}_m \geq 9$)

Figure 4.2 shows the experimental solubility data obtained in alkaline pH range in dilute to concentrated NaCl systems compared with the solubility data reported in the literature (Eriksen et al., 1992; Warwick et al., 2007). The figure clearly shows that the solubility of Tc(IV) increases with a well-defined slope of +1 at $\text{pH}_m \geq 11$. With increasing ionic strength up to 5.0 M NaCl, the solubility decreases almost one order of magnitude but retains the same slope (dashed lines in Figure 4.2). The slope analysis is consistent with the reported solubility data by Eriksen et al. (1992) [43], which defines the formation of the TcO(OH)₃⁻ species in equilibrium with TcO₂·1.6H₂O(s). Assuming the solubility control by the same solid phase, the same aqueous species can be expected to exist in NaCl systems in the present study. Significantly lower Tc(IV) solubility is reported by Warwick et al. (2007) [24] for $12 \leq \text{pH} \leq 14$. This can be caused by differences in the

crystallinity of the solid phase controlling the solubility of Tc(IV). Unfortunately, the authors did not characterise the solid phase controlling the solubility and did not use constant ionic strength conditions in the solubility experiments.

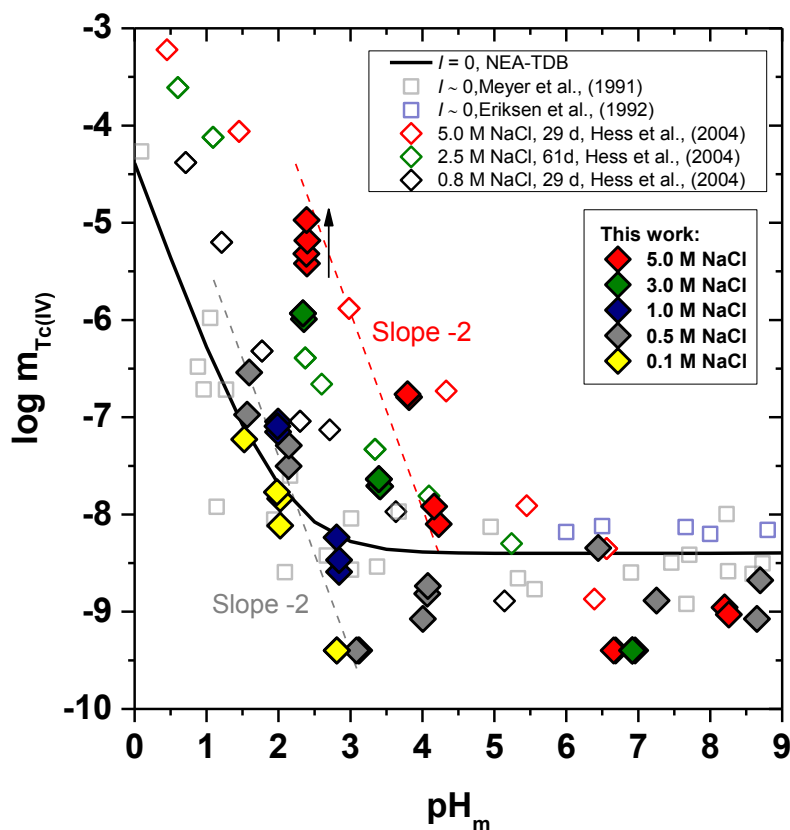


Figure 4.1 Experimental solubility data obtained in this work and reported in the literature under acidic to weakly alkaline pH conditions. Solid line corresponds to the overall solubility curve of $\text{TcO}_2 \cdot 1.6\text{H}_2\text{O}(\text{s})$ calculated with the NEA-TDB for $I = 0$.

Solubility data obtained in 0.1 M NaCl is slightly higher than predicted by thermodynamic calculations conducted for $I = 0$ using NEA-TDB data selection. The NEA-TDB review based its selection on a single solubility study focussing in this pH-region [43], although acknowledging that solubility might be underestimated due to experimental shortcoming of the method used by the authors to determine the Tc(IV) concentration.

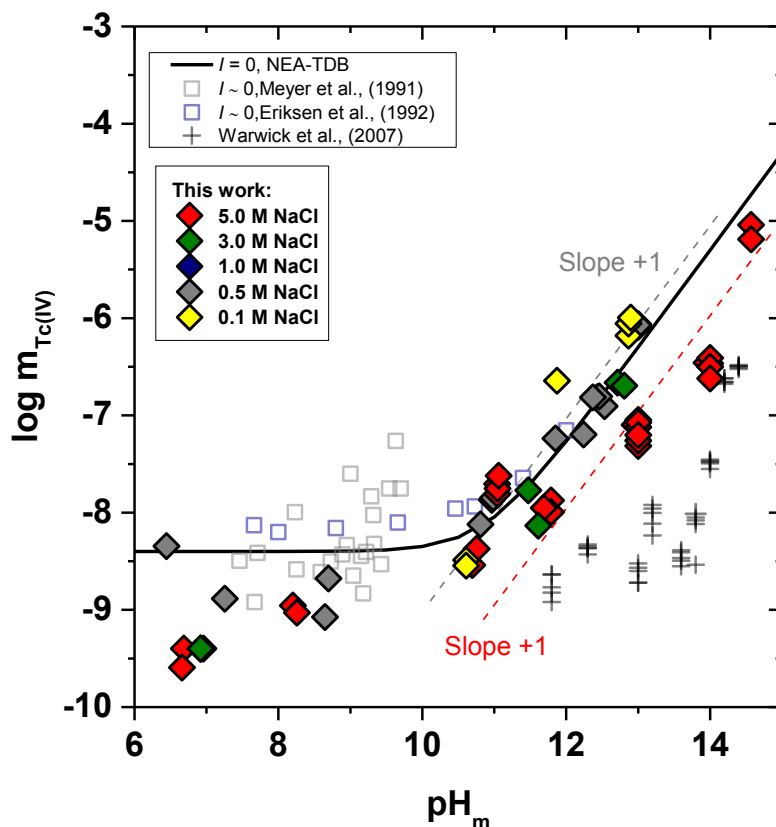


Figure 4.2 Experimental solubility data obtained in this work and reported in the literature under alkaline to hyperalkaline pH conditions. Solid line corresponds to overall solubility curve of $\text{TcO}_2 \cdot 1.6\text{H}_2\text{O}(\text{s})$ calculated with the NEA-TDB data for $I = 0$.

4.1.2 Solubility data of Tc(IV) in dilute to concentrated MgCl₂ solutions

Figure 4.3 shows the experimental solubility data obtained in the present work in dilute to concentrated MgCl₂ systems. Under acidic conditions, the solubility data in 0.25 M MgCl₂ is slightly higher than the solubility curve reported by NEA-TDB [35] probably because of the slight increase of ionic strength. The solubility of Tc(IV) is significantly increased (up to 5 orders of magnitude) with increasing ionic strength in acidic MgCl₂ media. This increase leads to nearly the same solubility as the data obtained in NaCl solutions with similar ionic strength. The solubility curve becomes pH-independent in 4.5 M MgCl₂ solutions with $\text{pH}_m \leq 2$ (dotted lines in Figure 4.3). A similar behaviour was observed by Hess et al. (2004) [88] at $\text{pH}_c \leq 0.1$ and $\text{pH}_c \leq 0.8$ for $I \sim 0$ and 5.0 M NaCl system, respectively. Hess and co-workers rationalized this behaviour considering a solid phase transformation from $\text{TcO}_2 \cdot x\text{H}_2\text{O}(\text{s})$ to $\text{TcCl}_4(\text{s})$ and assuming the predominance of $\text{TcCl}_4(\text{aq})$ in the aqueous phase. In the present work, the aqueous phase of these samples has been investigated with XAFS analysis and is discussed in Section 4.2. Slow kinetics are observed in the samples with $[\text{MgCl}_2] \geq 2 \text{ M}$, where equilibrium conditions (stable pH_m and $[\text{Tc}]$ readings) are only attained after 200 days of contact time. After attaining equilibrium conditions, it is seen that the solubility of all evaluated MgCl₂ systems follow a very well-defined slope of -2 within the pH-range 2 to 6 (depending upon salt concentration). This is in agreement with the solubility data obtained in the

present work in NaCl system and indicate that 2 H⁺ are consumed in the chemical reaction controlling the solubility in this pH region.

The solubility of Tc(IV) shows a pH-independent behaviour at $4 \leq \text{pH}_m \leq 9$ in 0.25 M MgCl₂ in analogy with NaCl systems. The pH-independent region shortens with increasing the ionic strength. The same hydrolysis species (TcO(OH)₂(aq)) is suggested in this pH region as in NaCl system (see Section 4.1.1).

In 4.5 M MgCl₂ systems, a steep increase of solubility can be observed at $\text{pH}_m \geq 8$. A similar increase in solubility under weakly alkaline conditions was previously reported for Zr(IV) and An(IV) in concentrated CaCl₂ solutions [39, 40, 63]. This increase in solubility was explained with the formation of ternary Ca-Zr(IV)/An(IV)-OH species based on spectroscopic evidence (EXAFS) and model calculations. Similar Mg-Tc(IV)-OH species are suspected to form for Tc(IV) in concentrated MgCl₂ solutions. For a better understanding of the solubility behaviour of Tc(IV) in this pH region, these experiments were extended up to $\text{pH}_m = 12$ in CaCl₂ system and are discussed in detail in the following section.

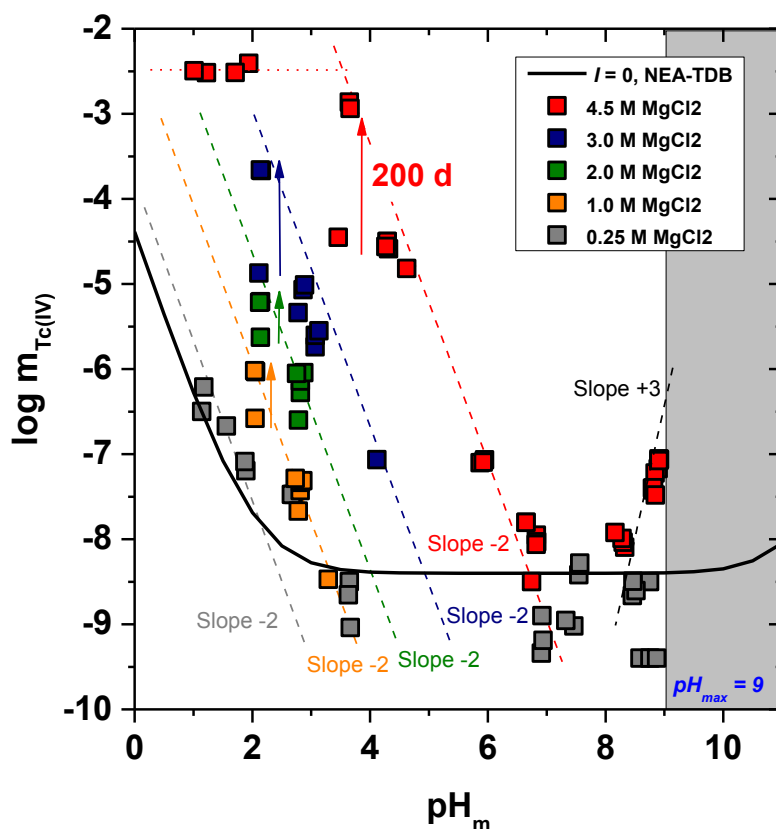


Figure 4.3 Experimental solubility data obtained in MgCl₂ system for $2 \leq \text{pH}_m \leq 9$. Solid line corresponds to the overall solubility curve of TcO₂·1.6H₂O(s) calculated with the NEA-TDB for $I = 0$.

4.1.3 Solubility data of Tc(IV) in dilute to concentrated CaCl₂ solutions

The experimental solubility data obtained in CaCl₂ systems with $7 \leq \text{pH}_m \leq 12$ are shown in Figure 4.4. The solubility of Tc(IV) in 0.25 M CaCl₂ shows a pH-independent behaviour up to $\text{pH}_m = 11$. For more concentrated CaCl₂ systems, the solubility shows an abrupt increase in solubility, which follows very slow kinetics. In 4.5 M CaCl₂, the solubility increase 3 orders of magnitude between $\text{pH}_m = 9.5$ and $\text{pH}_m = 10$ with a well-defined slope of +3 (dashed line in Figure 4.4). This system shows also very slow kinetics at $\text{pH}_m \geq 10.5$, where equilibrium conditions are not attained even after 500 days. Very similar behaviour was reported by Altmaier et al. [63] and Fellhauer et al. [39] for Zr(IV) and An(IV) in concentrated CaCl₂ systems. The authors explained this significant increase of solubility with the formation of ternary Ca-Zr(IV)/An(IV)-OH complexes with high number of hydroxide ligands. Note also that Fellhauer [89] observed very strong kinetics in the formation of ternary Ca-Np-OH species for pH values close to pH_{max} . The Ca-complexes which are spectroscopically and thermodynamically proven for Zr(IV) and An(IV), are evaluated for Tc(IV) in Section 4.3. The possibility of solid phase transformation occurring in this pH region is also discussed in Section 4.2.

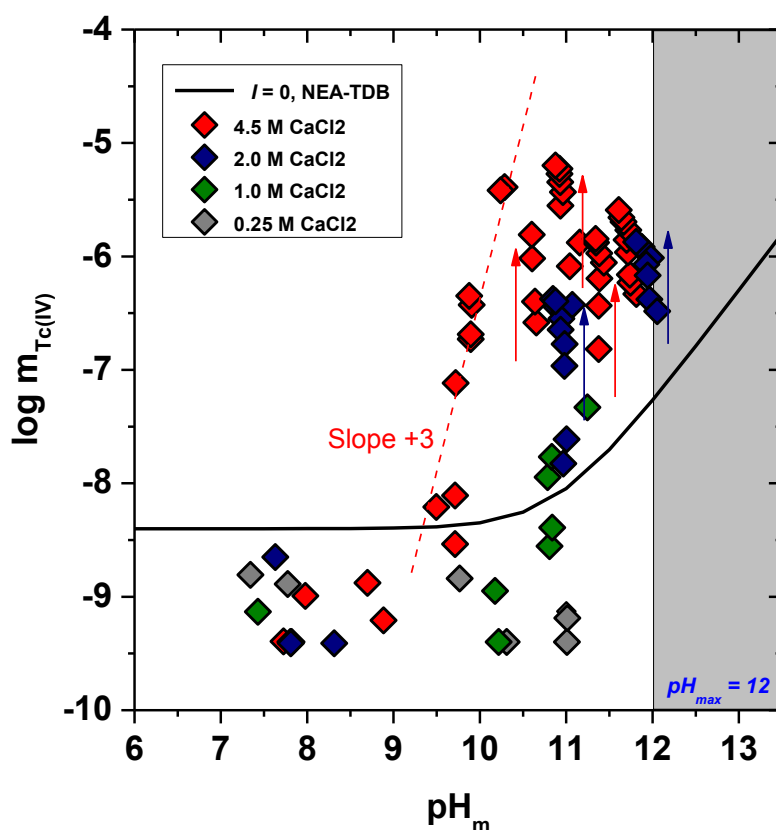


Figure 4.4 Experimental solubility data obtained in CaCl₂ system for $7 \leq \text{pH}_m \leq 12$. Solid line corresponds to the overall solubility curve of TcO₂·1.6H₂O(s) calculated with the NEA-TDB for $I = 0$.

4.2 Tc aqueous and solid phase characterisation

4.2.1 Tc aqueous phase characterisation

4.2.1.1 Tc redox speciation (solvent extraction)

Solvent extraction was performed for selected samples containing relatively high Tc concentration in solution ($\geq 10^{-6.5}$ M) in order to further assess a contribution of Tc(VII) to the solubility. Table 4.1 shows the results of redox distribution of Tc in NaCl and MgCl₂ solutions. In NaCl media, solvent extraction results confirm the predominance of Tc(IV). This observation is consistent with the predictions based on the measured pH and E_h values and the Tc *Pourbaix* diagrams reported in Chapter 3. In 4.5 M MgCl₂ media, the results show that 13% of total aqueous Tc is Tc(IV) at $\text{pH}_m = 2$. The presence of Tc(IV) increases towards alkaline pH region and becomes predominant (~ 94 %) at $\text{pH}_m = 9$. Similar solvent extraction results are reported for Tc(VII)/Tc(IV) redox experiments in Chapter 3. The redox state of Tc in the aqueous phase and the potential contribution of Cl⁻ in the complex formation are discussed in detail in the next section in connection with XANES/EXAFS measurements.

Table 4.1 Tc(IV) content in the aqueous phase of selected samples as quantified by solvent extraction. Reducing chemicals and measured pH_m and E_h for each sample also provided.

Background Eleytrolyte	Reducing system	pH_m^a	E_h^b (mV)	%Tc(IV) ^c
0.5 M NaCl	Na ₂ S ₂ O ₄	12.4	-670	99
5.0 M NaCl	Sn(II)	2.5	80	99
5.0 M NaCl	Na ₂ S ₂ O ₄	13.0	-540	98
5.0 M NaCl	Na ₂ S ₂ O ₄	14.0	-580	98
4.5 M MgCl ₂	Sn(II)	2.0	n.m.	13
4.5 M MgCl ₂	Sn(II)	4.0	-50	52
4.5 M MgCl ₂	Fe Powder	8.9	-170	91
4.5 M MgCl ₂	Sn(II)	9.0	-175	94

a: ± 0.05 ; **b:** ± 50 mV; **c:** $\pm 10\%$; **n.m.** = not measured

4.2.1.2 XANES/EXAFS

XANES and EXAFS data were collected at INE-Beamline for Actinide Research at ANKA and evaluated by Dr. Kathy Dardenne for the aqueous Tc containing phase of the solubility sample at $\text{pH}_m = 2$ in 4.5 M MgCl₂ in the presence of 1 mM SnCl₂ (see Figure 4.3). Tc(IV) content in this sample quantified by solvent extraction was 13% (see Table 4.1). The XANES spectrum of the sample is compared to both Tc(IV) and Tc(VII) reference in Figure 4.5. The shape and energy position of the inflection point of the XANES profile unequivocally confirms the clear predominance of Tc(IV) in this sample. This confirms that reducing conditions were successfully maintained in the solubility

experiment and indicates that solvent extraction data in concentrated MgCl₂ solutions is not correct. This observation also highlights the limitations of the solvent extraction method under highly saline conditions. The k^2 -weighted Tc K-edge EXAFS $\chi(k)$ together and the Fourier transform of the sample are shown in Figure 4.5 (middle) and Figure 4.5 (bottom), respectively. The structural parameters resulting from the EXAFS fit are shown in Table 4.2.

Table 4.2 Structural parameters obtained from the EXAFS evaluation of a Tc aqueous sample in 4.5 M MgCl₂ at pH_m = 2.

Sample	Path	CN [†]	R(Å)	$\sigma^2(\text{Å}^2)$	$\Delta E_0(\text{eV})$	%R [‡]
R-space [1.0–2.5Å]	Tc-O	4.5	2.20	0.002	-0.094	0.001
k -range [2.0–8.5 Å ⁻¹]	Tc-Cl	1.5	2.52	0.001		
	Tc-Tc	1.0	2.77	0.001		

[†]CN(Coordination number), [‡]R(Residual)

Fit errors: CN:± 20% ; R:0.01 Å, σ^2 : 0.001 Å²

Besides the O-shell at 2.20 Å, the fit of this sample unambiguously identifies the contribution of backscattering Cl-atoms at 2.52 Å. The substitution of Tc-Cl backscattering by oxygen significantly worsens the fit. On the other hand, the addition of Tc-Tc backscattering significantly improves the fit and thus has been retained in the final fitting model. This observation argues towards the formation of Tc(IV) oligomers/polymers as reported in previous spectroscopic studies [44].

In spite of the high [Tc] of the sample chosen for EXAFS analysis, the quality of the spectra collected is limited and only data for $k \leq 8.5 \text{ Å}^{-1}$ has been considered in the fit. Consequently, the information gained has been mostly considered from a qualitative perspective: i) confirms the oxidation state of +IV and falsifies the solvent extraction results pointing to the presence of Tc(VII), ii) indicates formation of the Cl-complexes in concentrated brine solutions under acidic conditions and iii) provides strong hints on the formation of Tc(IV) oligomers/polymers under acidic conditions, consistent with previously reported data [44].

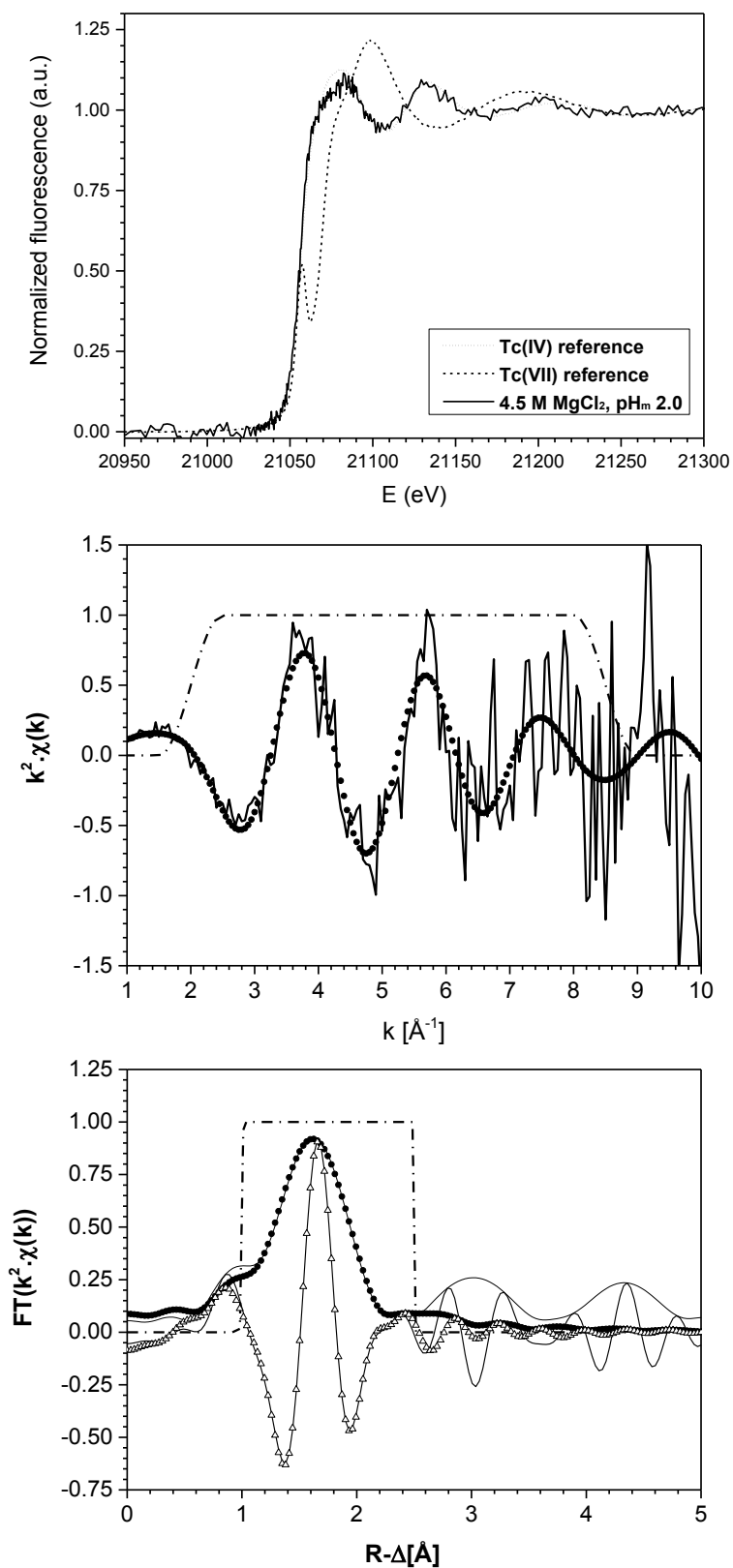


Figure 4.5 Tc K-edge XANES (top), k^2 -weighted EXAFS $\chi(k)$ (middle) and Fourier transform (bottom) of the sample at pH_m = 2 in 4.5 M MgCl₂ system solution. Data are depicted as solid lines, fits as circles and triangles. Dash dot lines correspond to the data window used for the fit.

4.2.2 Solid phase characterization (XRD, SEM–EDS and chemical analysis)

The solid phase of selected solubility samples was investigated by XRD, SEM–EDS and quantitative chemical analysis. The outcome of this characterization is summarized in Table 4.3, together with the experimental conditions of the investigated samples.

Table 4.3 Experimental conditions of investigated samples and XRD, SEM–EDS and chemical analysis results.

Background Electrolyte	Reducing system	pH _m ^a	XRD	SEM–EDS	Chemical analysis
				Na:Tc	Na:Tc
0.5 M NaCl	Na ₂ S ₂ O ₄	12.4	am	1.04	<0.01
5.0 M NaCl	Sn(II)	2.5	am	0.08	<0.01
5.0 M NaCl	Na ₂ S ₂ O ₄	13.0	n.m.	0.58	<0.01
5.0 M NaCl	Na ₂ S ₂ O ₄	14.0	am	0.08	<0.01
				Mg:Tc	Mg:Tc
0.25 M MgCl ₂	Sn(II)	2.0	am	0.0	< 0.01
4.5 M MgCl ₂	Sn(II)	4.0	am	2.3	< 0.01
4.5 M MgCl ₂	Fe Powder	8.9	n.m.	0.8	25.0 ^b
4.5 M MgCl ₂	Sn(II)	9.0	n.m.	0.0	0.3 ^b
				Ca:Tc	Ca:Tc
2.0 M CaCl ₂	Sn(II)	10.9	am, CaSn(OH) ₆	0.72	n.m.
2.0 M CaCl ₂	Na ₂ S ₂ O ₄	11.8	am	1.41	n.m.
4.5 M CaCl ₂	Sn(II)	10.9	am, (11.6)	1.09	2.7
4.5 M CaCl ₂	Na ₂ S ₂ O ₄	11.7	am	1.29	1.6
4.5 M CaCl ₂	Sn(II)	11.4	am, (11.6)	1.48	n.m.
4.5 M CaCl ₂	Sn(II)	10.7	am, (11.6)	1.62	n.m.

a: ± 0.05, **n.m.** = not measured

b: pH = pH_{max}, presence of Mg-OH-Cl(s) expected.

Figure 4.6 shows the XRD spectra of selected samples in NaCl and MgCl₂ systems. All spectra show broad patterns, reflecting the amorphous character of the solid phases controlling the solubility in these systems (Figure 4.6). Note that Tc(IV) oxide normally exists as a hydrated amorphous solid phase (TcO₂·xH₂O), which provides no marked reflections by powder XRD. The crystalline TcO₂(cr) has been reported to form by thermal decomposition of NH₄TcO₄ [90, 91] and is not expected in experiments conducted via precipitation at room temperature.

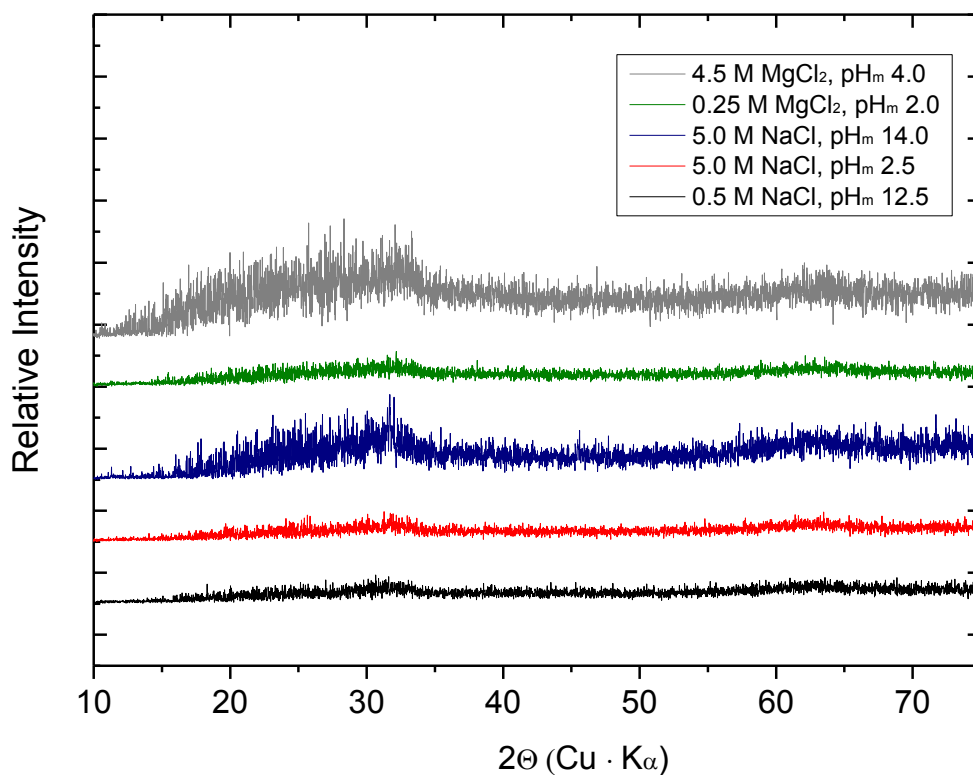
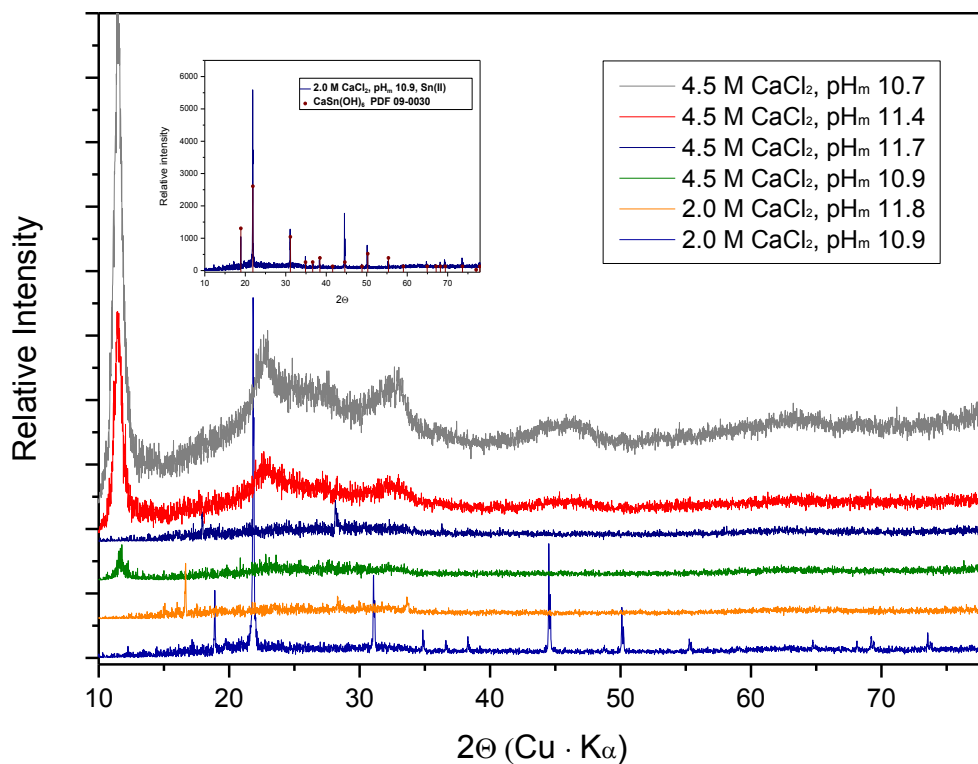
Figure 4.6 XRD spectra of solid phases of selected samples in NaCl and MgCl₂ systems.Figure 4.7 XRD spectra of solid phases of selected samples in CaCl₂ system.

Figure 4.7 shows the XRD patterns of selected samples in CaCl₂ system. Sharp features are observed in the sample at $\text{pH}_m = 10.9$ in 2.0 M CaCl₂ with Sn(II) as a reducing chemical. This pattern has unequivocally been identified as CaSn(OH)₆ (JCPDS–File 09 – 0030) [70]. This crystalline phase has been also identified in SEM images of the same sample (Figure 4.10, left), but it is not observed in any other sample analysed.

XRD patterns of the samples in 4.5 M CaCl₂ at $10.5 \leq \text{pH}_m < 11.7$ show the presence of an unknown broad peak at $2\Theta = 11.6$. This feature could not be assigned to any previously reported Tc compound, and may hint towards the transformation of TcO₂·xH₂O into a more stable Ca-Tc(IV)-OH phase. Provided the absence of thermodynamic equilibrium within the considered time frame, a more detailed investigation of this particular system has been disregarded within the context of this PhD thesis.

Figure 4.8 show some of the SEM images of the solid phases in NaCl system defined in Table 4.3. All investigated samples show amorphous Tc aggregates as main component, in good agreement with XRD observations. The particle size of these aggregates varies between 50 and 80 nm. An additional compound (spot A in Figure 4.8) is only observed in the SEM images of the samples with Na₂S₂O₄. The presence of S is also detected by EDS for these spots, thus hinting towards the precipitation of Na₂S₂O₄ or its degradation products on the surface of TcO₂·xH₂O(s). The Na:Tc ratios measured by SEM–EDS are listed in Table 4.3 as overall mean values of the atom percentages. Note that, in contrast to quantitative chemical analysis, a significant amount of Na is observed for samples in Na₂S₂O₄ in 0.5 M and 5.0 M NaCl and $\text{pH}_m = 12.4$ and 13.0, respectively. These results are considered to be biased by the presence of Na₂S₂O₄ on the surface of TcO₂·xH₂O(s), and therefore the Na:Tc ratio determined by quantitative chemical analysis which is not surface sensitive but reflects the entire bulk solid composition is considered more reliable for the definition of the solid phase controlling the solubility in this study. The quantitative chemical analysis clearly indicates the absence of Na in the bulk solid phase.

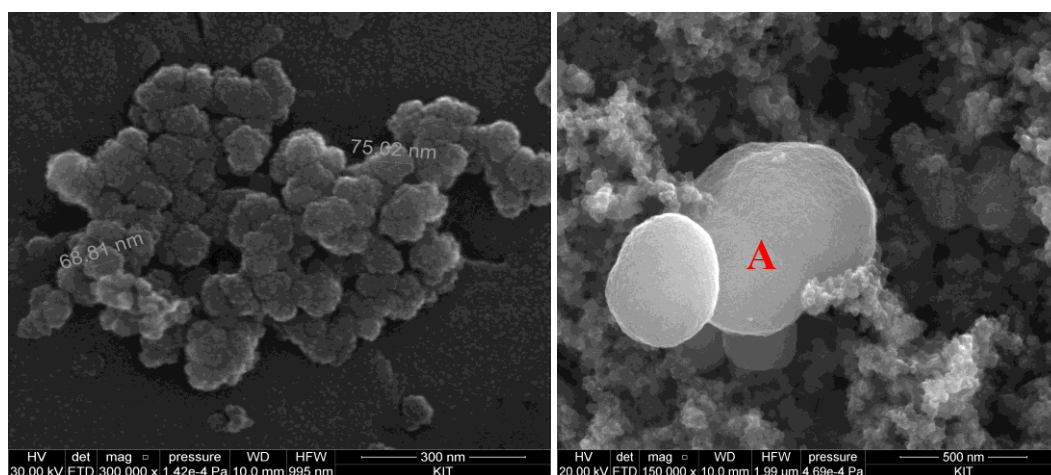


Figure 4.8 SEM images of the solubility samples at $\text{pH}_m = 12.4$ in 0.5 M NaCl (left) and at $\text{pH}_m = 14.0$ in 5.0 M NaCl (right).

Figure 4.9 shows selected SEM images of the solid phases in MgCl₂ system defined in Table 4.3. In all systems, SEM shows amorphous Tc aggregates as main component, in good agreement with the NaCl system and XRD observations. In alkaline systems with $\text{pH}_m \approx \text{pH}_{\text{max}}$, the presence of Mg-OH-Cl(s) phase can be observed (spot B in Figures 4.9, right) in good agreement with the high concentration of Mg determined by chemical analysis.

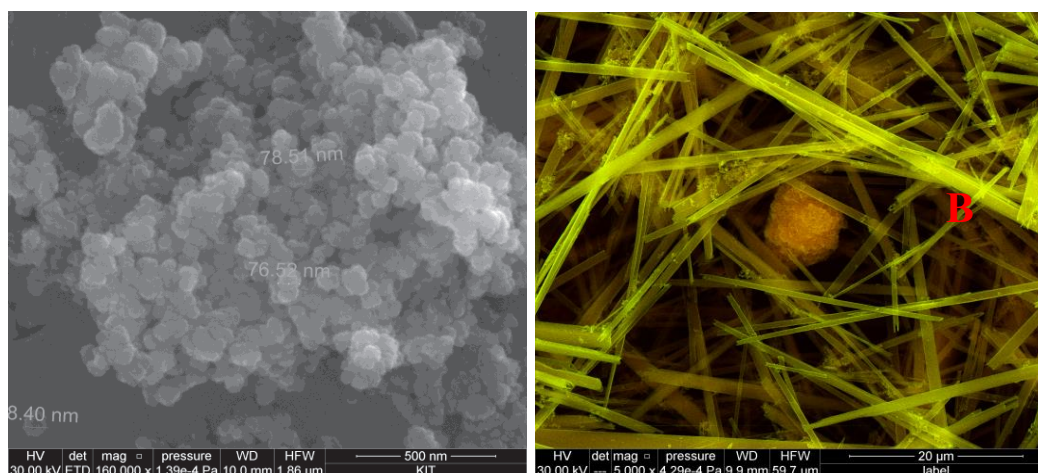


Figure 4.9 SEM images of the solubility samples at $\text{pH}_m = 4.0$ in 4.5 M MgCl₂ (left) and at $\text{pH}_m = 9.0$ in 4.5 M MgCl₂ (right). The right picture uses false colour to mark different solid phases.

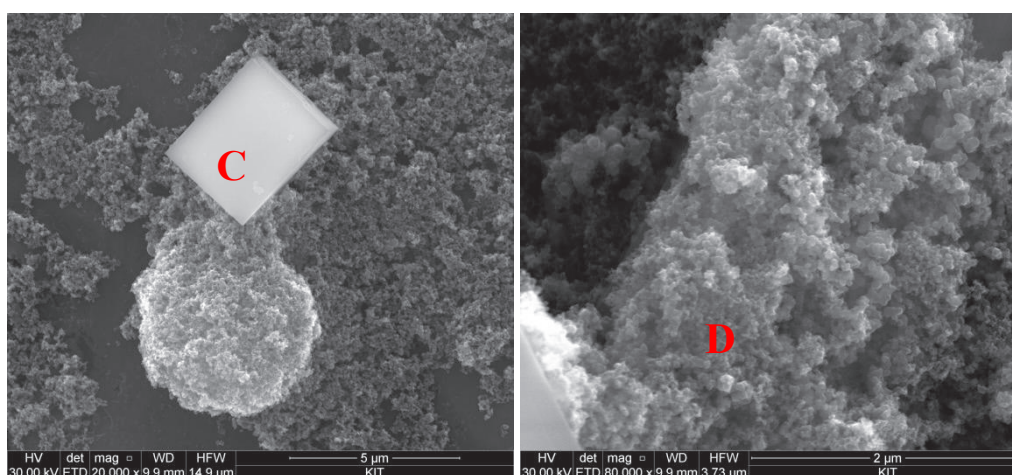


Figure 4.10 SEM images of the solubility samples at $\text{pH}_m = 10.9$ in 2.0 M CaCl₂ (left) and at $\text{pH}_m = 11.4$ in 4.5 M CaCl₂ (right).

The SEM images of the solid phases in CaCl₂ system defined in Table 4.3 are shown in Figure 4.10. A crystalline compound is seen (spot C) in the sample at $\text{pH}_m = 10.9$ in 2.0 M CaCl₂, in which the sharp XRD peaks are also observed. The atomic distribution of this crystalline phase indicates a Ca:Sn ratio of 1:1, confirming the identified species as CaSn(OH)₆ by XRD. Elemental analysis of the solubility samples at $10.5 \leq \text{pH}_m < 11.7$ in 4.5 M CaCl₂ solutions show the precipitation of CaCl₂ and corresponding Ca-hydroxychlorides as well as Sn and S compounds, which are coming from degradation/oxidation of reducing systems i.e. SnCl₂ and Na₂S₂O₄, respectively. Despite of that,

Ca:Tc \approx 1:1 is observed on the amorphous Tc-like phases (spot D in Figure 4.10) by subtracting all other elements. This observation may hint towards solid phase transformation to Ca-Tc(IV)-OH in that region.

Quantitative chemical analyses (Table 4.3) show the absence of Na in the Tc solid phases controlling the solubility in NaCl system, even for those phases equilibrated in 5.0 M NaCl solutions. Similarly, no Mg is detected in solid phases controlling the solubility under acidic conditions in 4.5 M MgCl₂, whereas very high Mg concentration are observed in alkaline samples where pH = pH_{max}. In these samples, precipitated Mg-hydroxochlorides are very clearly seen on SEM images (Figure 4.9, right). These observations clearly hint to the absence of Na and Mg as component of the Tc(IV) solid phase controlling the solubility in NaCl and MgCl₂ systems, respectively. In CaCl₂ system, most of the samples described in Table 4.3 were not measured by quantitative chemical analysis because of unforeseen technical problems resulting in a loss of the samples. The only two measured samples indicate the presence of a significant amount of Ca in the solid. Although precipitation of CaCl₂ and/or calcium hydroxochlorides is observed on SEM pictures, EDS analysis of amorphous Tc spots (D spot in Figure 4.10) gives a clear correlation between Ca and Tc (with Ca:Tc \approx 1:1) suggesting the possible formation of ternary Ca-Tc(IV)-OH solid phase.

All these results hint towards TcO₂·xH₂O(am) as solid phase controlling the solubility of Tc(IV) in all evaluated NaCl and MgCl₂ systems within the entire pH region and in CaCl₂ system up to pH_m = 10.5. Provided the very good agreement between experimental solubility data measured in this work in dilute systems and thermodynamic calculations using NEA–TDB selection, it can be postulated that the same number of hydration waters ($x = 1.6$ in TcO₂·xH₂O) applies also to the solid phase synthesized in this work. This reasonable hypothesis remains to be confirmed by thermogravimetric and differential thermal analysis (TG-DTA). The uncertainty associated with the number of hydration waters has a limited impact in NaCl systems, where the activity of water has a noticeable but relatively minor change from $I = 0$ (log $a_w = 0$) to 5.0 M (log $a_w = -0.11$).

Besides the solubility control imposed by TcO₂·1.6H₂O(s), the formation of a ternary Ca-Tc(IV)-OH phase is suspected in alkaline CaCl₂ systems with pH_m \geq 10.5. Longer equilibrium times as well as complementary characterisation of these samples, i.e. EXAFS analysis need to be provided for definitive conclusions on the formation of Ca-Tc(IV)-OH phase.

4.3 Tc(IV) chemical, thermodynamic and activity models

Experimental solubility data and speciation information described in Sections 4.1 and 4.2 are evaluated in terms of comprehensive chemical, thermodynamic and activity models using both SIT and Pitzer approaches. In a first step, the chemical, thermodynamic and activity models reported in two relevant publications (Neck and Fanghänel, (1999) [92]; Hess et al., 2004 [88]) were analysed if they can adequately explain the new experimental observations obtained in this work. As this was not the case, based upon the new solubility data, slope analysis and the solid and aqueous phase characterisation performed in the present work, an improved chemical model was developed in combination with NEA–TDB data selections and recent spectroscopic evidences reported in the literature. Based on this new chemical model, thermodynamic and activity models were subsequently

derived by fitting the available solubility data. The criteria considered for the selection of a final model have been the following:

- adequate explanation of the experimental solubility data generated in this work in dilute to concentrated NaCl, MgCl₂ and CaCl₂ solutions
- good agreement with available spectroscopic data
- consistency with NEA–TDB (whenever possible)
- coherence of the activity model: SIT and Pitzer ion interaction parameters are compared with data available in the literature, and evaluated with respect to expected trends according with charge extrapolations/analogies

4.3.1 Chemical and thermodynamic model reported in Neck and Fanghänel (1999)

Neck and Fanghänel assessed the solubility of Tc(IV) from acidic to alkaline pH conditions and estimated a thermodynamic and (Pitzer) activity model for the system Na⁺–K⁺–Mg²⁺–Ca²⁺–Cl[–]–SO₄^{2–}–H₂O (25°C) systems [92]. Neck and Fanghänel used the chemical model selected in NEA–TDB and did not consider any additional Tc(IV) species potentially forming in concentrated brine solutions (e.g Tc(IV)-Cl and Ca/Mg-Tc(IV)-OH species). The authors retained in most of the cases the same stability constants as in NEA–TDB. Pitzer ion interaction coefficients were estimated according to charge correlations and chemical analogies and not validated against independent experimental evidence. The stability constants and estimated activity coefficients by the authors are summarized in Table 4.4 and Table 4.5, respectively.

The model proposed by Neck and Fanghänel was used to calculate the solubility of Tc(IV) in 0.1 M, 0.5 M, 1.0 M, 3.0 M and 5.0 M NaCl solutions. The resulting curves are compared in Figure 4.11 with experimental solubility data generated in this work. Calculations for MgCl₂ and CaCl₂ systems (also reported by the authors) have not been considered in this exercise. Figure 4.11 shows that the trend predicted by the authors shares qualitative similarities with the experimental observations, i.e. increase of solubility in acidic pH region and decrease of solubility in alkaline pH region with increasing ionic strength. However, significant disagreement between the model calculations and experimental data can be observed, especially for concentrated brines, clearly hinting towards an inappropriate activity model. Consequently, thermodynamic and activity models estimated by Neck and Fanghänel have been disregarded in the present work.

Table 4.4 Chemical and thermodynamic model reported by Neck and Fanghänel (1999) for solubility and hydrolysis of Tc(IV).

<i>Reactions</i>	<i>log *K°</i>
TcO ₂ . 1.6H ₂ O(s)+2H ⁺ ⇌ TcO ²⁺ + 2H ₂ O(l)	-5.8 ± 1.0
TcO ₂ . 1.6H ₂ O(s)+ H ⁺ ⇌ TcO(OH) ⁺ + H ₂ O(l)	-5.9 ± 0.6*
TcO ₂ . 1.6H ₂ O(s) ⇌ TcO(OH) ₂ (aq) + 0.6 H ₂ O(l)	-8.4 ± 0.5*
TcO ₂ . 1.6H ₂ O(s) + 0.4 H ₂ O(l) ⇌ TcO(OH) ₃ ⁻ + H ⁺	-19.1 ± 0.5

*reported value in NEA–TDB.

4 Solubility and hydrolysis of Tc(IV) in dilute to concentrated NaCl, MgCl₂ and CaCl₂ solutions

Table 4.5 Pitzer binary and mixing parameters estimated by Neck and Fanghänel (1999) for Tc(IV) hydrolysis species.

<i>i</i>	<i>j</i>	Binary Parameters		
		$\beta^{(0)}$	$\beta^{(1)}$	$C^{(\phi)}$
TcO ²⁺	Cl ⁻	0.3	1.7	0
TcO(OH) ⁺	Cl ⁻	0.1	0.2	0
TcO(OH) ₃ ⁻	Na ⁺	0	0.1	0
	Mg ²⁺	0.3	1.7	0
	Ca ²⁺	0.3	1.7	0

<i>i</i>	<i>j, j'</i>	Mixing Parameters
TcO ²⁺	c, c' = Na ⁺ , Mg ²⁺ , Ca ²⁺ , K ⁺ a, a' = Cl ⁻ , SO ₄ ²⁻	$\theta_{cc'/aa'} = 0$
TcO(OH) ⁺		$\psi_{acc'/caa'} = 0$
TcO(OH) ₃ ⁻		
TcO(OH) ₂ (aq)	c = Na ⁺ , Mg ²⁺ , Ca ²⁺ , K ⁺ a = Cl ⁻ , SO ₄ ²⁻	$\lambda_{n/c} = 0$ $\lambda_{n/a} = -0.15$

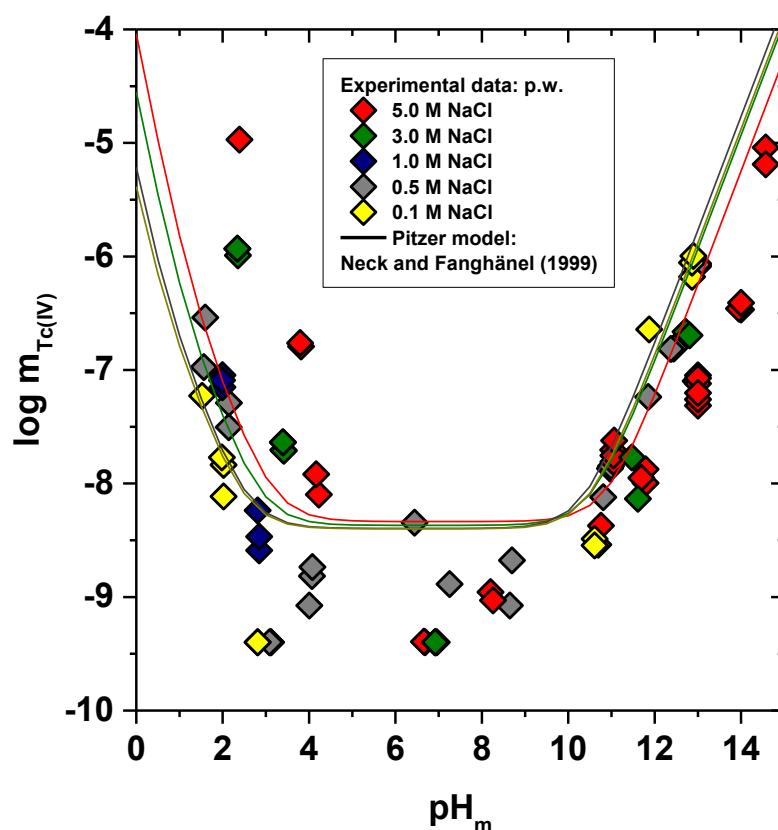


Figure 4.11 Comparison of experimental solubility data generated in this work in NaCl solutions with thermodynamic calculations conducted for the same boundary conditions using the model reported in Neck and Fanghänel (1999).

4.3.2 Use of chemical and thermodynamic models reported in Hess et al. (2004)

Hess and co-workers performed Tc(IV) solubility experiments in dilute to concentrated HCl and NaCl solutions from very acidic (up to 6.0 M HCl) to near-neutral pH conditions (see details in Section 1.2.3) [88]. The thermodynamic model was derived for the system Tc(IV)–Na⁺–Cl[–]–H⁺–OH[–]–H₂O considering solubility data in combination with solid and aqueous phase speciation/characterisation. Pitzer parameters were estimated using charge-based chemical analogies [93]. In addition to Tc(IV) hydrolysis species selected in NEA–TDB, the authors reported the formation of TcCl₄(aq) and TcCl₆^{2–} species at pH_c ≤ 1 and I ≥ 2.5 M. The transformation of TcO₂·1.6H₂O(s) to TcCl₄(s) was also proposed to take place in very acidic pH conditions. Thermodynamic and activity models reported by the authors are summarized in Table 4.6 and Table 4.7, respectively. In this study, the thermodynamic model for the solubility of Tc(IV) in acidic NaCl system is calculated by using the thermodynamic and activity model derived by Hess and co-workers.

Figure 4.12 shows the comparison of experimental solubility data generated in this work in NaCl systems with the corresponding thermodynamic calculations performed using the Pitzer model in Hess et al. The figure shows that the calculated solubility based upon the model of Hess et al. cannot adequately explain the experimental data points generated in the present work. Neither in dilute nor in concentrated NaCl systems does a satisfying agreement exist. This is mainly due to the predominance of TcO(OH)⁺ species defined by Hess et al. within 2 ≤ pH_c ≤ 5 (slope of –1 in the solubility curve) and the well-defined slope of –2 observed in the solubility data generated in this work. Note that Hess and co-workers defined the slope (log[Tc] vs. pH_m) of –1 in dilute systems (and thus the predominance of TcO(OH)⁺) after only 11 days of equilibration time. In the present work, the slope of –2 (shown with dashed line in figure 4.12) was obtained after 600 days of equilibration time.

Table 4.6 Chemical model and log^{*}K^o values reported by Hess et al. (2004) for the solubility and hydrolysis of Tc(IV).

<i>Reactions</i>	<i>log[*]K^o</i>
TcO ₂ ·1.6H ₂ O(s)+2H ⁺ ⇌ TcO ²⁺ + 2H ₂ O(l)	<4*
TcO ₂ ·1.6H ₂ O(s)+ H ⁺ ⇌ TcO(OH) ⁺ + H ₂ O(l)	–4 ± 0.3
TcO ₂ ·1.6H ₂ O(s) ⇌ TcO(OH) ₂ (aq) + 0.6 H ₂ O(l)	–8.4 ± 0.5*
TcCl ₄ (s) ⇌ TcCl ₄ (aq)	–3.7 ± 0.5

*reported value in NEA–TDB.

4 Solubility and hydrolysis of Tc(IV) in dilute to concentrated NaCl, MgCl₂ and CaCl₂ solutions

Table 4.7 Pitzer binary and mixing parameters estimated by Hess et al. (2004) for solubility of Tc(IV).

<i>i</i>	<i>j</i>	Binary Parameters		
		$\beta^{(0)}$	$\beta^{(1)}$	$C^{(\phi)}$
TcO ²⁺	Cl ⁻	0.3053	1.7090	0.002
TcO(OH) ⁺	Cl ⁻	-0.053	0.0396	0.008
TcCl ₆ ²⁻	H ⁺	0.0196	1.1130	0.00497
<i>i</i>	<i>j, j'</i>	Mixing Parameters		
TcO ²⁺	H ⁺	$\theta_{cc'/aa'} = 0.092$		
	H ⁺ - Cl ⁻	$\Psi_{acc'/caa'} = -0.015$		
TcO(OH) ⁺	H ⁺	$\theta_{cc'/aa'} = 0.036$		
	H ⁺ - Cl ⁻	$\Psi_{acc'/caa'} = -0.04$		
TcO(OH) ₂	NaCl	$\lambda_{n/c,a} = 0$		

Na⁺ - H₂PO₄⁻ used to estimate TcO(OH)⁺ - Cl⁻, Ca²⁺ - Cl⁻ used to estimate TcO²⁺ - Cl⁻, Na⁺ - H⁺ and Na⁺ - H⁺ - Cl⁻ used to estimate TcO(OH)⁺ - H⁺ and TcO(OH)⁺ - H⁺ - Cl⁻, Ca²⁺ - H⁺ and Ca²⁺ - H⁺ - Cl⁻ used to estimate TcO²⁺ - H⁺ and TcO²⁺ - H⁺ - Cl⁻.

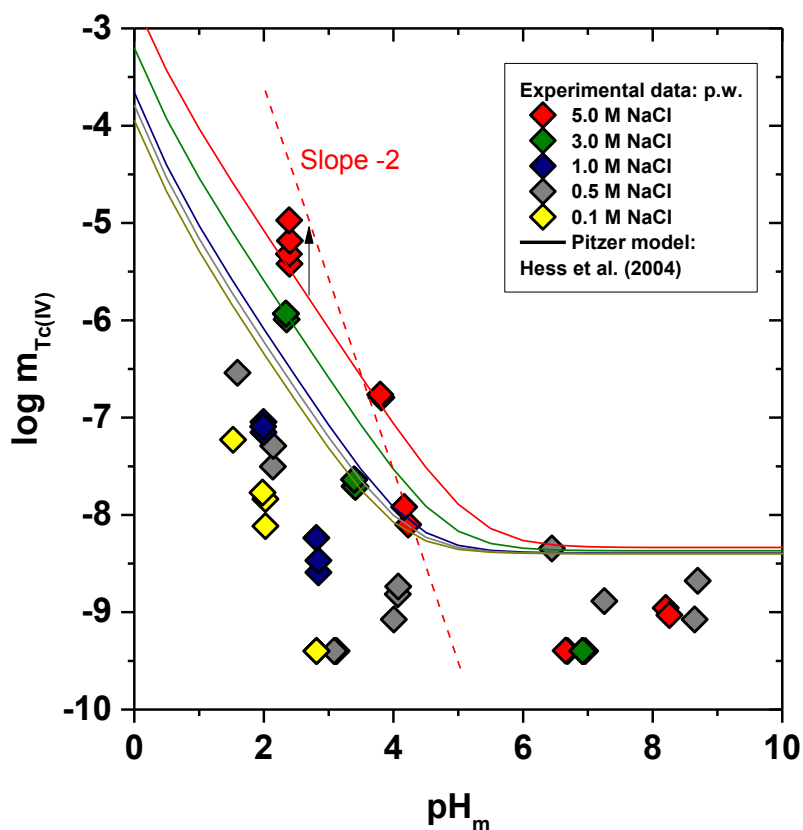


Figure 4.12 Comparison of experimental solubility data generated in this work in NaCl solutions with thermodynamic calculations conducted for the same boundary conditions using the model reported in Hess et al. (2004).

Figure 4.13 shows the time evolution of the solubility data obtained by Hess et al. in dilute system in comparison with the solubility determined in this work in 0.1 M NaCl. The figure clearly shows that the solubility behaviour of Tc(IV) after 11 days is significantly different than the solubility data at longer equilibration times. Tc concentration at $\text{pH}_c \geq 2$ decreases one order of magnitude up to 65 days, whereas it increases with very slow kinetics in highly acidic pH conditions. Similar behaviour is also observed in the present work. Furthermore, the slope of the solubility curve clearly changes from -1 to -2 within this timeframe. The former can be interpreted with the predominance of $\text{TcO}(\text{OH})^+$ (as considered by the authors in their thermodynamic model), whereas the use of the solubility data at longer equilibration times confirms the consumption of 2H^+ in the solubility reaction and thus the predominance of TcO^{2+} (or analogue oligomeric/polymeric species). Consequently, the chemical model proposed in Hess et al. has been disregarded in the present work.

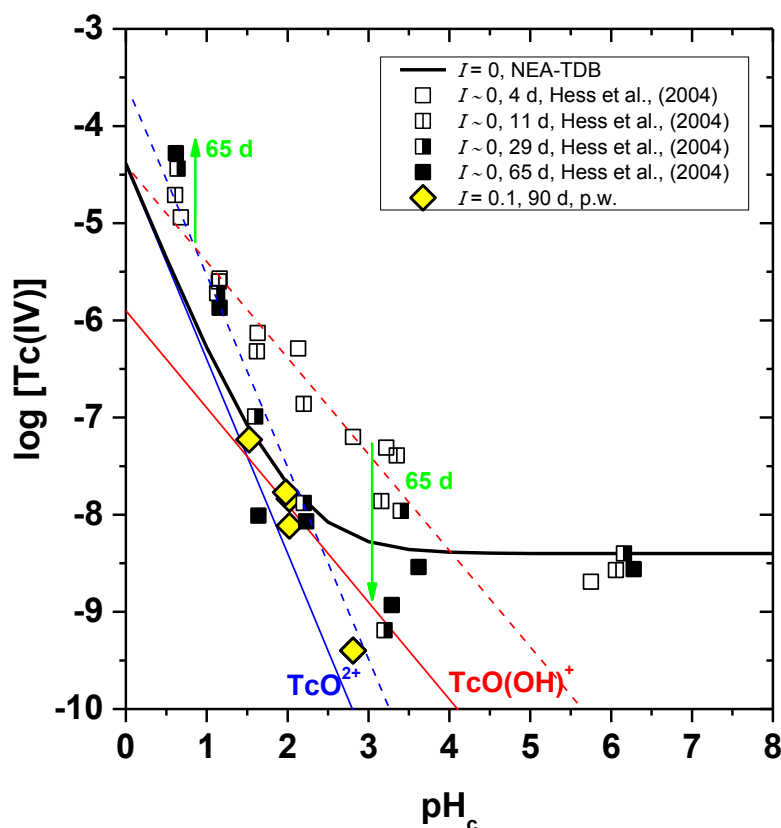


Figure 4.13 Experimental solubility data of Tc(IV) in 0.1 M NaCl (p.w.) and in a dilute system (absence of background electrolyte, Hess et al. (2004)). Solid lines correspond to overall solubility curve of $\text{TcO}_2 \cdot 1.6\text{H}_2\text{O}(\text{s})$ and underlying Tc(IV) aqueous speciation as calculated with the NEA-TDB for $I = 0$.

4.3.3 Improved chemical, thermodynamic and activity models derived in this work

Solubility calculations performed using the thermodynamic and activity models reported in the Neck and Fanghänel (1999) and Hess et al. (2004) cannot properly explain the experimental solubility data obtained in the present work in dilute to concentrated salt systems. No activity model is provided in the current NEA-TDB selection, and thus only calculations at $I \sim 0$ can be performed. Consequently,

this section aims at developing a comprehensive chemical, thermodynamic and activity model valid for the system $\text{Tc}^{4+}\text{-Na}^+\text{-Mg}^{2+}\text{-Ca}^{2+}\text{-H}^+\text{-Cl}^-\text{-OH}^-\text{-H}_2\text{O}$ at 25°C in dilute to concentrated brine systems. In the first step, a correct chemical model is defined based on slope analysis, solid phase characterization and spectroscopic evidence generated in this work and available from literature. In a consecutive step, new thermodynamic data and activity models were derived by fitting the solubility data using SIT or Pitzer approaches.

4.3.3.1 Acidic pH conditions ($\text{pH}_m \leq 4$)

The experimental data obtained in the present study show that the solubility of Tc(IV) increases with increasing ionic strength in the acidic pH region independent of the matrix salt system. The increase of the solubility is identical in NaCl and MgCl₂ solutions of similar ionic strength. The slope ($\log [\text{Tc}]$ vs. pH_m) of -2 is defined from solubility data in all investigated acidic systems at $0.1 \text{ M} \leq I \leq 13.5 \text{ M}$, indicating that 2 H^+ are consumed in the solubility reaction. No solid phase transformation is observed within this pH region by XRD, SEM-EDS and chemical analysis. The number of hydration water molecules (x in $\text{TcO}_2 \cdot x\text{H}_2\text{O}$) is considered 1.6 due to the very similar solubility behaviour of dilute NaCl and MgCl₂ systems under acidic conditions compared to thermodynamic calculations at $I=0$ using NEA-TDB. Aqueous phase characterisation by solvent extraction and XANES analysis confirm that no oxidation of Tc(IV) occurred during the studies. A pH-independent solubility behaviour is observed at $\text{pH}_m \leq 3.5$ in 4.5 M MgCl₂ system. EXAFS fit of the sample at $\text{pH}_m = 2$ in 4.5 M MgCl₂ system demonstrates the presence of Cl-atoms in the first coordination shell of Tc, thus confirming the formation of chlorocomplexes in these conditions. This observation agrees well with the data reported in Hess et al. (2004), who also observed a pH-independent solubility behaviour in very acidic pH region at $I \geq 2.5 \text{ M}$ and the presence of Tc(IV)-Cl species in solution as confirmed by UV-VIS. All these samples showing a pH-independent solubility behaviour at $\text{pH}_m \leq 2$ have been disregarded in this section for deriving chemical and thermodynamic model. Hence, the chemical model in the acidic pH region is derived based on the slope analysis and solid phase characterisation gained in the present study in combination with spectroscopic evidence reported in the literature.

NEA-TDB selected two cationic hydrolysis species forming in the acidic pH region, namely TcO^{2+} (prevailing at $\text{pH} \leq 1.5$) and $\text{TcO}(\text{OH})^+$ (prevailing at $1.5 \leq \text{pH} \leq 2.5$). Chemical reactions and corresponding equilibrium constants for the formation of these species are provided in Eq (4.3) and Eq (4.4), respectively.



The slope ($\log [\text{Tc}]$ vs. pH_m) of -2 estimated in the present work from solubility data is consistent with the formation of TcO^{2+} species. Note that the definition of the $\text{TcO}(\text{OH})^+$ species is not needed to properly explain the experimentally determined solubility data in this work, and thus has been disregarded in the chemical model proposed in this work.

A number of spectroscopic studies dedicated to Tc(IV) speciation under acidic conditions have been published after the release of the NEA–TDB update book on U, Np, Pu, Am and Tc [21, 44-47, 94]. These studies strongly hint towards the predominance of polynuclear Tc(IV) species of the type $Tc_nO_p^{(4n-2p)+}$ in the acidic pH-range, instead of the currently considered monomeric species TcO^{2+} and $TcOOH^+$. Vichot and co-workers investigated the aqueous speciation of Tc(IV) in Cl^- and SO_4^{2-} media at $pH = 1.5$ and $I \leq 3$ [44]. Based on the interpretation of EXAFS data, the authors suggested the formation of small-size polynuclear species independently of the composition of the considered solution. The participation of chloride in the first coordination sphere of Tc(IV) was disregarded by the authors on the basis of EXAFS data. Based on a latter study with focus on UV-VIS spectroscopy, the same authors proposed the formation of the trimer $Tc_3O_4^{4+}$ at $pH \leq 3$, which shows clear analogies with the cluster $Mo_3O_4 \cdot 9H_2O^{4+}$ known for Mo(IV) [45]. Poineau and co-workers also confirmed the formation and stability of polyatomic $Tc_nO_p^{(4n-2p)+}$ species up to $pH = 3$ [21, 46, 47]. Note further that trimeric species of Zr(IV) are also considered to play a relevant role in the solubility of Zr(IV) under acidic conditions [63].

Based on the spectroscopic evidence published on the formation and relevance of polyatomic Tc(IV) species under acidic conditions, the predominance of a trimeric species $Tc_3O_n^{(12-2n)}$ has been considered in the chemical model proposed in this work. The formation of such species must be consistent with the slope of -2 in the chemical reaction controlling the solubility at $pH_m \leq 4$, considering $TcO_2 \cdot 1.6H_2O$ as the solubility controlling solid phase. This leads to the chemical reaction in Eq (4.5).



which is defined by $\log {}^*K'_{s,Tc_3O_5^{2+}}$ and $\log {}^*K^o_{s,Tc_3O_5^{2+}}$ according to;

$$\log {}^*K'_{s,Tc_3O_5^{2+}} = 1/3 \log [Tc_3O_5^{2+}] - 2/3 \log [H^+] \quad (4.6)$$

$$\log {}^*K^o_{s,Tc_3O_5^{2+}} = \log {}^*K'_{s,Tc_3O_5^{2+}} + 1/3 \log \gamma_{Tc_3O_5^{2+}} - 2/3 \log \gamma_{H^+} + 1.93 \log a_w \quad (4.7)$$

Conditional stability constants for reaction (4.5) are experimentally determined from solubility data generated in this work in 0.1 M, 0.5 M, 1.0 M, 3.0 M and 5.0 M NaCl and 0.25 M, 1.0 M, 2.0 M, 3.0 M and 4.5 M MgCl₂ solutions. The $\log {}^*K^o_{s,Tc_3O_5^{2+}}$ value is determined by extrapolating the calculated conditional $\log {}^*K'_{s,Tc_3O_5^{2+}}$ to $I = 0$ according to Eq (4.7) by using the SIT or Pitzer formalism. This approach leads also to the determination of SIT and Pitzer ion interaction coefficients for $Tc_3O_5^{2+}$.

SIT approach

Eq (4.8) shows the linearization of Eq. (4.7) according to the SIT formalism.

$$\begin{aligned} \log {}^*K'_{s,Tc_3O_5^{2+}} - 2/3 D + 1.93 \log a_w = \log {}^*K^o_{s,Tc_3O_5^{2+}} \\ - [1/3\epsilon(Tc_3O_5^{2+}, Cl^-) - 2/3\epsilon(H^+, Cl^-)] \cdot m_{Cl^-} \end{aligned} \quad (4.8)$$

SIT-plots ($\log {}^*K'_{s,\text{Tc}_3\text{O}_5^{2+}} - 2/3 D + 1.93 \log a_w$ vs. m_{salt}) based on Eq (4.8) are shown in Figure 4.14 and Figure 4.15 for both NaCl and MgCl₂ systems, respectively. The activity of water for each ionic strength was taken from NEA–TDB.

The intercept and the slope obtained by linear SIT regression in Figure 4.14 represent $\log {}^*K_{s,\text{Tc}_3\text{O}_5^{2+}}^o$ and $-\Delta\varepsilon = 1/3 \varepsilon(\text{Tc}_3\text{O}_5^{2+}, \text{Cl}^-) - 2/3 \varepsilon(\text{H}^+, \text{Cl}^-)$ in NaCl media. The value of $\log {}^*K_{s,\text{Tc}_3\text{O}_5^{2+}}^o$ is found as -1.56 ± 0.10 . The slope of the linear SIT regression is $0.20 \pm 0.01 \text{ kg}\cdot\text{mol}^{-1}$, which results in $\varepsilon(\text{Tc}_3\text{O}_5^{2+}, \text{Cl}^-) = -0.36 \pm 0.03 \text{ kg}\cdot\text{mol}^{-1}$ considering $\varepsilon(\text{H}^+, \text{Cl}^-) = 0.12 \pm 0.01 \text{ kg}\cdot\text{mol}^{-1}$ as reported in NEA–TDB. The same calculations are performed for the MgCl₂ system based on Figure 4.15, resulting in $\log {}^*K_{s,\text{Tc}_3\text{O}_5^{2+}}^o = -1.47 \pm 0.30$ and $\varepsilon(\text{Tc}_3\text{O}_5^{2+}, \text{Cl}^-) = -0.30 \pm 0.07$. Stability constants and ion interaction coefficients determined in NaCl and MgCl₂ systems agree well with each other. Larger uncertainties are observed in MgCl₂ systems, probably because of the known limitations of SIT at very high ionic strengths. The final selection considered in this work relies on the weighted average of the values obtained in NaCl and MgCl₂, respectively:

$$\log {}^*K_{s,\text{Tc}_3\text{O}_5^{2+}}^o = -1.53 \pm 0.16 \qquad \varepsilon(\text{Tc}_3\text{O}_5^{2+}, \text{Cl}^-) = -0.34 \pm 0.10$$

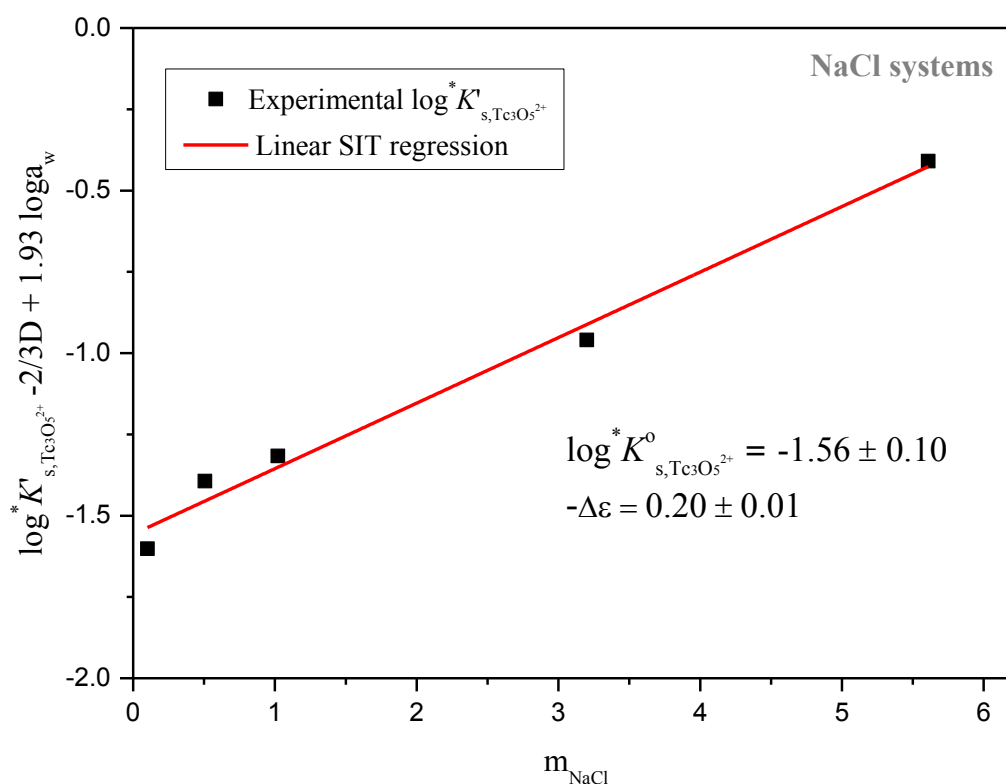


Figure 4.14 SIT-plot for the solubility reaction $\text{TcO}_2 \cdot 1.6\text{H}_2\text{O}(\text{s}) + 2/3\text{H}^+ \rightleftharpoons 1/3\text{Tc}_3\text{O}_5^{2+} + 1.93\text{H}_2\text{O}$ considering experimental $\log {}^*K'_{s,\text{Tc}_3\text{O}_5^{2+}}$ determined in NaCl media.

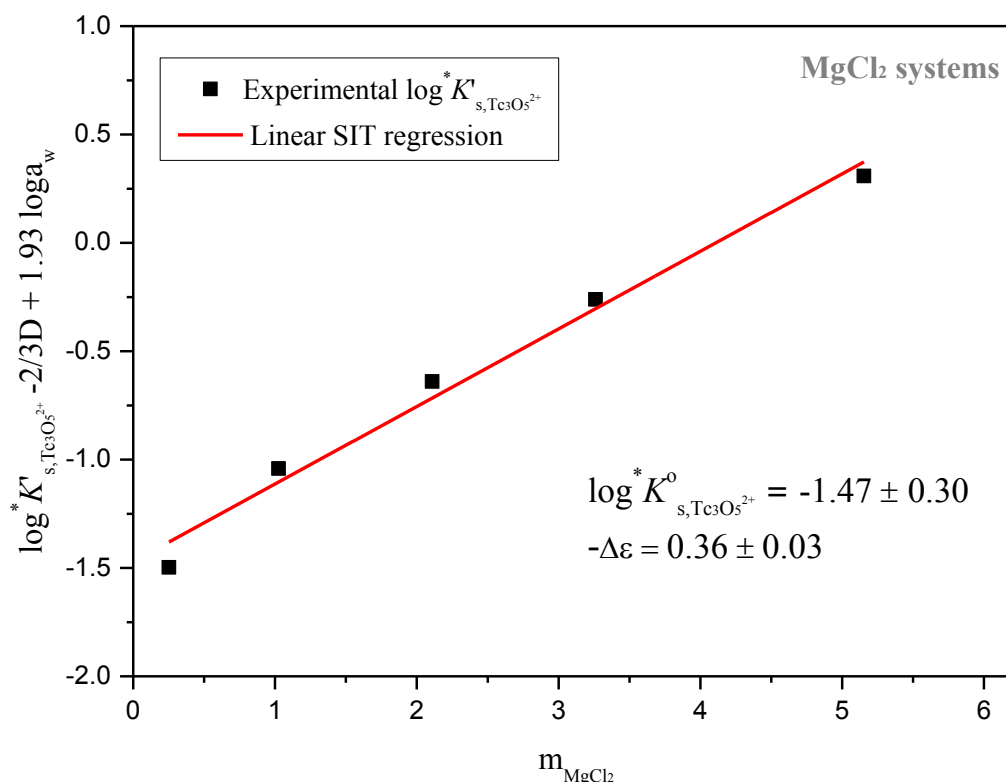


Figure 4.15 SIT-plot for the solubility reaction $\text{TcO}_2 \cdot 1.6\text{H}_2\text{O}(\text{s}) + 2/3\text{H}^+ \rightleftharpoons 1/3\text{Tc}_3\text{O}_5^{2+} + 1.93\text{H}_2\text{O}$ considering experimental $\log^* K'_{s, \text{Tc}_3\text{O}_5^{2+}}$ determined in MgCl_2 media.

The SIT ion interaction parameter determined for $\text{Tc}_3\text{O}_5^{2+}$ is much lower than the expectations for a typical divalent cation, $\varepsilon(\text{M}^{2+}, \text{Cl}^-) = 0.15 \pm 0.10 \text{ kg} \cdot \text{mol}^{-1}$ based on charge correlations [53]. However, the use of charge analogies for very large or oligomeric species must be considered with precaution. The effect of size and the distribution of the formal charge throughout the voluminous species can lead to large deviations with respect to monomeric/simple species. Note that Fellhauer [89] recently reported similar SIT ion interaction coefficient for the monomeric but very large divalent cationic species $\text{Ca}_3[\text{NpO}_2(\text{OH})_5]^{2+}$, $\varepsilon(\text{Ca}_3[\text{NpO}_2(\text{OH})_5]^{2+}, \text{Cl}^-) = -0.20$.

Pitzer approach

Conditional solubility constants determined in NaCl and MgCl_2 systems were fitted according to Eq (4.7) and considering Pitzer formalism. The values of $\log \gamma_{\text{H}^+}$ and a_w in equation (4.7) are calculated from the parameters reported by Harvie et al. [79]. The binary parameter $C^{(0)}$ and the mixing parameters $\theta(\text{Tc}_3\text{O}_5^{2+}, \text{Na}^+)$ and $\Psi(\text{Tc}_3\text{O}_5^{2+}, \text{Cl}^-, \text{Na}^+)$ are set to zero. $\log^* K_{s, \text{Tc}_3\text{O}_5^{2+}}^0$, $\beta^{(0)}$ and $\beta^{(1)}$ were fitted simultaneously for NaCl and MgCl_2 systems by minimizing the difference between experimental and modelled $\log^* K'_{s, \text{Tc}_3\text{O}_5^{2+}}$ in both systems. The resulting values are:

$$\log^* K_{s, \text{Tc}_3\text{O}_5^{2+}}^0 = -1.56 \pm 0.10 \quad \beta^{(0)} = -0.20 \text{ kg} \cdot \text{mol}^{-1} \quad \beta^{(1)} = 1.30 \text{ kg} \cdot \text{mol}^{-1}$$

Figure 4.16 shows experimental and calculated $\log^* K'_{s, \text{Tc}_3\text{O}_5^{2+}}$ for NaCl and MgCl_2 systems. The figure shows that both SIT and Pitzer model derived in this work reproduce very well the experiment-

tally determined $\log {}^*K'_{s,\text{Tc}_3\text{O}_5^{2+}}$ values. Note that the calculations of $\log {}^*K'_{s,\text{Tc}_3\text{O}_5^{2+}}$ with the SIT model were obtained by using the weighted average of $\log {}^*K^o_{s,\text{Tc}_3\text{O}_5^{2+}}$ and $\epsilon(\text{Tc}_3\text{O}_5^{2+}, \text{Cl}^-)$ obtained in NaCl and MgCl₂ systems.

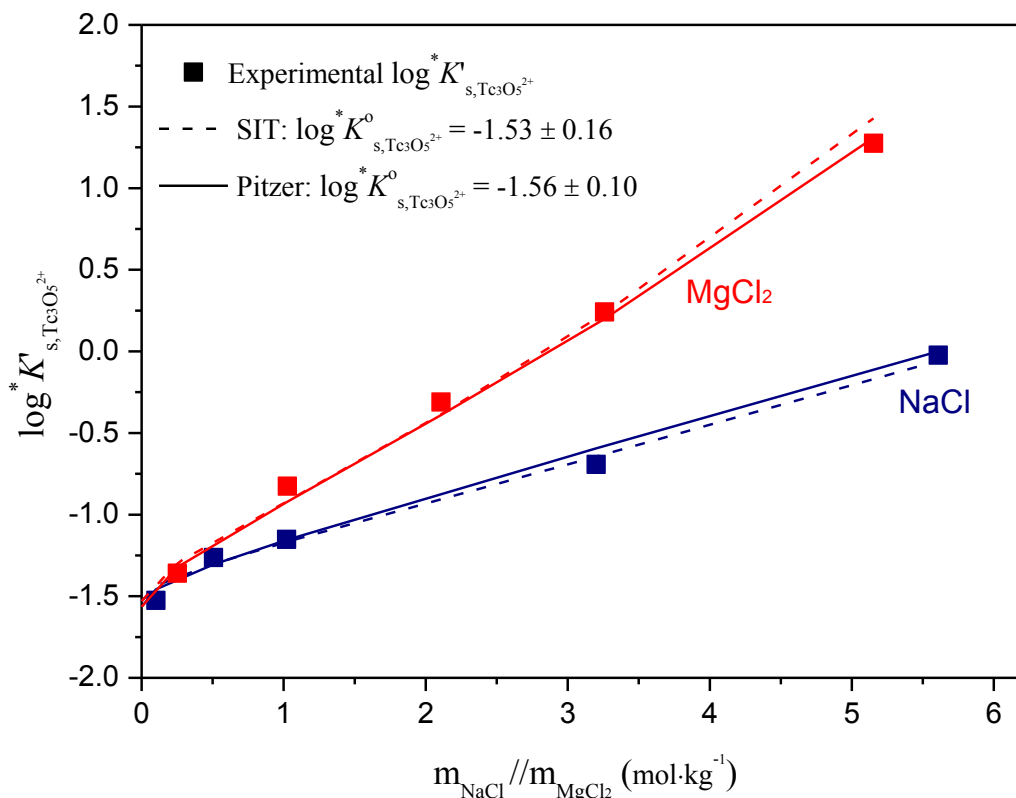
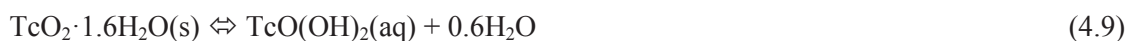


Figure 4.16 Conditional equilibrium constants $\log {}^*K'_{s,\text{Tc}_3\text{O}_5^{2+}}$ as a function of the NaCl and MgCl₂ molality; experimental values (symbols) and calculated functions based on the SIT (dashed line) and Pitzer models (solid line).

4.3.3.2 Weakly acidic to weakly alkaline pH conditions ($4 \leq \text{pH}_m \leq 8 / 10$)

The solubility of Tc(IV) follows a pH-independent behaviour within $4 \leq \text{pH}_m \leq 10$ and $4 \leq \text{pH}_m \leq 8$ for NaCl and MgCl₂/CaCl₂ systems, respectively. No ionic strength dependence is observed for the solubility data within this pH region, agreeing well with known tendencies for neutral species. Consistent with the NEA-TDB selection, the chemical reaction controlling the solubility of Tc(IV) within this pH region can be defined as:



which can be described according with the following equations;

$$\log {}^*K'_{s,\text{TcO}(\text{OH})_2} = \log [\text{TcO}(\text{OH})_2] \quad (4.10)$$

$$\log {}^*K^o_{s,\text{TcO}(\text{OH})_2} = \log {}^*K'_{s,\text{TcO}(\text{OH})_2} + \log \gamma_{\text{TcO}(\text{OH})_2} + 0.6 \log a_{\text{H}_2\text{O}} \quad (4.11)$$

SIT and Pitzer ion interaction coefficients for TcO(OH)₂(aq) have been considered zero in the present work and consequently $\log \gamma_{\text{TcO(OH)}_2}$ equals zero. $\log {}^*K_{\text{s,TcO(OH)}_2}^o$ can be calculated as the average Tc concentration at $4 \leq \text{pH}_m \leq 10$ with a small contribution of activity of water. In this study, $\log {}^*K_{\text{s,TcO(OH)}_2}^o = -8.8 \pm 0.5$ is determined for the chemical equilibrium in Eq (4.9), agreeing well with the current NEA–TDB selection of $\log {}^*K_{\text{s,TcO(OH)}_2}^o = -8.4 \pm 0.5$.

On the other hand, this model leads to questioning the fate of polymeric hydrolysis species which have been proven to exist in acidic pH region by spectroscopic means (see Section 4.2.1.2). Following this trend, zero-charged polymeric hydrolysis species could be also expected under near-neutral pH conditions. Sundrehagen (1979) evaluated the formation of Tc(IV) polymeric species as a function of Tc concentration and pH. The author reported that the formation of polymeric Tc(IV) can be avoided at $[\text{Tc}] \leq 10^{-6.8}$ [95]. The formation of oligomeric neutral hydrolysis species has been previously reported for Zr(IV) [96]. The formation of these species is only relevant at $[\text{Zr}] \geq 10^{-6}$ M, whereas monomeric species prevail at lower metal concentrations. Extrapolating this behaviour to Tc(IV), it can be postulated that $[\text{Tc}] \geq 10^{-8.8}$ M is insufficient to stabilize an oligomeric structure. TcO(OH)₂(aq) selected in the NEA–TDB has therefore been retained in this work, although admittedly a definitive proof of concept is still missing.

4.3.3.3 Alkaline pH conditions (pH_m ≥ 10) in NaCl system

As discussed in Section 4.1.2, a clear slope of +1 is defined by the solubility data in this pH region from dilute to concentrated NaCl systems. This observation is consistent with the chemical model selected in the NEA–TDB;



which can be described with the following equations;

$$\log {}^*K'_{\text{s,TcO}(\text{OH})_3^-} = \log[\text{TcO}(\text{OH})_3^-] + \log[\text{H}^+] \quad (4.13)$$

$$\log {}^*K_{\text{s,TcO}(\text{OH})_3^-}^o = \log {}^*K'_{\text{s,TcO}(\text{OH})_3^-} + \log \gamma_{\text{s,TcO}(\text{OH})_3^-} + \log \gamma_{\text{H}^+} - 0.4 \log a_{\text{H}_2\text{O}} \quad (4.14)$$

The conditional equilibrium constants are experimentally determined with the solubility data in 0.1 M, 0.5 M, 3.0 M and 5.0 M NaCl according to Eq (4.13). Eq (4.14) can be applied using either SIT or Pitzer approaches to derive $\log {}^*K_{\text{s,TcO}(\text{OH})_3^-}^o$ and corresponding ion interaction parameters.

SIT approach

Eq (4.15) shows the linearization of Eq. (4.14) according to SIT formalism.

$$\begin{aligned} \log {}^*K'_{\text{s,TcO}(\text{OH})_3^-} - 2D - 0.4 \log a_w = \log {}^*K_{\text{s,TcO}(\text{OH})_3^-}^o \\ + [\varepsilon(\text{TcO}(\text{OH})_3^-, \text{Na}^+) + \varepsilon(\text{H}^+, \text{Cl}^-)] \cdot m_{\text{NaCl}} \end{aligned} \quad (4.15)$$

Figure 4.17 shows the SIT regression obtained according to Eq (4.15). The intercept is determined as -19.27 ± 0.10 and corresponds to $\log {}^*K_{s,\text{TcO}(\text{OH})_3^-}^o$. This value is in excellent agreement with the value currently selected in the NEA–TDB, $\log {}^*K_{s,\text{TcO}(\text{OH})_3^-}^o = -19.3 \pm 0.9$ but permits to significantly decrease the associated uncertainty. The ion interaction coefficient $\varepsilon(\text{TcO}(\text{OH})_3^-, \text{Na}^+)$ is calculated as $0.10 \pm 0.02 \text{ kg}\cdot\text{mol}^{-1}$ from the slope of the linear regression ($-\Delta\varepsilon = \varepsilon(\text{TcO}(\text{OH})_3^-, \text{Na}^+) + \varepsilon(\text{H}^+, \text{Cl}^-)$). This value is in line with the SIT ion interaction coefficient expected for a typical monovalent anion $\varepsilon(\text{M}^-, \text{Na}^+) = -0.05 \pm 0.10 \text{ kg}\cdot\text{mol}^{-1}$.

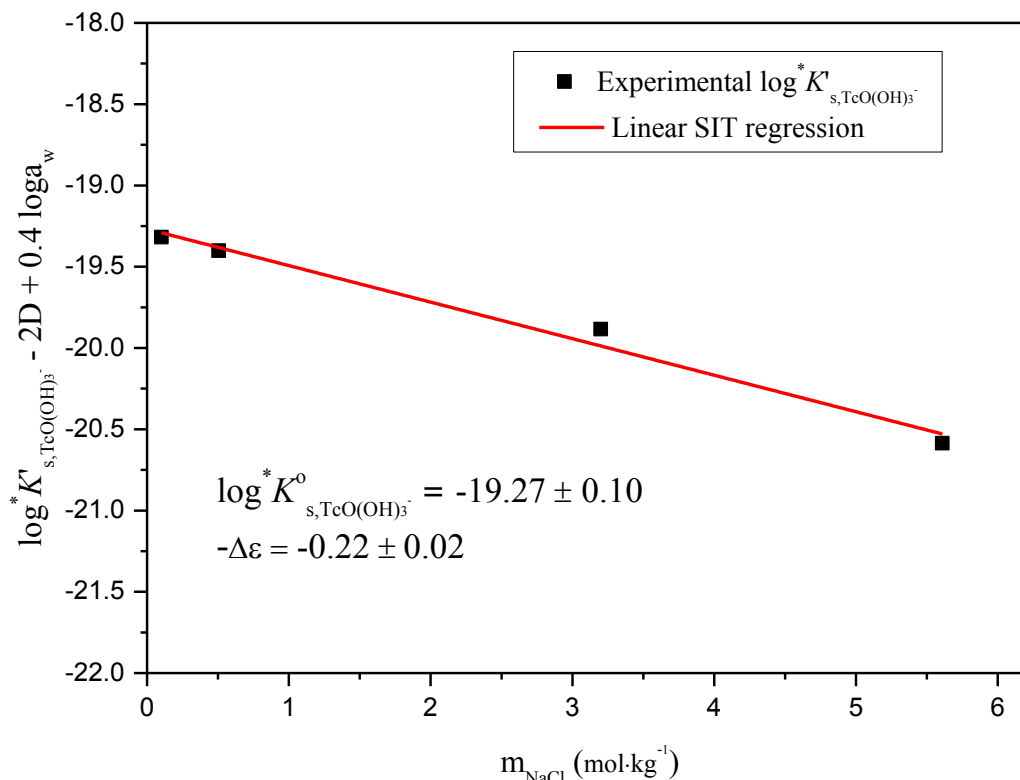


Figure 4.17 SIT-plot for the solubility reaction $\text{TcO}_2 \cdot 1.6\text{H}_2\text{O}(\text{s}) + 0.4 \text{H}_2\text{O} \Leftrightarrow \text{TcO}(\text{OH})_3^- + \text{H}^+$ considering experimental $\log {}^*K'_{s,\text{TcO}(\text{OH})_3^-}$ determined in this work.

Pitzer approach

Conditional solubility constants determined in alkaline NaCl systems were fitted according to Eq (4.14) considering the Pitzer formalism. The values of $\log \gamma_{\text{H}^+}$ and a_w in equation (4.14) are calculated from the parameters reported by Harvie et al. [79]. The mixing parameters $\theta(\text{TcO}(\text{OH})_3^-, \text{Cl}^-)$ and $\Psi(\text{TcO}(\text{OH})_3^-, \text{Cl}^-, \text{Na}^+)$ are set to zero. $\log {}^*K_{s,\text{TcO}(\text{OH})_3^-}^o$, $\beta^{(0)}$ and $\beta^{(1)}$ and $C^{(\Phi)}$ were fitted for 0.1 M, 0.5 M, 3.0 M and 5.0 M NaCl systems by minimizing the difference between experimental and modelled $\log {}^*K'_{s,\text{TcO}(\text{OH})_3^-}$. The resulting values are:

$$\log {}^*K_{s,\text{TcO}(\text{OH})_3^-}^o = -19.32 \pm 0.10 \quad \beta^{(0)} = 0.006 \text{ kg}\cdot\text{mol}^{-1}$$

$$\beta^{(1)} = 0.30 \text{ kg}\cdot\text{mol}^{-1} \quad C^{(\Phi)} = 0.04 \text{ kg}^2\cdot\text{mol}^{-2}$$

The ionic strength dependence of $\log^* K'_{s, \text{TcO}(\text{OH})_3^-}$ plotted in Figure 4.18 show that both SIT and Pitzer models can explain the experimentally determined $\log^* K'_{s, \text{TcO}(\text{OH})_3^-}$ values. However, although in this particular case SIT and Pitzer approaches result in more or less the same data, it should be kept in mind that the Pitzer model is more accurate than SIT approach at high ionic strength conditions and should definitely be favoured in related modelling exercises under saline conditions.

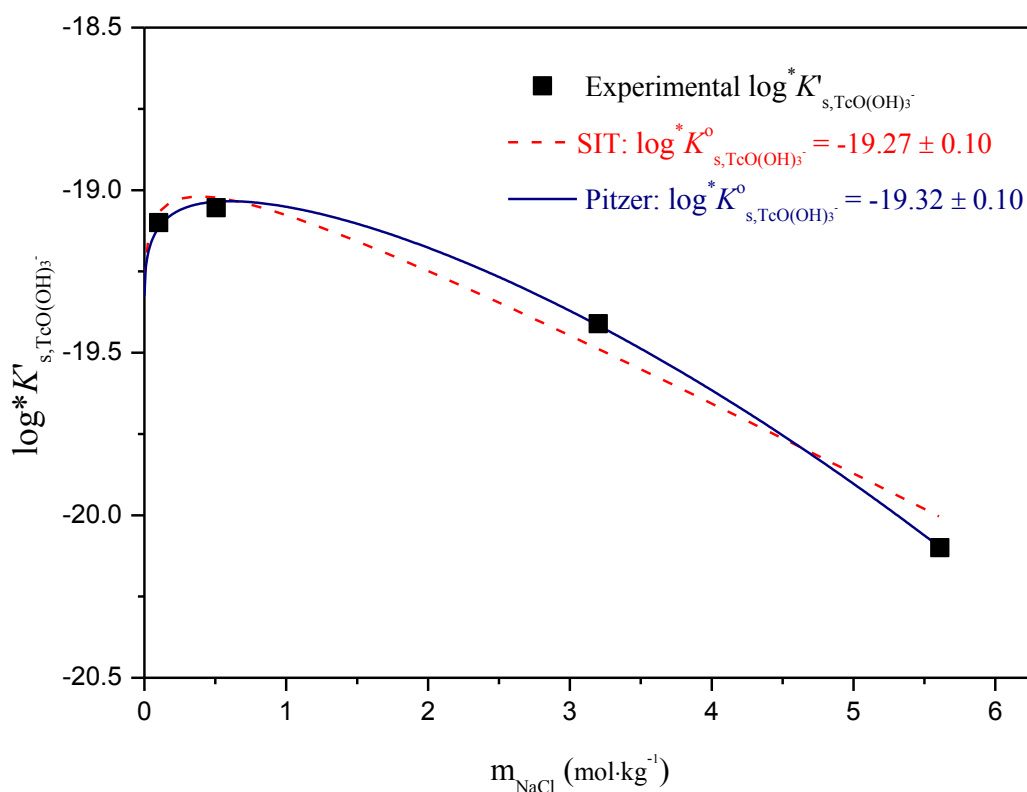


Figure 4.18 Conditional equilibrium constants $\log^* K'_{s, \text{TcO}(\text{OH})_3^-}$ as a function of the NaCl molality; experimental values (symbols) and calculated functions based on the SIT (dashed line) and Pitzer model (solid line).

4.3.3.4 Alkaline pH conditions ($\text{pH}_m \geq 8$) in MgCl₂ and CaCl₂ systems

A steep and significant increase of solubility is observed in alkaline MgCl₂ and CaCl₂ systems at $\text{pH}_m \geq 8$. This observation cannot be explained by the chemical model derived for NaCl solutions described above and necessitates an extension of the chemical model for respective MgCl₂ and CaCl₂ systems.

An increase in solubility in MgCl₂ solutions can be only observed in 4.5 M systems, likely because of the pH limitations caused by the precipitation of Mg(OH)₂ and Mg-oxychlorides at $\text{pH}_m \sim 9$. Consequently, these series cannot be used for systematically extrapolating data to $I = 0$ using SIT or Pitzer approaches. In the case of CaCl₂ solutions, a similar effect limits the systems to $\text{pH}_{\text{max}} \sim 12$. The same behaviour as in 4.5 M MgCl₂ has been observed for the systems with $[\text{CaCl}_2] \geq 1.0$ M. These data have been used to derive a thermodynamic model, with samples showing very slow kinetics having been disregarded for the model development.

Solubility data define a slope of +3, indicating the release of 3 H⁺ in the chemical reaction controlling the solubility in this pH region. Provided the predominance of the solid phase TcO₂·1.6H₂O(s), the aqueous species TcO(OH)₃⁻ is insufficient to explain the observed slope, and a new species holding the moiety [TcO(OH)₅³⁻] must be defined. Note that this species has a coordination environment fully occupied by O- and OH- ligands (CN_{max} of Tc(IV) = 6).

Several studies focussing on the solubility of actinides (III/IV/V) and Zr(IV) have clearly shown the participation of Ca in the complex formation in concentrated CaCl₂ systems and alkaline pH conditions [38, 39, 63, 89]. The formation of these species is also confirmed by EXAFS for Ca₃[Zr(IV)(OH)₆]⁴⁺ and Ca₄[Th(IV)(OH)₈]⁴⁺ species. In most of the cases, the formation of these species was accompanied by the full occupancy of the coordination number of the central metal atom. Based on these previous evidences and considering the slope analysis of solubility data in MgCl₂ and CaCl₂, the formation of Ca-Tc(IV)-OH species can be also postulated. Considering TcO₂·1.6H₂O as solid phase controlling the solubility, the release of 3H⁺ is deduced and the solubility reaction in this pH region can be described as Eq. (4.16).



which can be described with the following equations

$$\log {}^*K'_{\text{s,Ca}_n\text{TcO}(\text{OH})_5^{(2n-3)}} = \log \left[\text{Ca}_n\text{TcO}(\text{OH})_5^{(2n-3)} \right] + 3 \log [\text{H}^+] - n \log [\text{Ca}^{2+}] \quad (4.17)$$

$$\begin{aligned} \log {}^*K^o_{\text{s,Ca}_n\text{TcO}(\text{OH})_5^{(2n-3)}} &= \log {}^*K'_{\text{s,Ca}_n\text{TcO}(\text{OH})_5^{(2n-3)}} + \log \gamma_{\text{s,Ca}_n\text{TcO}(\text{OH})_5^{(2n-3)}} \\ &+ 3 \log \gamma_{\text{H}^+} - n \log \gamma_{\text{Ca}^{2+}} - 2.4 \log a_{\text{H}_2\text{O}} \end{aligned} \quad (4.18)$$

Neither spectroscopic data nor slope analysis are available for Ca_nTcO(OH)₅⁽²ⁿ⁻³⁾ species to assess the number of Ca²⁺ in this complexation reaction. Consequently, a pure modelling exercise based on the solubility data in CaCl₂ solutions has been used to derive the number of Ca atoms in this species.

Conditional stability constants are experimentally determined from solubility data available in 1.0 M, 2.0 M and 4.5 M CaCl₂. The value of log ^{*}K^o is calculated by extrapolating the results in high ionic strength to I = 0 according to Eq (4.18). In a first step, log ^{*}K^o values and ion interaction coefficients are calculated using the SIT approach considering four different chemical species and modelling options: Ca_n[TcO(OH)₅]⁽²ⁿ⁻³⁾ with n = 1-4. In a second step, the best chemical model derived by SIT has been used to derive log ^{*}K^o_{s,Ca_nTcO(OH)₅⁽²ⁿ⁻³⁾. In a separate modelling step, ion interaction coefficients according to Pitzer formulism were derived.}

SIT approach

To determine the unknown number of Ca atoms in Ca_nTcO(OH)₅⁽²ⁿ⁻³⁾ complex, n value in Ca_nTcO(OH)₅⁽²ⁿ⁻³⁾ complex is set to 1 to 4. Note that the slope in all these options remains +3. The resulting solubility reactions are shown in Eq (4.19) to Eq (4.22).



SIT linear regressions derived for reactions (4.19) to (4.22) are described with the following equations and are plotted in Figure 4.19.

$$\begin{aligned} \log {}^*K'_{\text{s,Ca}[\text{TcO}(\text{OH})_5]^-} - 2.4 \log a_w &= \log {}^*K^o_{\text{s,Ca}[\text{TcO}(\text{OH})_5]^-} \\ &- [\varepsilon(\text{Ca}[\text{TcO}(\text{OH})_5]^- , \text{Ca}^{2+}) + 6 \varepsilon(\text{H}^+ , \text{Cl}^-) - 2 \varepsilon(\text{Ca}^{2+} , \text{Cl}^-)] \cdot m_{\text{CaCl}_2} \end{aligned} \quad (4.23)$$

$$\begin{aligned} \log {}^*K'_{\text{s,Ca}_2[\text{TcO}(\text{OH})_5]^+} + 4D - 2.4 \log a_w &= \log {}^*K^o_{\text{s,Ca}_2[\text{TcO}(\text{OH})_5]^+} \\ &- [2 \varepsilon(\text{Ca}_2[\text{TcO}(\text{OH})_5]^+ , \text{Cl}^-) + 6 \varepsilon(\text{H}^+ , \text{Cl}^-) - 4 \varepsilon(\text{Ca}^{2+} , \text{Cl}^-)] \cdot m_{\text{CaCl}_2} \end{aligned} \quad (4.24)$$

$$\begin{aligned} \log {}^*K'_{\text{s,Ca}_3[\text{TcO}(\text{OH})_5]^{3+}} - 2.4 \log a_w &= \log {}^*K^o_{\text{s,Ca}_3[\text{TcO}(\text{OH})_5]^{3+}} \\ &- [2 \varepsilon(\text{Ca}_3[\text{TcO}(\text{OH})_5]^{3+} , \text{Cl}^-) + 6 \varepsilon(\text{H}^+ , \text{Cl}^-) - 6 \varepsilon(\text{Ca}^{2+} , \text{Cl}^-)] \cdot m_{\text{CaCl}_2} \end{aligned} \quad (4.25)$$

$$\begin{aligned} \log {}^*K'_{\text{s,Ca}_4[\text{TcO}(\text{OH})_5]^{5+}} - 12D - 2.4 \log a_w &= \log {}^*K^o_{\text{s,Ca}_4[\text{TcO}(\text{OH})_5]^{5+}} \\ &- [2 \varepsilon(\text{Ca}_4[\text{TcO}(\text{OH})_5]^{5+} , \text{Cl}^-) + 6 \varepsilon(\text{H}^+ , \text{Cl}^-) - 8 \varepsilon(\text{Ca}^{2+} , \text{Cl}^-)] \cdot m_{\text{CaCl}_2} \end{aligned} \quad (4.26)$$

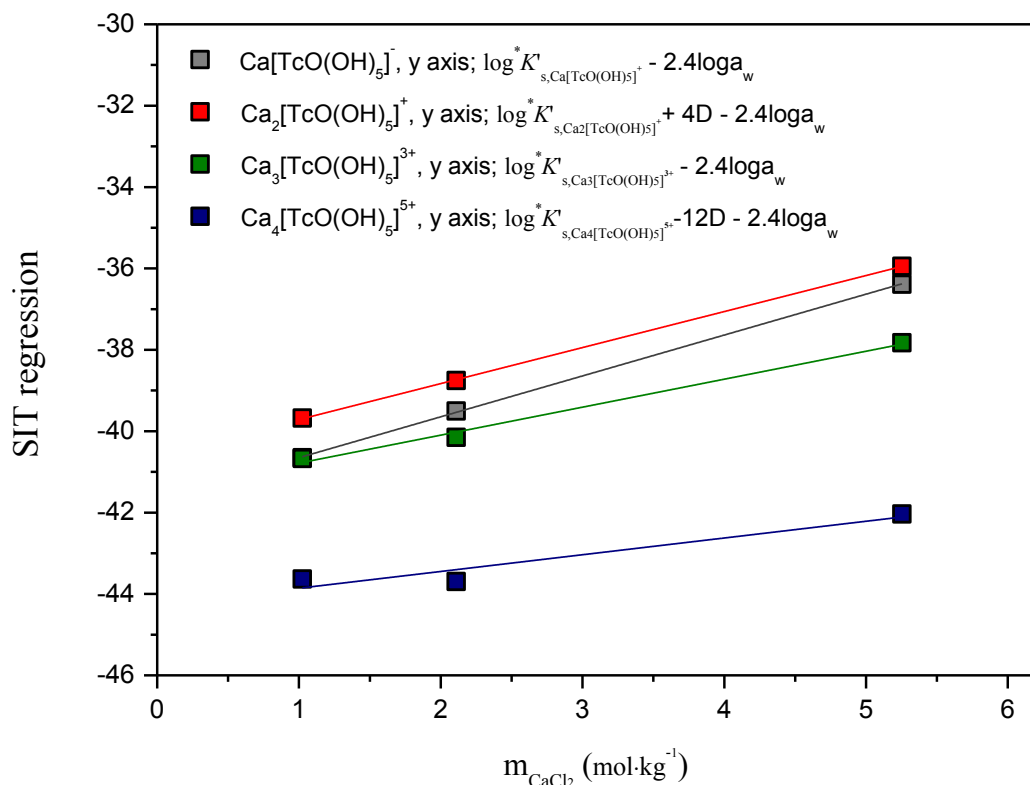


Figure 4.19 SIT-plot for the solubility reactions $\text{TcO}_2 \cdot 1.6\text{H}_2\text{O}(\text{s}) + n\text{Ca}^{2+} + 2.4\text{H}_2\text{O} \rightleftharpoons \text{Ca}_n\text{TcO}(\text{OH})_5^{(2n-3)} + 3\text{H}^+$ with $n = 1 - 4$ considering the conditional values for $\log^* K'_{s,\text{Ca}_n\text{TcO}(\text{OH})_5^{(2n-3)}}$ determined in this work.

Table 4.8 summarizes the $\log^* K'_{s,\text{Ca}_n\text{TcO}(\text{OH})_5^{(2n-3)}}$ and ε_{ij} values determined by intercept and slope of the corresponding SIT-plots, respectively, as well as the experimental stability constants and the difference between experimental and calculated $\log^* K'_{s,\text{Ca}_n\text{TcO}(\text{OH})_5^{(2n-3)}}$ values (quality parameter). Ion interaction coefficients are calculated from the slope of SIT-plots by subtracting the value of $\varepsilon(\text{H}^+, \text{Cl}^-) = 0.12 \pm 0.01 \text{ kg}\cdot\text{mol}^{-1}$ and $\varepsilon(\text{Ca}^{2+}, \text{Cl}^-) = 0.14 \pm 0.01 \text{ kg}\cdot\text{mol}^{-1}$ as reported in the NEA-TDB. The final selection of the chemical model for CaCl₂ solutions under alkaline conditions has been based on the following criteria:

- Minimum deviation between experimental and calculated conditional constants need to be obtained (quality parameter in Table 4.8);
- Reasonable values of SIT ion interaction coefficients need to be chosen. SIT ion interaction coefficients have an analogy between the identically charged species, such as $\varepsilon(\text{M}^+, \text{Cl}^-) = 0.05 \pm 0.1 \text{ kg}\cdot\text{mol}^{-1}$ and $\varepsilon(\text{M}^{2+}, \text{Cl}^-) = 0.15 \pm 0.1 \text{ kg}\cdot\text{mol}^{-1}$. It is known that these parameters deviate from the estimated values with increasing the radius of the ion (see Table 4.9);
- Stoichiometry of the complex should retain a certain consistency with previously reported ternary systems Ca–M(III/IV/V)–OH, with M = Zr, Tc and An (see Table 4.10) with respect to ionic radii and coordination number of M;

- The plot of $\log {}^*K'_{s, Ca_n TcO(OH)_5^{(2n-3)}}$ vs. CaCl₂ concentration (see Figure 4.20) should give a smooth shape without jumps or turning points.

Species CaTcO(OH)₅⁻ and Ca₄TcO(OH)₅⁵⁺ were directly disregarded because of the very large and clearly unrealistic values of ϵ and quality parameters, respectively. The species Ca₂TcO(OH)₅⁺ shows the lowest quality parameter, but retains a very negative SIT ion interaction coefficient. On the contrary, the species Ca₃TcO(OH)₅³⁺ has the second largest quality parameter, whereas the SIT ion interaction coefficient is more moderate. Both species show a smooth shape in Figure 4.20, which do not allow a clear selection of one or the other.

Most of the SIT ion interaction coefficients reported in the literature for Ca-M(III/IV/V)-OH species with charges between +2 and +4 (M = Zr, Tc, An) are positive or very close to 0 (Table 4.9). Only Fellhauer [89] recently reported $\epsilon = -0.20$ for the species Ca₃[NpO₂(OH)₅]²⁺. Based on those values, $\epsilon = -0.52$ quantified for the species Ca₂[TcO(OH)₅]⁺ appears as a unexpectedly large, which would hint towards the possible formation of the species Ca₃[TcO(OH)₅]³⁺.

In all previously reported ternary Ca–M–OH species holding the maximum number of OH-ligands (in most of the cases the maximum coordination number, see Table 4.10), the number of Ca atoms considered in the selected chemical model was three. This applies to the large actinide ions ($90 \leq Z \leq 96$, $1.09 \leq r [\text{Å}] \leq 1.19$), but also to Zr with $Z = 40$ and $r = 0.86 \text{ Å}$ for a coordination number of 6. In spite of the smaller size of Tc(IV) ions with coordination number of 6 ($r = 0.79 \text{ Å}$), the formation of the species Ca₃TcO(OH)₅³⁺ has been finally favoured in the chemical model for Tc(IV) in concentrated CaCl₂ solutions. No spectroscopic “proof of concept” (e.g. EXAFS) can be obtained for this hypothesis due to the low Tc concentration reached in these systems ($[\text{Tc}]_{\text{aq}} \leq 10^{-5} \text{ M}$). It is to note that the existence of the Ca₃TcO(OH)₅³⁺ species has recently been proposed on the basis of quantum chemical calculations using Density Functional theory (DFT) performed by Robert Polly (KIT-INE). However, as this ongoing quantum chemical calculations should be mentioned in support of the adopted speciation scheme derived in this work, a detailed discussion of these comprehensive calculations is out of the scope of this PhD thesis.

Table 4.8 $\log {}^*K^0$ and ϵ_{ij} values obtained by SIT regression for Ca_nTcO(OH)₅⁽²ⁿ⁻³⁾ species.

Species	$\log {}^*K'_{\text{experimental}}$				Outcome of SIT – plot		
	1.0 M	2.0 M	4.5 M	$\log {}^*K^0$	j	ϵ_{ij}	Quality
Ca[TcO(OH) ₅] ⁻	-40.71	-39.67	-37.18	-41.66	Ca ²⁺	-1.44 ± 0.03	$\Delta = 0.07$
Ca₂[TcO(OH)₅]⁺	-40.72	-40.00	-37.90	-40.60	Cl⁻	-0.52 ± 0.10	$\Delta = 0.04$
Ca₃[TcO(OH)₅]³⁺	-40.73	-40.32	-38.62	-41.47	Cl⁻	-0.28 ± 0.05	$\Delta = 0.26$
Ca ₄ [TcO(OH) ₅] ⁵⁺	-40.74	-40.64	-39.34	-44.27	Cl ⁻	-0.01 ± 0.07	$\Delta = 0.58$

4 Solubility and hydrolysis of Tc(IV) in dilute to concentrated NaCl, MgCl₂ and CaCl₂ solutions

Table 4.9 ϵ_{ij} values obtained by SIT regression for Ca-Zr(IV)-OH, Ca-An(IV/V)-OH and Ca-M(III)-OH species in literature.

<i>Species</i>			
<i>i</i>	<i>j</i>	ϵ_{ij}	Reference
Ca[M(III)(OH) ₃] ²⁺	Cl ⁻	0.05 ± 0.04	[97]
Ca ₂ [M(III)(OH) ₄] ³⁺	Cl ⁻	0.29 ± 0.07	[97]
Ca ₃ [M(III)(OH) ₆] ³⁺	Cl ⁻	0.00 ± 0.06	[97]
Ca ₂ [Zr(IV)(OH) ₆] ²⁺	Cl ⁻	0.1 ± 0.10	[63]
Ca ₃ [Zr(IV)(OH) ₆] ⁴⁺	Cl ⁻	0.4 ± 0.07	[63]
Ca ₄ [An(IV)(OH) ₈] ⁴⁺	Cl ⁻	-0.01 ± 0.10	[39, 63]
Ca[Np(V)O ₂ (OH) ₂] ⁺	Cl ⁻	-0.07	[89]
Ca ₃ [Np(V)O ₂ (OH) ₅] ²⁺	Cl ⁻	-0.20	[89]

Table 4.10 Formal charge, effective ionic radii and number of Ca atoms considered in the ternary Ca-M-OH species reported in the literature for M = Zr(IV), Th(IV), Np(V) and Cm(III) and evaluated in this work for Tc(IV). Only species with greatest number of OH-ligands are considered in the comparison.

Element	Z	An-OH	Formal charge	Effective ion radius (M ⁿ⁺ or MO ₂ ⁿ⁺) [Å]	Number of Ca in the complex	Reference
Zr(IV)	40	[Zr(OH) ₆] ²⁻	-2	0.86 (CN = 6) ^a [98] 1.03 (CN = 9) ^a [98]	3	[63]
Tc(IV)	43	[TcO(OH) ₅] ³⁻	-3	0.79 (CN = 6) ^a [98]	1-4 (?)	p.w.
Th(IV)	90	[Th(OH) ₈] ⁴⁺	-4	1.19 (CN = 8) ^a [98]	4	[63]
Np(V)	93	[NpO ₂ (OH) ₅] ⁴⁺	-4	1.12 ^b [99]	3	[89]
Cm(III)	96	[Cm(OH) ₆] ³⁻	-3	1.09 (CN = 8) ^a [98]	3	[38]

a. crystal radius; **b.** in aqueous solution

In the 4.5 M MgCl₂ system, the solubility starts to increase with a slope of +3 at pH_m ≥ 8, approximately 1 pH-unit earlier than in 4.5 M CaCl₂ systems. This increase is likely caused by the formation of Mg₃[TcO(OH)₅]³⁺ species in analogy with Ca₃[TcO(OH)₅]³⁺. Since the available solubility data for the MgCl₂ system is insufficient due to the limitations in pH, the ion interaction coefficient calculated for $\epsilon(\text{Ca}_3[\text{TcO}(\text{OH})_5]^{3+}, \text{Cl}^-) = -0.28 \pm 0.05$ is used for $\epsilon(\text{Mg}_3[\text{TcO}(\text{OH})_5]^{3+}, \text{Cl}^-)$ to extrapolate the conditional stability constant at 4.5 M MgCl₂ to $I = 0$ and calculate accordingly $\log {}^*K_{s, \text{Mg}_3\text{TcO}(\text{OH})_5}^0 = -40.06 \pm 0.50$. The value obtained is significantly higher than $\log {}^*K_{s, \text{Ca}_3\text{TcO}(\text{OH})_5}^0 = -41.47 \pm 0.20$, as expected in the view of the greater solubility observed for MgCl₂ systems for the same alkaline pH values.

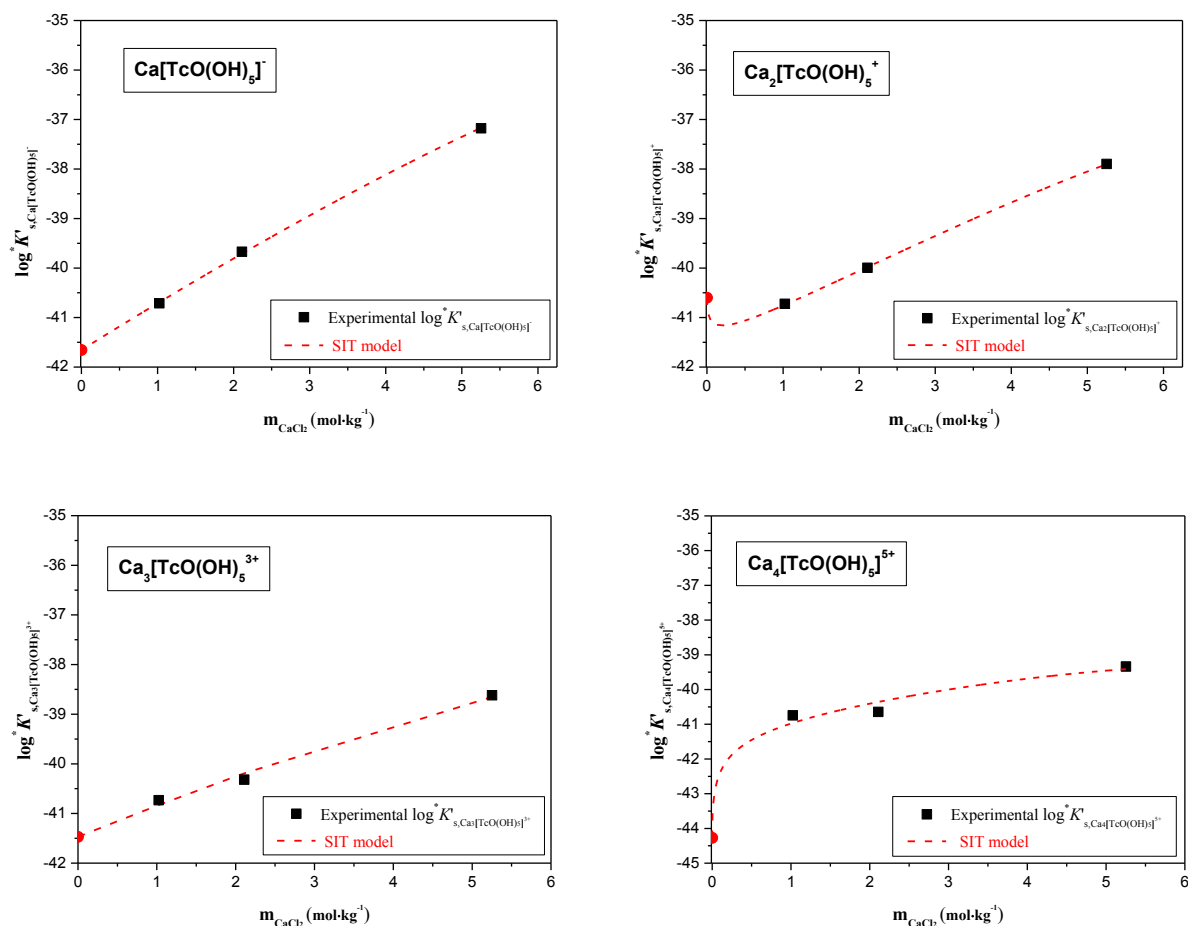


Figure 4.20 Conditional equilibrium constants $\log^* K'_{s,\text{Ca}n\text{TcO}(\text{OH})_5^{(2n-3)}}$ as a function of the CaCl₂ molality; experimental data and calculated functions based on the SIT approach.

Pitzer approach

The species $\text{Ca}_3[\text{TcO}(\text{OH})_5]^{3+}$ has been selected for the chemical model of Tc(IV) based on the discussion provided in the previous section according to the SIT approach. Conditional solubility constants determined in CaCl₂ systems were also fitted according to Eq. (4.18) and considering the Pitzer formulism. The values of $\log \gamma_{H^+}$ and a_w in equation (4.18) are calculated from the parameters reported by Harvie et al. [79]. Some parameters were fixed due to the ionic strength limitations (too many parameters need to be fitted by 3 available ionic strengths). $\beta^{(1)}$ was fixed to value 4.30 according to literature recommendations [38, 39, 100]. The binary parameter $C^{(\text{D})}$ and the mixing parameters $\theta(\text{Ca}_3[\text{TcO}(\text{OH})_5]^{3+}, \text{Ca}^{2+})$ and $\Psi(\text{Ca}_3[\text{TcO}(\text{OH})_5]^{3+}, \text{Cl}^-, \text{Ca}^{2+})$ were set to zero. $\log^* K_{s,\text{Ca}_3\text{TcO}(\text{OH})_5}^0$ and $\beta^{(0)}$ were fitted for CaCl₂ systems by minimizing the difference between experimental and modelled $\log^* K'_{s,\text{Ca}_3\text{TcO}(\text{OH})_5}^{3+}$ in 1.0 M, 2.0 M and 4.5 M CaCl₂ systems. The resulting values are:

$$\log^* K_{s,\text{Ca}_3\text{TcO}(\text{OH})_5}^0 = -41.48 \pm 0.10 \quad \beta^{(0)} = 0.08 \text{ kg} \cdot \text{mol}^{-1} \quad \beta^{(1)} = 4.30 \text{ kg} \cdot \text{mol}^{-1}$$

Figure 4.21 shows experimental and calculated $\log^* K'_{s, \text{Ca}_3\text{TcO}(\text{OH})_5^{3+}}$ for CaCl₂ systems. The figure shows that both SIT and Pitzer model derived in this work reproduce very well the experimentally determined $\log^* K'_{s, \text{Ca}_3\text{TcO}(\text{OH})_5^{3+}}$ values.

As same as in SIT calculation of Mg₃[TcO(OH)₅]³⁺ species, the Pitzer parameters calculated for Ca₃[TcO(OH)₅]³⁺ are used for Mg₃[TcO(OH)₅]³⁺ to extrapolate the conditional stability constant at 4.5 M MgCl₂ to $I = 0$ and to calculate accordingly $\log^* K^o_{s, \text{Mg}_3\text{TcO}(\text{OH})_5^{3+}} = -40.34 \pm 0.50$.

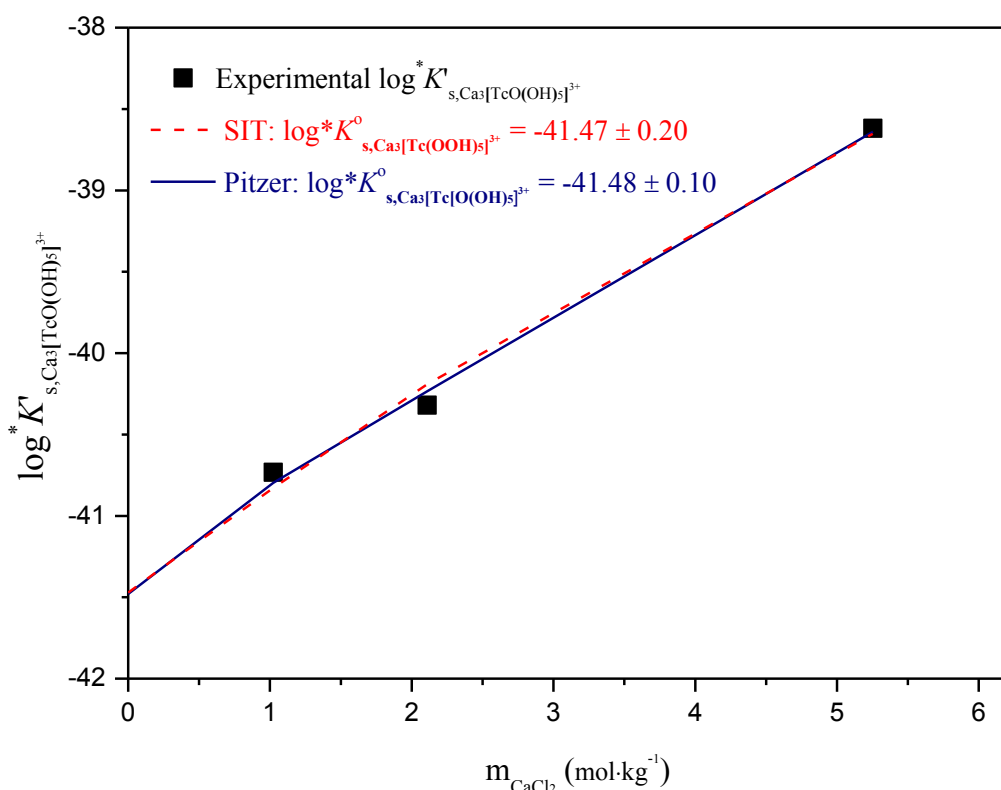


Figure 4.21 Conditional equilibrium constants $\log^* K'_{s, \text{Ca}_3\text{TcO}(\text{OH})_5^{3+}}$ as a function of the CaCl₂ molality; experimental values (symbols) and calculated functions based on the SIT (dashed line) and Pitzer model (solid line).

4.4 Chemical, thermodynamic and activity model for the system $\text{Tc}^{4+} - \text{Na}^+ - \text{Mg}^{2+} - \text{Ca}^{2+} - \text{H}^+ - \text{Cl}^- - \text{OH}^- - \text{H}_2\text{O}$

In Section 4.3, the chemical, thermodynamic and activity models are derived for Tc(IV) solubility in NaCl, MgCl₂ and CaCl₂ systems using SIT and Pitzer approaches. Standard stability constants determined according to the newly developed chemical models are summarized in Table 4.11. The chemical model developed for Tc(IV) solubility in the present work differs from NEA–TDB data selection in the acidic pH region where the new spectroscopic evidences are available since the publication of last update book of NEA–TDB. Also, new complexes have been derived in alkaline MgCl₂ and CaCl₂ systems based on the very different solubility behaviour observed under these conditions. The ion interaction coefficients derived for newly generated Tc(IV) species are shown in Table 4.12. Figure 4.22, 4.23 and 4.24 show all the experimental solubility data determined in the

present work, together with the thermodynamic calculations performed using the Pitzer activity model. The underlying aqueous species for each system (shown in Table 4.11) are shown in the figures. The newly determined thermodynamic models for Tc(IV) solubility in dilute to concentrated saline solutions can properly explain the experimental solubility data in the present work, as well as the experimental solubility data at $I \sim 0$ considered in NEA–TDB selection for the selection of Tc(IV) thermodynamic data. It is to note that the present work gives a first comprehensive description of Tc(IV) solubility in NaCl, MgCl₂ and CaCl₂ solutions ranging from dilute to highly saline systems. Based upon these new solubility and speciation studies, it was possible to derive new and improved comprehensive thermodynamic models following both SIT and Pitzer approaches.

Table 4.11 Stability constants determined by SIT and Pitzer models for the formation of Tc(IV) aqueous species in NaCl, MgCl₂ and CaCl₂ solutions.

Chemical Reactions	SIT	Pitzer
	$\log^* K^o$	$\log^* K^o$
$\text{TcO}_2 \cdot 1.6\text{H}_2\text{O}(\text{s}) + 2/3 \text{H}^+ \Leftrightarrow 1/3\text{Tc}_3\text{O}_5^{2+} + 1.93 \text{H}_2\text{O}$	-1.53 ± 0.16	-1.56 ± 0.10
$\text{TcO}_2 \cdot 1.6\text{H}_2\text{O}(\text{s}) \Leftrightarrow \text{TcO}(\text{OH})_2 + 0.6 \text{H}_2\text{O}$	-8.80 ± 0.50	-8.80 ± 0.50
$\text{TcO}_2 \cdot 1.6\text{H}_2\text{O}(\text{s}) + 0.4\text{H}_2\text{O} \Leftrightarrow \text{TcO}(\text{OH})_3^- + \text{H}^+$	-19.27 ± 0.10	-19.32 ± 0.10
$\text{TcO}_2 \cdot 1.6\text{H}_2\text{O}(\text{s}) + 3\text{Mg}^{2+} + 2.4\text{H}_2\text{O} \Leftrightarrow \text{Mg}_3[\text{TcO}(\text{OH})_5]^{3+} + 3\text{H}^+$	-40.06 ± 0.50	-39.74 ± 0.50
$\text{TcO}_2 \cdot 1.6\text{H}_2\text{O}(\text{s}) + 3\text{Ca}^{2+} + 2.4\text{H}_2\text{O} \Leftrightarrow \text{Ca}_3[\text{TcO}(\text{OH})_5]^{3+} + 3\text{H}^+$	-41.47 ± 0.20	-41.48 ± 0.10

Table 4.12 Ion interaction coefficients for Tc hydrolysis species in NaCl, MgCl₂ and CaCl₂ media at 25 °C; SIT ion interaction coefficients: ϵ_{ij} [kg mol^{-1}] and Pitzer parameters: $\beta^{(0)}$, $\beta^{(1)}$, λ_{ij} , $\Theta_{ii'}$ in [$\text{kg} \cdot \text{mol}^{-1}$], $C^{(\phi)}$ and $\Psi_{iji'}$ in [$\text{kg}^2 \cdot \text{mol}^{-2}$].

Species		SIT	Pitzer				
i	j	ϵ_{ij}	Binary parameters		Mixing parameters		
			$\beta^{(0)}$	$\beta^{(1)}$	$C^{(\phi)}$	$\Theta_{ii'}$	$\Psi_{iji'}$
$\text{Tc}_3\text{O}_5^{2+}$	Cl^-	-0.34 ± 0.1	-0.20	1.3	0	0	0
$\text{TcO}(\text{OH})_3^-$	Na^+	0.10 ± 0.02	0.01	0.3	0.04	0	0
$\text{Ca}_3[\text{TcO}(\text{OH})_5]^{3+}$	Cl^-	-0.28 ± 0.04	0.08	4.3*	0	0	0
$\text{Mg}_3[\text{TcO}(\text{OH})_5]^{3+}$	Cl^-	-0.28 ± 0.04	0.08	4.3*	0	0	0
$\text{TcO}(\text{OH})_2$	NaCl/MgCl ₂	0	0	0	0	0	0

*Fixed value for the corresponding charge type, according to [100]

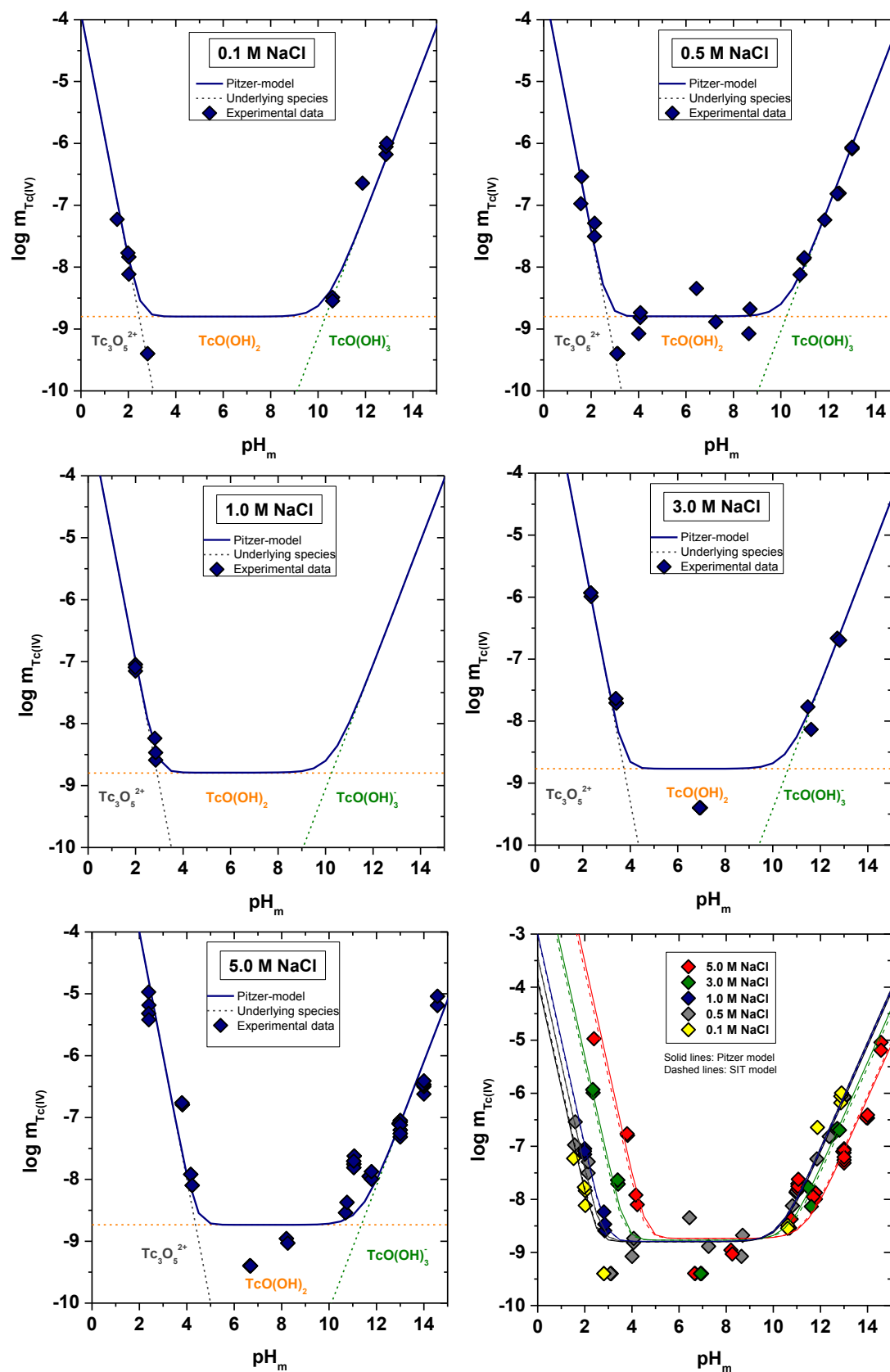


Figure 4.22 Solubility and speciation calculations for Tc(IV) in NaCl systems performed with the chemical, thermodynamic and Pitzer activity model derived in this work. Experimental data corresponding to equilibrium values determined in this work.

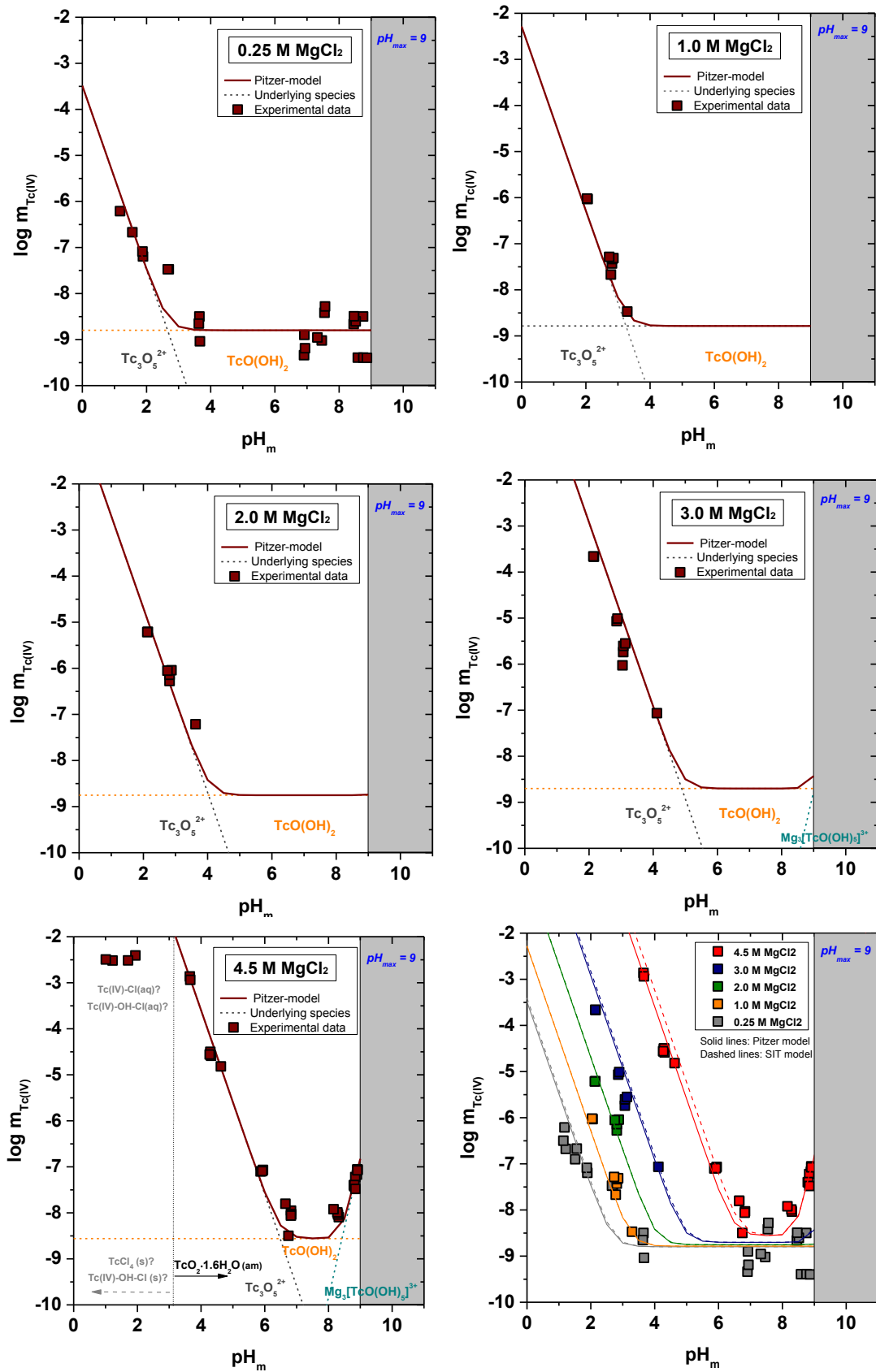


Figure 4.23 Solubility and speciation calculations for Tc(IV) in MgCl₂ systems performed with the chemical, thermodynamic and Pitzer activity model derived in this work. Experimental data corresponding to equilibrium values determined in this work.

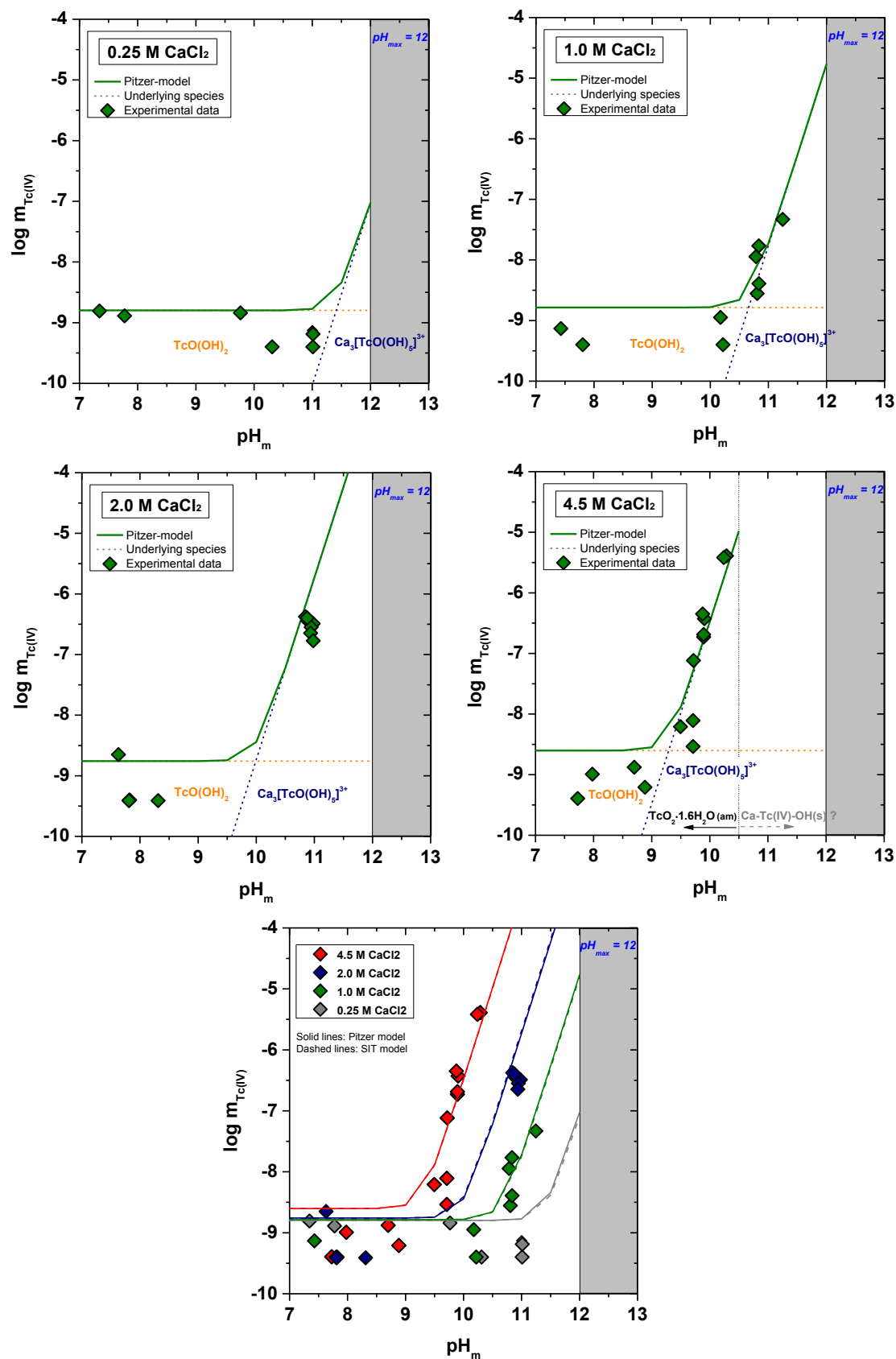


Figure 4.24 Solubility and speciation calculations for Tc(IV) in CaCl₂ systems performed with the chemical, thermodynamic and Pitzer activity model derived in this work. Experimental data corresponding to equilibrium values determined in this work.

4.5 Conclusion for Tc(IV) solubility

This part of the PhD thesis was dedicated to the investigation of Tc(IV) solubility in dilute to concentrated NaCl, MgCl₂ and CaCl₂ solutions from acidic to alkaline pH conditions. Experimentally measured solubility data in dilute NaCl and MgCl₂ solutions agree very well with the experimental solubility data reported in previous studies in dilute systems as well as with thermodynamic calculations considering NEA–TDB selection. In the acidic pH range, a very significant increase in the solubility (up to 4 orders of magnitude) is observed following a well-defined slope of -2 . Based on this slope analysis and considering previous spectroscopic evidence, the Tc₃O₅²⁺ species was proposed dominant in these conditions for all evaluated systems. New spectroscopic evidence on the formation of an oligomeric Tc(IV) species with chloride ligands has also been gained in this work.

In neutral pH region, a pH-independent solubility reaction prevails in all evaluated systems, consistently with the current NEA–TDB selection. No ionic strength effect is observed up to $I = 13.5$ M. $\log^* K_{S, \text{TcO}(\text{OH})_2}^o$ is determined in the present work as -8.8 ± 0.5 , which agrees well within the uncertainties with the value selected in the NEA–TDB, also permitting to importantly reduce uncertainties.

In the alkaline pH region, the solubility of Tc(IV) increases with a slope of $+1$ in NaCl system, indicating the predominance of TcO(OH)₃⁻ as reported for diluted systems in NEA–TDB. The solubility decreases about one order of magnitude with increasing the ionic strength, although the same aqueous speciation is retained. $\log^* K_{S, \text{TcO}(\text{OH})_3}^o$ determined in this work is in a very good agreement with the NEA–TDB.

In alkaline MgCl₂ and CaCl₂ systems, a steep increase of the solubility is observed with a well-defined slope of $+3$. Based on the slope analysis, model calculations and analogy with An(IV) and Zr(IV) systems, the formation of Mg₃[TcO(OH)₅]³⁺ and Ca₃[TcO(OH)₅]³⁺ species is proposed. At $\text{pH}_m \geq 10.5$ in concentrated CaCl₂ systems, a solid phase transformation is rather likely to occur, based on the solubility behaviour and XRD observations. An accurate assessment of this interesting phenomenon is foreseen after the completion of this thesis.

This work provides new and extended experimental data of Tc(IV) solubility behaviour in dilute to concentrated NaCl, MgCl₂ and CaCl₂ systems and subsequently comprehensive chemical, thermodynamic and activity model in acidic to hyper-alkaline pH region for the system Tc⁴⁺–Na⁺–Mg²⁺–Ca²⁺–H⁺–Cl⁻–OH⁻–H₂O at 25°C. It is the first time that the solubility and speciation of the Tc(IV) system has been investigated in such a comprehensive and systematic way, spanning a wide variation of pH conditions and extending from dilute to highly concentrated saline systems. New and improved thermodynamic data were derived following both the SIT and Pitzer approaches. The thermodynamic data generated in this work are to be implemented in national and international thermodynamic databases, and will allow more accurate geochemical model calculations in a variety of relevant conditions (dilute, saline, cementitious) relevant for performance assessment purposes.

5 Reduction and uptake of Tc by Fe(II) minerals in dilute to concentrated saline systems

This chapter of the PhD thesis is dedicated to investigate the reduction and uptake mechanism of Tc by Fe(II) minerals. In a first part, the experiments were performed in the presence of magnetite and mackinawite in the 0.1 M NaCl system and the Tc retention mechanism investigated as a function of initial Tc concentration and Tc loading on the Fe(II) minerals. In a second part, the experiments were specifically focussed on highly saline conditions, e.g., 5.0 M NaCl and 4.5 M MgCl₂ systems in the presence of magnetite, mackinawite and siderite. In all investigated systems, the samples were equilibrated for 4 to 6 of weeks, and pH_c, E_h and Tc concentration were measured for a quantitative interpretation of the sorption processes. In both systems, XANES/EXAFS measurements of separated solid phases were performed in ESRF (ROBL beamline, Grenoble, France) in cooperation with A. C. Scheinost. Evaluated data are discussed in the following sections as a function of ionic strength.

5.1 Reduction and uptake of Tc by magnetite and mackinawite in 0.1 M NaCl

5.1.1 Quantitative evaluation of the wet chemistry data

The reduction and uptake of Tc in the presence of magnetite (Fe₃O₄) and mackinawite (FeS) in 0.1 M NaCl was investigated as a function of initial Tc concentration ($2 \cdot 10^{-4}$ M and $2 \cdot 10^{-5}$ M) and Tc loading of the solid Fe phases (400 ppm, 600 ppm and 900 ppm). Experimental conditions and measured pH_c, E_h and Tc concentration in the Fe mineral suspensions after 6 weeks of equilibration time are summarized in Table 5.1. For magnetite samples, measured E_h values are slightly below the thermodynamically calculated Tc(VII)/Tc(IV) redox borderline, whereas significantly lower E_h values are found in the mackinawite system (Figure 5.1). In both systems, Tc concentrations measured in solution decrease to values below the detection limit of LSC within 6 weeks, suggesting that TcO₄⁻ is completely reduced to Tc(IV) and quantitatively removed from the aqueous phase.

5 Reduction and uptake of Tc by Fe(II) minerals in dilute to concentrated saline systems

Table 5.1 Experimental conditions and measured pH_c , E_h and $[\text{Tc}]_{\text{final}}$ of Tc sorbed by magnetite and mackinawite in 0.1 M NaCl system (after 6 weeks of equilibration time).

Fe mineral	Tc loading (ppm)	$[\text{Tc}]_0^{\text{a}}$	pH_c^{b}	E_h (mV) ^c	$[\text{Tc}]_{\text{final}}$
Magnetite-1	400	$2 \cdot 10^{-4}$	9.28	-149	$\leq 4 \cdot 10^{-10} \text{ d}$
Magnetite-2	600	$2 \cdot 10^{-4}$	9.16	-146	$\leq 4 \cdot 10^{-10} \text{ d}$
Magnetite-3	900	$2 \cdot 10^{-4}$	9.08	-139	$\leq 4 \cdot 10^{-10} \text{ d}$
Magnetite-4	400	$2 \cdot 10^{-5}$	9.12	-138	$\leq 4 \cdot 10^{-10} \text{ d}$
Magnetite-5	600	$2 \cdot 10^{-5}$	8.90	-121	$\leq 4 \cdot 10^{-10} \text{ d}$
Magnetite-6	900	$2 \cdot 10^{-5}$	8.68	-109	$\leq 4 \cdot 10^{-10} \text{ d}$
Mackinawite-7	400	$2 \cdot 10^{-4}$	9.07	-315	$\leq 4 \cdot 10^{-10} \text{ d}$
Mackinawite-8	600	$2 \cdot 10^{-4}$	9.16	-381	$\leq 4 \cdot 10^{-10} \text{ d}$
Mackinawite-9	900	$2 \cdot 10^{-4}$	8.99	-309	$\leq 4 \cdot 10^{-10} \text{ d}$
Mackinawite-10	400	$2 \cdot 10^{-5}$	9.02	-289	$\leq 4 \cdot 10^{-10} \text{ d}$
Mackinawite-11	600	$2 \cdot 10^{-5}$	8.91	-280	$\leq 4 \cdot 10^{-10} \text{ d}$
Mackinawite-12	900	$2 \cdot 10^{-5}$	8.83	-271	$\leq 4 \cdot 10^{-10} \text{ d}$

a: initial Tc(VII) concentration; **b:** ± 0.05 ; **c:** ± 50 mV; **d:** detection limit

Figure 5.2a and Figure 5.2b show the SEM pictures of magnetite and mackinawite samples, respectively. The pictures show a very different morphology for both phases. Thus, magnetite is characterized by aggregates of small particles, whereas mackinawite shows a platelet-based structure. In both cases, particle size agrees well with data previously reported for Fe minerals synthesized by the same method [75, 101, 102]. Note that the crystallinity of the magnetite synthesized in this work is significantly lower (e. g. smaller particle size) than such obtained using the standard method described by Schwertmann and Cornell [103] who used the higher temperature ($T = 80$ °C).

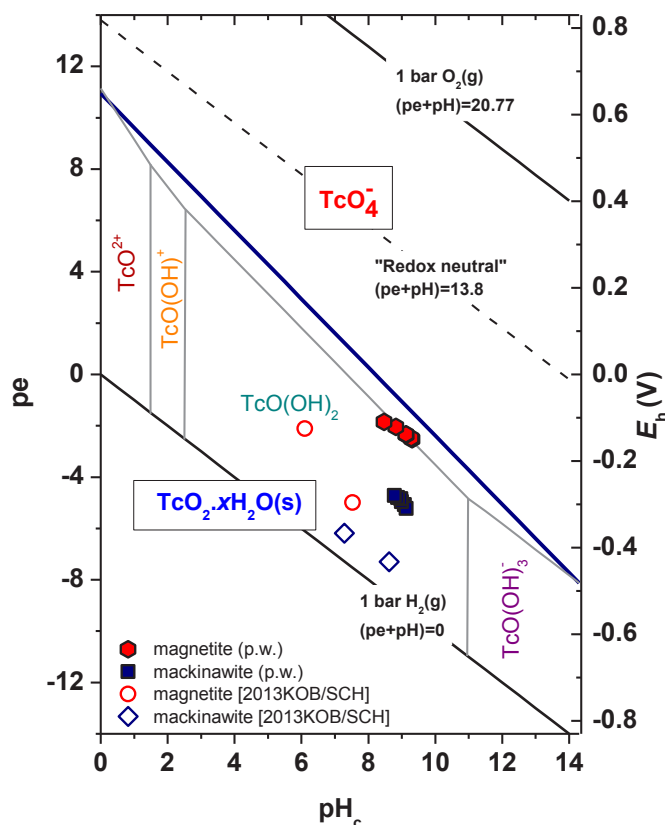


Figure 5.1 Experimental pH_c and E_h values of Tc samples in 0.1 M NaCl and presence of magnetite and mackinawite. Measurements performed after 6 weeks of equilibration time (directly before sampling for EXAFS measurements). Solid blue line represents the 50:50 equilibrium line for Tc(VII)/Tc(IV) calculated at $I = 0.1$ M according to the reaction $\text{TcO}_4^- + 4 \text{H}^+ + 3\text{e}^- \rightleftharpoons \text{TcO}_2 \cdot 1.6\text{H}_2\text{O}(\text{s}) + 0.4 \text{H}_2\text{O}$. Calculations performed using NEA–TDB thermodynamic data and ionic strength corrections as discussed in Chapter 3. Black solid and dashed lines indicate upper and lower decomposition lines of water and “redox neutral” ($\text{pe} + \text{pH} = 13.8$) conditions. Experimental pH_c and E_h determined in the study of Kobayashi et al. [73] for magnetite and mackinawite systems are also included for comparison.

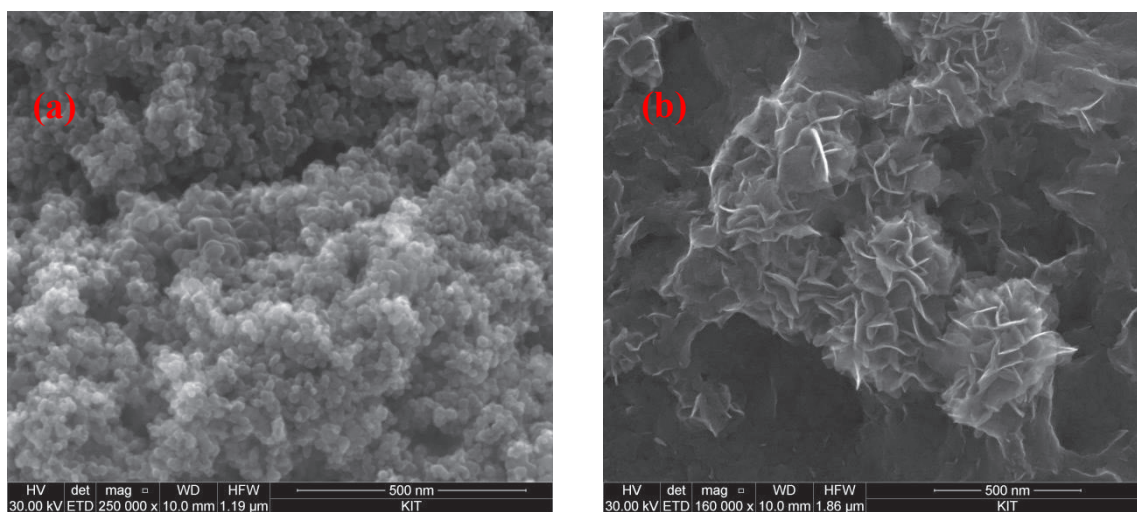


Figure 5.2 SEM pictures of Tc sorbed magnetite (a) and mackinawite (b) investigated in this work.

5.1.2 Structural interpretation of Tc uptake: EXAFS/XANES

5.1.2.1 Magnetite

Figure 5.3a shows the XANES spectra measured at the Tc K-edge for Tc sorbed magnetite samples. All investigated samples show similar features and edge position. The absence of any pre-edge feature at 21050 eV confirms the absence of Tc(VII) (lower detection limit < 5%) and predominance of Tc(IV). The k^3 -weighted EXAFS spectra and the Fourier Transforms for all magnetite samples are shown in Figure 5.3b and Figure 5.3c, respectively. A good reconstruction of the experimental XANES and EXAFS spectra (red lines in Figure 5.3) was possible using two different Tc species present in the magnetite samples.

The grouping is also visible from the Fourier Transform Magnitudes: while the first peak at $R \approx 1.5 \text{ \AA}$ (distance uncorrected for phase shift) corresponding to backscattering of the Tc-O coordination shell is very similar for all six samples, a double peak in the 2.3 to 3.5 \AA range is more split for the lower initial Tc concentration, and less split for the higher initial Tc concentration. To elucidate the structural differences between both groups, EXAFS shell fitting was performed. The required paths were calculated with FEFF (8.2) using an atomic cluster based on the structure of magnetite [104], where the central, photon-absorbing Fe cation was replaced by Tc. Furthermore, a Tc-Tc backscattering path was created by replacing two backscattering Fe atoms at radial distances of 2.97 \AA and 3.48 \AA by Tc. Note that these distances are sufficiently similar to the Tc-Tc distances in TcO_2 , with two short Tc-Tc distances at 2.60 and 3.09 \AA , and longer distances at 3.6 \AA [105], to provide a reliable EXAFS fit model. Structural parameters resulting from the EXAFS fits are shown in Table 5.2.

Magnetite samples with the same $[\text{Tc}]_0$ (either $2 \cdot 10^{-4} \text{ M}$ or $2 \cdot 10^{-5} \text{ M}$) show very similar EXAFS spectra regardless of the final Tc loading. The first shell in all investigated samples corresponds to the backscattering of oxygen. The fit of this shell results in a coordination number (CN) of 6 at $2.03 \pm 0.01 \text{ \AA}$, in good agreement with the octahedral coordination environment expected for Tc(IV). In those samples with lower $[\text{Tc}]_0$ ($2 \cdot 10^{-5} \text{ M}$, samples 4–6), the second and third shells can be properly fitted with Tc-Fe paths at $3.09 \pm 0.01 \text{ \AA}$ and $3.52 \pm 0.01 \text{ \AA}$, corresponding to edge-sharing and corner-sharing positions in the magnetite structure. In all cases, the best fit is obtained by also considering Tc-Tc backscattering at $2.58 \pm 0.01 \text{ \AA}$. Note that in those samples with higher $[\text{Tc}]_0$ ($2 \cdot 10^{-4} \text{ M}$, samples 1–3), the coordination number of the Tc backscatterer is larger than for samples with lower $[\text{Tc}]_0$, whereas the coordination number of the second Fe shell is lower. This can be interpreted as the formation of $[\text{TcO}_2]$ -dimers/polymers on the surface of magnetite in addition to the incorporation of monomeric Tc(IV) species to the magnetite structure.

The relatively large coordination numbers fitted for Tc-Fe₁ (CN = 3–5) and Tc-Fe₂ (CN = 3–4) paths hint towards the partial incorporation of Tc into the structure of magnetite. As discussed in Section 1.2.4, both complete incorporation of Tc into the magnetite structure and formation of TcO_2 -like dimers/polymers on the surface were reported by different authors [26, 32, 51, 52, 73]. However, none of the available studies has investigated the effect of initial Tc concentration and solid to liquid ratio (or loading) as performed in the present work, but rather focussed on a given $[\text{Tc}]$ and loading. Kobayashi and co-workers [73] conducted Tc uptake experiments with magnetite under analogous $[\text{Tc}]_0$ and loading ($2 \cdot 10^{-5} \text{ M}$ and 400 ppm, respectively), but significantly lower pH values

(6–7.5). The authors observed the complete incorporation of Tc(IV) in the structure of magnetite. The differences in the prevailing uptake mechanism observed in this work and in Kobayashi et al. are interpreted in connection with differences in magnetite solubility in both systems. As shown in Figure 5.4, the solubility of magnetite in the pH_c range 6–7.5 ($\text{pe} + \text{pH}_c = 4$, see Figure 5.1) (Kobayashi et al., 2013) is significantly larger than at $\text{pH}_c \sim 9$ ($\text{pe} + \text{pH}_c = 7$, see Figure 5.1) (this work). Higher concentrations of Fe in solution are expected to promote a greater recrystallization rate, thus facilitating the incorporation of Tc(IV) in the structure of magnetite. These observations strongly suggest that the mechanism driving the retention of Tc by magnetite strongly depends on the initial Tc concentration and pH, and to a significantly lesser extent on the loading at the surface of magnetite.

Table 5.2 Structural parameters determined for Tc uptake by magnetite in 0.1 M NaCl and varying $[\text{Tc}]_0$ and loading.

Fe mineral	Sample		Path	CN [†]	R(Å)	$\sigma^2(\text{Å}^2)$	$\Delta E_0(\text{eV})$	%R [‡]
	$[\text{Tc}]_0$	Upload (ppm)						
Magnetite	$2 \cdot 10^{-4}$	400	Tc-O	6.2	2.03	0.0047	3.8	7.3
			Tc-Tc	2.3	2.58	0.0085		
			Tc-Fe ₁	3.0	3.08	0.0100		
			Tc-Fe ₂	4.1	3.52	0.0084		
Magnetite	$2 \cdot 10^{-4}$	600	Tc-O	6.4	2.03	0.0046	3.7	8.1
			Tc-Tc	2.9	2.58	0.0084		
			Tc-Fe ₁	2.6	3.07	0.0100		
			Tc-Fe ₂	4.3	3.52	0.0089		
Magnetite	$2 \cdot 10^{-4}$	900	Tc-O	6.0	2.03	0.0044	4.3	7.9
			Tc-Tc	2.2	2.58	0.0068		
			Tc-Fe ₁	2.9	3.09	0.0100		
			Tc-Fe ₂	4.8	3.53	0.0100		
Magnetite	$2 \cdot 10^{-5}$	400	Tc-O	6.0	2.03	0.0051	3.8	7.3
			Tc-Tc	1.8	2.58	0.0099		
			Tc-Fe ₁	3.6	3.09	0.0100		
			Tc-Fe ₂	5.0	3.51	0.0097		
Magnetite	$2 \cdot 10^{-5}$	600	Tc-O	6.1	2.03	0.0049	3.6	8.5
			Tc-Tc	1.6	2.58	0.0100		
			Tc-Fe ₁	4.0	3.09	0.0100		
			Tc-Fe ₂	4.0	3.51	0.0075		
Magnetite	$2 \cdot 10^{-5}$	900	Tc-O	6.0	2.02	0.0046	3.7	7.6
			Tc-Tc	1.6	2.59	0.0100		
			Tc-Fe ₁	4.8	3.08	0.0100		
			Tc-Fe ₂	3.6	3.51	0.0059		

[†]CN(Coordination number), [‡]R(Residual)

Fit errors: CN: $\pm 25\%$; R: 0.01 Å , σ^2 : 0.002 Å^2

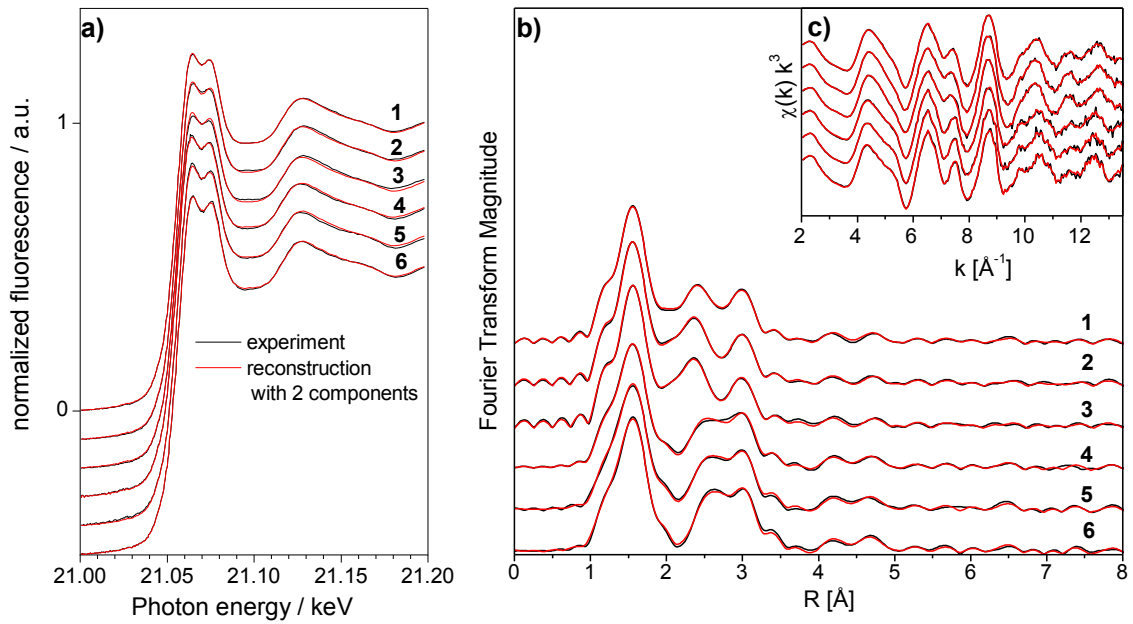


Figure 5.3 Tc-K edge XAS spectra of Tc sorbed on magnetite in 0.1 M NaCl a) XANES, b) k^3 -weighted EXAFS spectra, c) corresponding Fourier Transform magnitude. Black lines represent the experimental data, the red lines represent their reconstruction with two principal components.

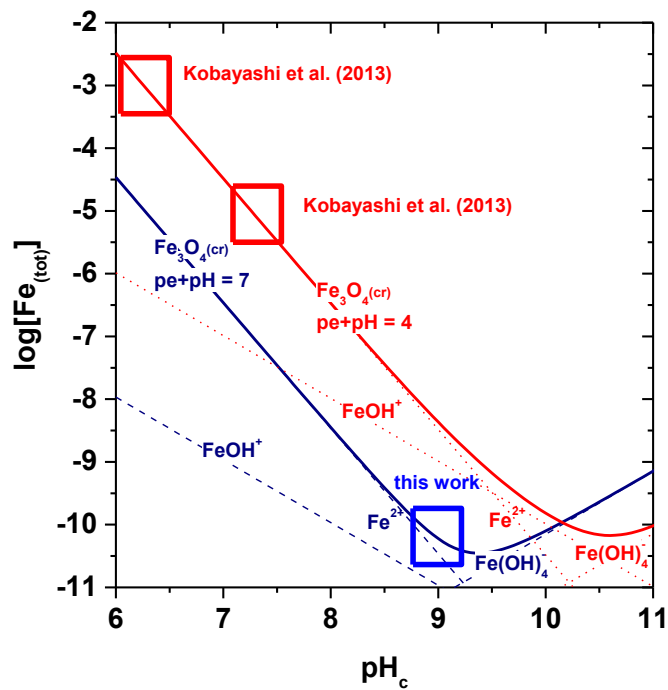


Figure 5.4 Solubility of magnetite ($\text{Fe}_3\text{O}_4(\text{cr})$) calculated for $\text{pe} + \text{pH} = 4$ (red, Kobayashi et al., 2013) and $\text{pe} + \text{pH} = 7$ (blue, this work) using ThermoChimie TDB [106].

5.1.2.2 Mackinawite

Figure 5.5a shows the XANES spectra of Tc K-edge for samples 7 to 12, corresponding to Tc sorbed on mackinawite. As in the case of Tc uptake by magnetite, all investigated mackinawite samples do not show the pre-edge feature at 21050 eV characteristic of Tc(VII), thus indicating the complete reduction of Tc(VII) to Tc(IV) within the timeframe of the experiment. A good reconstruction of the experimental XANES and EXAFS spectra (see Figure 5.5a.) was possible using two different Tc species present in the mackinawite samples. Fourier Transforms and the k^3 -weighted EXAFS spectra for all mackinawite samples with corresponding best fit models are shown in Figure 5.5b and Figure 5.5c, respectively. The structural parameters resulting from the EXAFS fit, using FEFF 8.2 calculated paths of an atomic cluster based on the structure of TcS₂ [107] are shown in Table 5.3. Note that the shortest Tc-S path at 2.30 Å was replaced by Tc-O, and a Tc-Tc path at 2.90 Å was replaced by Tc-Fe to provide the necessary structural flexibility.

Regardless of the initial Tc concentration ($2 \cdot 10^{-4}$ M or $2 \cdot 10^{-5}$ M), and in confirmation of the results of the PCA analysis, the Fourier-transformed spectra show an increase of the peak at $R \approx 1.5$ Å and a decrease of the peak at $R \approx 1.9$ Å (both distances not corrected for phase shift) with increasing Tc loading. These two peaks could be fitted with Tc-O and Tc-S backscattering paths at 2.01 ± 0.01 Å and 2.37 ± 0.01 Å, respectively. The distances fitted for the Tc-S path are in good agreement with data available in the literature for Tc-sulphide compounds (2.30–2.50 Å) [29]. The number of O- and S-backscatterer in the first coordination shell is directly related with the Tc loading. Hence, greater S coordination numbers (and consequently lower O coordination numbers) are fitted for those samples with lower Tc upload, and *vice versa*. The outer shells are fitted with Tc-Fe and Tc-Tc paths at 2.71 ± 0.01 Å and 2.80 ± 0.01 Å, respectively. The Tc-Tc distance is well in line with TcS₂ [107]. The addition of the Tc-Fe shell significantly improved the overall fit. Throughout the experimental conditions, their CNs are small and do not change significantly. Since the distances are larger than the ones expected in mackinawite, these results suggest formation of a mixed Tc-Fe sulphide phase with very limited long-range order.

Analogous species/moieties were previously reported in the literature, based on spectroscopic evidences obtained under different experimental conditions. Kobayashi et al. [73] suggested the formation of a TcS₂-like phase based on their XANES data, in experiments conducted with $[Tc]_0 = 2 \cdot 10^{-5}$ M and 200 ppm Tc loading. With a significantly higher loading (99000 ppm) and $[Tc]_0$ ($1.5 \cdot 10^{-4}$ M), Liu et al. [30] reported the immobilization of Tc by mackinawite as a TcO₂-like phase (Tc-O path at 1.99 ± 0.02 Å with CN = 6). Provided the very high loading and $[Tc]_0$, the main component was identified as TcO₂·xH₂O(s) by the authors. These observations are in line with our experimental data and spectroscopic findings: i) there is a clear and systematic effect of loading on the retention of Tc by mackinawite; ii) a component with predominance of Tc-S interactions in the first shell forms in mackinawite systems with low Tc loadings; iii) TcO₂-like phase (likely surface precipitate or colloidal Tc(IV)) starts to form with increasing loading, becoming predominant at the very high loadings used by Liu and co-workers (99000 ppm). Note that the method used in [73], [30] and in the present work for the synthesis of mackinawite was exactly the same.

5 Reduction and uptake of Tc by Fe(II) minerals in dilute to concentrated saline systems

Table 5.3 Structural parameters determined for Tc uptake by mackinawite in 0.1 M NaCl and varying $[Tc]_0$ and loading.

Sample			Path	CN [†]	R(Å)	$\sigma^2(\text{Å}^2)$	$\Delta E_0(\text{eV})$	%R [‡]
Fe mineral	$[Tc]_0$	Upload (ppm)						
Mackinawite	$2 \cdot 10^{-4}$	400	Tc-O	1.8	2.00	0.01	5.6	5.2
			Tc-S	4.2	2.37	0.0036		
			Tc-Fe	0.3	2.71	0.0025		
			Tc-Tc	0.5	2.80	0.0025		
Mackinawite	$2 \cdot 10^{-4}$	600	Tc-O	1.7	2.01	0.01	6.0	5.7
			Tc-S	4.3	2.37	0.0065		
			Tc-Fe	0.4	2.74	0.0032		
			Tc-Tc	0.9	2.80	0.0032		
Mackinawite	$2 \cdot 10^{-4}$	900	Tc-O	3.0	2.02	0.01	5.2	6.5
			Tc-S	3.0	2.37	0.0064		
			Tc-Fe	0.5	2.70	0.0024		
			Tc-Tc	0.4	2.80	0.0024		
Mackinawite	$2 \cdot 10^{-5}$	400	Tc-O	1.5	2.01	0.01	6.0	4.8
			Tc-S	4.5	2.37	0.007		
			Tc-Fe	0.4	2.70	0.0035		
			Tc-Tc	0.7	2.80	0.0035		
Mackinawite	$2 \cdot 10^{-5}$	600	Tc-O	2.0	2.01	0.01	5.8	5.4
			Tc-S	4.0	2.37	0.0077		
			Tc-Fe	0.6	2.71	0.0041		
			Tc-Tc	0.8	2.80	0.0041		
Mackinawite	$2 \cdot 10^{-5}$	900	Tc-O	2.8	2.02	0.01	5.4	5.6
			Tc-S	3.2	2.37	0.0068		
			Tc-Fe	0.6	2.71	0.0038		
			Tc-Tc	0.7	2.80	0.0038		

[†]CN(Coordination number), [‡]R(Residual)

Fit errors: CN: $\pm 25\%$;R:0.01 Å, σ^2 : 0.002 Å²

In contrast to these observations, Livens et al. [31] reported the formation of a TcS₂-like phase ($d_{Tc-S} = 2.42 \pm 0.02$ Å and CN = 6) in the presence of relatively high loadings (10000 ppm) of Tc on 300 mg mackinawite. A direct comparison of the data by Livens and co-workers with the present study cannot be accomplished, because of the different method used for the synthesis of mackinawite and the very limited experimental description provided by the authors, which (among others) omits information on S:L, $[Tc]_0$ and pH.

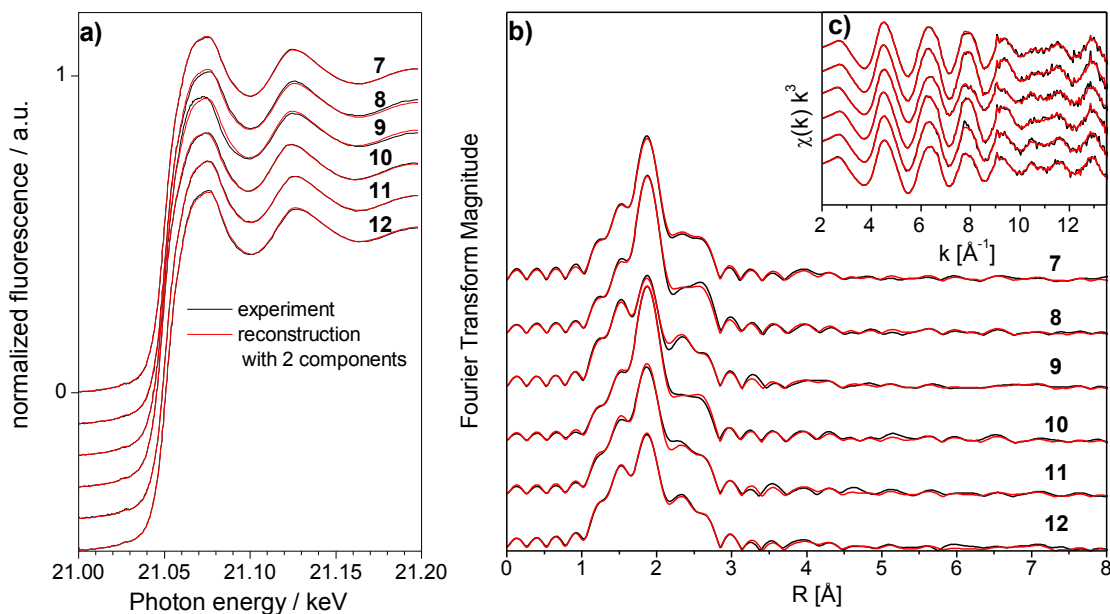


Figure 5.5 Tc-K edge XAS spectra of Tc sorbed on mackinawite in 0.1 M NaCl a) XANES, b) k^3 -weighted EXAFS spectra, c) corresponding Fourier Transform magnitude. Black lines represent the experimental data, the red lines represent their reconstruction with two principal components.

5.2 Reduction and uptake of Tc by magnetite, mackinawite and siderite in concentrated NaCl and MgCl₂ solutions

5.2.1 Quantitative evaluation of the wet chemistry data

E_h and pH_c values measured in the Fe mineral suspensions (magnetite, mackinawite and siderite) with Tc after 4 weeks equilibration time are summarized in Table 5.4 and Figure 5.6. In all cases, experimental E_h values are below the observed Tc(VII)/Tc(IV) reduction borderline. In analogy to previous observations for other reducing systems reported in this work (see chapter 3), E_h values in 4.5 M MgCl₂ media are significantly higher than in 5.0 M NaCl (~2 pe-units) at the same pH_c . As discussed previously, this observation can be attributed to the impact of high [Cl⁻] and/or [Mg²⁺] on the redox couple controlling the redox conditions of the system.

R_d values (calculated as $R_d = \frac{[Tc]_s}{[Tc]_{aq}} \cdot \frac{V}{m}$ ($L \cdot kg^{-1}$)) for the uptake of Tc by Fe phases in 5.0 M NaCl and 4.5 M MgCl₂ have been calculated under the assumption of final sample equilibration and no interfering solubility processes. These preliminary exercises are summarized in Table 5.4 and need to be confirmed in further studies. According to the calculation, a stronger uptake is observed in 5.0 M NaCl ($4.6 \leq \log R_d$ ($L \cdot kg^{-1}$) ≤ 7.2) compared to sorption samples in 4.5 M MgCl₂ ($3.0 \leq \log R_d$ ($L \cdot kg^{-1}$) ≤ 4.1).

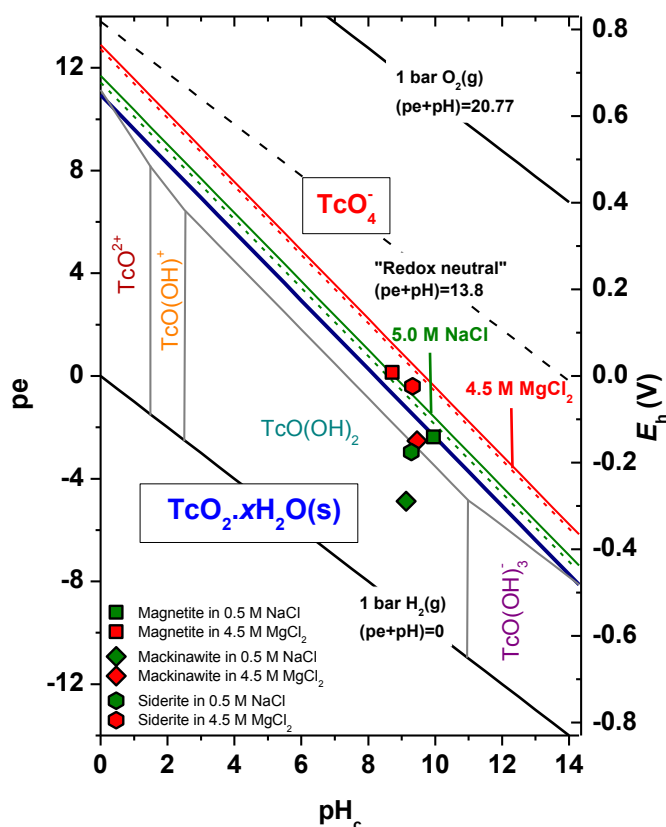


Figure 5.6 Measured pH_c and E_h values of Tc sorbed magnetite, mackinawite and siderite (after 4 weeks equilibration time) in 5.0 M NaCl and 4.5 M MgCl_2 solutions. Solid blue line represents the 50:50 equilibrium line between Tc(VII)/Tc(IV) oxidation states reaction with; $\text{TcO}_4^- + 4 \text{H}^+ + 3\text{e}^- \leftrightarrow \text{TcO}_2 \cdot 1.6\text{H}_2\text{O}(\text{s}) + 0.4 \text{H}_2\text{O}$ calculated with NEA-TDB at $I = 0$. Black solid lines indicate upper and lower decomposition lines of water and “redox neutral” ($\text{pe} + \text{pH} = 13.8$) conditions. Dashed and solid lines correspond to Tc(VII)/Tc(IV) borderlines considering reaction (3.1), calculated by SIT and Pitzer approaches for $I = 5.0 \text{ M NaCl}$ (green dashed line: SIT, green solid line: Pitzer) and $I = 13.5 \text{ M MgCl}_2$ (red dashed line: SIT, red solid line: Pitzer).

Table 5.4 pH_c , E_h and $\log R_d$ values determined for the uptake of Tc by Fe minerals (after 4 weeks of equilibration time).

Fe mineral	Background Electrolyte	pH_c^a	E_h (mV) ^b	$\log R_d$ ($\text{L} \cdot \text{kg}^{-1}$) ^c
Magnetite	5.0 M NaCl	9.6	-140	4.7
Magnetite	4.5 M MgCl_2	8.7	10	3.0
Mackinawite	5.0 M NaCl	8.7	-290	7.2
Mackinawite	4.5 M MgCl_2	8.3	-150	4.1
Siderite	5.0 M NaCl	8.7	-175	6.0
Siderite	4.5 M MgCl_2	8.3	-25	3.8

a: ± 0.05 ; **b:** $\pm 50 \text{ mV}$; **c:** $\pm 10\%$ for $\log R_d \leq 3$; $\pm 50\%$ for $\log R_d \geq 3$

5.2.2 Redox speciation of Tc taken up by Fe(II) minerals: XANES

Figure 5.7 shows the Tc K-edge XANES spectra collected for Tc(VII) reacted with Fe(II) minerals. Note that the spectra were collected at a sample temperature of 10-15 K in He atmosphere to prevent changes of Tc oxidation state induced by atmospheric O₂ or by O-radicals produced by the high X-ray photon flux. All mineral samples have an edge position near 21058 keV and a white line position at 21065 to 21070 eV in line with Tc(IV), while the distinct pre-edge peak of Tc(VII) at 21050 keV is absent in these samples. Accordingly, Tc(VII) has been reduced to Tc(IV) in all the samples. The edge and white line positions as well as the fine structure is furthermore suggesting a coordination to O atoms; therefore, we find no evidence for the (partial) coordination of Tc(IV) by S atoms in the high-salt mackinawite systems. This is in contrast to previous findings at lower ionic strengths in this work and in the literature, where formation of a TcS₂-like phase was found after precipitating mackinawite in the presence of pertechnetate [29]. Tc(IV) coordinated to S was also found after sorption of pertechnetate to mackinawite at an ionic strength of 0.1 M [31, 73], pointing to a decisive role of ionic strength on the reaction product. This aspect relevant to high ionic strength conditions needs confirmation by more detailed investigations.

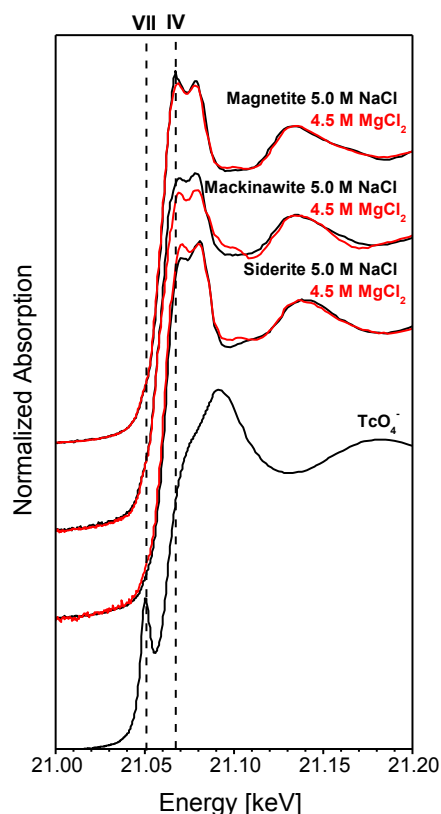


Figure 5.7 Tc K-edge XANES spectra of Tc(VII) reacted with magnetite, mackinawite and siderite in saline solutions.

5.3 Conclusion for Tc uptake studies by Fe(II) minerals

Tc reduction and uptake mechanisms by Fe(II) minerals (magnetite, mackinawite and siderite) were investigated in 0.1 M NaCl, 5.0 M NaCl and 4.5 M MgCl₂ systems. The results show that Tc(VII) is reduced to Tc(IV) in contact with these minerals in all investigated systems regardless of initial [Tc]₀, S:L and ionic strength. The observed reduction is also consistent with the Tc(VII)/Tc(IV) borderline thermodynamically calculated for each ionic strength.

In dilute NaCl systems, EXAFS data shows that the mechanism of Tc(IV) retention by magnetite and mackinawite is strongly dependent on the loading, [Tc]₀ and pH. Hence, Tc(IV) partly incorporates into the structure of magnetite at low [Tc]₀ ($2 \cdot 10^{-5}$ M), but forms TcO₂-dimers/ polymers at [Tc]₀ = $2 \cdot 10^{-4}$ M. A larger incorporated fraction is observed in those conditions favouring a higher solubility of magnetite (and thus a greater recrystallization degree), i.e. lower pH and E_h . No clear effect of loading has been observed for the uptake of Tc by this mineral. In contrast to magnetite, [Tc]₀ has no clear impact on the neighbouring atoms of Tc in mackinawite systems. Loading affects significantly the Tc retention mechanism in mackinawite systems: a TcS₂-like phase prevails at low loadings (400 ppm), whereas higher loadings favour the predominance of TcO₂-like phases, likely surface precipitates of colloidal Tc(IV) species.

In concentrated NaCl and MgCl₂ systems, Tc(VII) is reduced by magnetite, mackinawite and siderite under mildly alkaline conditions. Measured Tc concentration in the aqueous phase after 4 weeks equilibrium is significantly higher in 4.5 MgCl₂ solution than dilute systems or concentrated NaCl solutions. A similar behaviour is observed in Tc(VII)/Tc(IV) redox studies in the presence of reducing chemicals, as summarized in Chapter 3.

These results provide a very relevant step forward in the mechanistic understanding of Tc reduction/uptake by Fe(II) minerals relevant in the context of radioactive waste disposal.

6 Summary and Conclusion

This PhD thesis has successfully addressed three fundamental processes affecting the behaviour of technetium in the context of nuclear waste disposal, (i) redox transformations, (ii) solubility phenomena and (iii) sorption effects. As all these processes have been systematically evaluated from dilute solutions to concentrated saline systems (NaCl, MgCl₂ and CaCl₂), special attention has been dedicated to concentrated salt brine systems because of the drastic lack of previous studies and the potential relevance in the context of nuclear waste disposal in salt-rock formations. The results are described and quantified in terms of equilibrium thermodynamics of aqueous systems using both SIT and Pitzer to address ion-interaction processes. The thermodynamic data and model parameters derived in this work contribute to national and international database projects and significantly improve model calculations on Tc under repository relevant conditions. Relevant contribution of specific interphase processes and surface equilibria were identified in the case of the Tc sorption studies on iron minerals.

Redox behaviour of Tc(VII)/Tc(IV) was systematically investigated in the presence of different reducing chemical systems over the entire pH region in dilute to concentrated NaCl and MgCl₂ solutions in the first part of this work. Measured pH and E_h values were compared to thermodynamic calculations using NEA–TDB data selection and SIT/Pitzer activity models for Tc(VII) reported in the literature. The reduction of Tc(VII) to Tc(IV) was assessed by following the decrease in $[Tc]_0$ due to the formation of sparingly soluble oxo-hydroxides of Tc(IV), in combination with a solvent extraction method. The results show a good agreement between experimental E_h -pH measurements and thermodynamic calculations, thus highlighting the potential of using $pe + pH$ measurements as an accurate tools to predict the redox distribution of Tc in dilute solutions to concentrated saline systems. Experiments also confirm the reduction of Tc(VII) to Tc(IV) in MgCl₂ and NaCl concentrated brines under repository-relevant pH and E_h conditions, although strong kinetics are observed in MgCl₂ systems for those samples at the highest pH ($pH_c \approx pH_{max}$). This observation indicates the need of performing complementary undersaturation solubility experiments for deriving reliable thermodynamic and activity models for these systems.

Solubility and hydrolysis of Tc(IV) in dilute to concentrated saline systems was investigated in the second part of this PhD thesis. Information on redox transformations derived from the Tc redox experiments undertaken in the first part of this work enabled to adopt adequate redox conditions to ensure the predominance of Tc(IV) throughout the undersaturation solubility experiments. The experimentally measured solubility of Tc(IV) in dilute NaCl, MgCl₂ and CaCl₂ solutions agree very well with experimental data previously reported and with thermodynamic calculations considering NEA–TDB selection. The solubility curves show a typical amphoteric behaviour involving the formation of cationic and anionic hydrolysis species under acidic and alkaline pH conditions, respectively. In the neutral pH region, the pH-independent behaviour of the solubility is attributed to the chemical reaction $TcO_2 \cdot 1.6H_2O(s) \Leftrightarrow TcO(OH)_2(aq) + 0.6H_2O$ with a $\log^* K_{s,TcO(OH)_2}^\circ$ in good agreement with NEA–TDB data selection. With increasing ionic strength, a very significant increase in the solubility (up to 4 orders of magnitude) is observed following a well-defined slope of -2 in the acidic pH range. This observation is explained with the formation of the polynuclear species $Tc_3O_5^{2+}$,

which is supported by previous spectroscopic evidence published after the last update book of NEA–TDB. In alkaline MgCl_2 and CaCl_2 systems, a pronounced increase of the solubility close to the respective maximum pH values is explained by the formation of $\text{Mg}_3[\text{TcO}(\text{OH})_5]^{3+}$ and $\text{Ca}_3[\text{TcO}(\text{OH})_5]^{3+}$ species, based on slope analysis, model calculations and the analogy with An(IV) and Zr(IV) systems where similar ternary species were reported. The very slow kinetics observed at $\text{pH}_m \geq 10.5$ in concentrated CaCl_2 systems may indicate towards a slow solid phase transformation process, although further investigations are needed to confirm this hypothesis. Based on the newly generated experimental data, comprehensive chemical, thermodynamic and activity models using both SIT and Pitzer approaches are derived for the system Tc^{4+} – Na^+ – Mg^{2+} – Ca^{2+} – H^+ – Cl^- – OH^- – H_2O at 25 °C. These data represent a clear improvement with respect to the previous NEA–TDB thermodynamic selection, especially in view of the chemical models available in acidic conditions and concentrated alkaline brines, and the availability of complete activity models valid for NaCl, MgCl_2 and CaCl_2 background electrolytes. An experimentally well supported Pitzer model for Tc(IV) is made available within this study for the first time and will importantly impact the modelling of Tc(IV) chemistry in salt brine systems.

Tc reduction and uptake of Tc by Fe(II) minerals (magnetite, mackinawite and siderite) were investigated in 0.1 M NaCl, 5.0 M NaCl and 4.5 M MgCl_2 systems in the third part of this work. Tc(VII) is reduced to Tc(IV) by all considered Fe(II) minerals regardless of initial technetium concentration ($[\text{Tc}]_0$), solid to liquid ratio (S:L) and ionic strength. In spite of the observed reduction, sorption is found to be weaker in concentrated brine systems (5.0 M NaCl and 4.5 M MgCl_2), consistently with the higher solubility observed for the same systems in the second part of this thesis. Systematic experiments performed with magnetite and mackinawite in dilute NaCl systems as a function of S:L and initial technetium concentration indicate that the mechanism of Tc(IV) retention is strongly dependent on loading, $[\text{Tc}]_0$ and pH. In the magnetite system, $[\text{Tc}]_0$ and pH control the uptake mechanism as incorporation or surface reaction. Loading plays an important role for technetium retention by mackinawite, leading to the formation of TcO_2 -like or TcS_2 -like phases at high and low Tc concentration levels, respectively. These results highlight the need of coupling classical wet-chemistry techniques with advanced spectroscopic methods when assessing sorption processes and deriving an advanced model description beyond the limited “ K_d approach”.

Appendix

Appendix I

The formulism of the terms in the Pitzer equations;

$$F = -A^\phi \left[\frac{I^{1/2}}{1+bI^{1/2}} + \frac{2}{b} \ln(1+bI^{1/2}) \right] + \sum_c \sum_a m_c m_a B'_{ca} + \sum_{c<} \sum_{c'} m_c m_{c'} \Phi_{cc'} + \sum_{a<} \sum_{a'} m_a m_{a'} \Phi_{aa'} \quad (\text{AI.1})$$

$$B_{MX} = \beta_{MX}^{(0)} + \beta_{MX}^{(1)} f(\alpha_1 I^{1/2}) + \beta_{MX}^{(2)} f(\alpha_2 I^{1/2}) \quad (\text{AI.2})$$

$$B'_{MX} = [\beta_{MX}^{(1)} f'(\alpha_1 I^{1/2}) + \beta_{MX}^{(2)} f'(\alpha_2 I^{1/2})] / I \quad (\text{AI.3})$$

with

$$f(x) = 2 [1 - (1+x) \exp(-x)] / x^2 \quad (\text{AI.4})$$

$$f'(x) = -2 [1 - (1+x+x^2/2) \exp(-x)] / x^2 \quad (\text{AI.5})$$

and

$$C_{MX} = C_{MX}^\phi / 2 |z_M z_X|^{1/2} \quad (\text{AI.6})$$

A^ϕ is the Debye-Hückel constant for the osmotic coefficient 0.3915 at 25 °C, b is the universal parameter with the value of $1.2 \text{ kg}^{1/2} \cdot \text{mol}^{1/2}$, α_1 has the value of $2.0 \text{ kg}^{1/2} \cdot \text{mol}^{1/2}$ for 1-1, 2-1, 3-1 and even 4-1 salts (but $\alpha_1 = 1.4 \text{ kg}^{1/2} \cdot \text{mol}^{1/2}$ and $\alpha_2 = 12 \text{ kg}^{1/2} \cdot \text{mol}^{1/2}$ for the 2-2 electrolytes). The mixing coefficient for identically charged species is written as Eq (AI.7)

$$\Phi_{ij} = \theta_{ij} + {}^E\theta_{ij}(I) \quad (\text{AI.7})$$

$$\Phi_{ij}^\phi = \theta_{ij} + {}^E\theta_{ij}(I) + I {}^E\theta'_{ij}(I) \quad (\text{AI.8})$$

$$\Phi'_{ij} = {}^E\theta'_{ij}(I) \quad (\text{AI.9})$$

θ_{ij} is a coefficient only for anion-anion or cation-cation interactions. The electrostatic unsymmetrical effects ${}^E\theta_{ij}(I)$ and ${}^E\theta'_{ij}(I)$ are given as;

$${}^E\theta_{MN}(I) = \frac{z_M z_N}{4I} \left[J(x_{MN}) - \frac{1}{2} J(x_{MM}) - \frac{1}{2} J(x_{NN}) \right] \quad (\text{AI.10})$$

$${}^E\theta'_{MN}(I) = \frac{z_M z_N}{8I^2} \left[J'(x_{MN}) - \frac{1}{2} J'(x_{MM}) - \frac{1}{2} J'(x_{NN}) \right] - \frac{{}^E\theta_{MN}}{I} \quad (\text{AI.11})$$

If $z_M = z_N$, ${}^E\theta_{ij}(I) = {}^E\theta'_{ij}(I) = 0$. The value of $J(x)$ and $J'(x)$ can be calculated using two Chebyshev polynomial approximation reported in [41].

The activity coefficient for neutral species N is calculated by Eq (AI.12).

$$\ln \gamma_N = 2 (\sum_c m_c \lambda_{Nc} + \sum_a m_a \lambda_{Na} + \sum_n m_n \lambda_{Xn}) \quad (\text{AI.12})$$

Appendix II

Table A. I Thermodynamic data for Fe(II)/Fe(III) used to calculate Fe systems at acidic conditions.

Reaction	$\log^* K^\circ$	Reference
$\text{Fe}^{2+} \leftrightarrow \text{Fe}^{3+} + \text{e}^-$	-13.05	NEA-TDB [108]
$\text{Fe}^{3+} + \text{Cl}^- \leftrightarrow \text{FeCl}^{2+}$	1.52	NEA-TDB [108]
$\text{Fe}^{3+} + 2\text{Cl}^- \leftrightarrow \text{FeCl}_2^+$	2.22	NEA-TDB [108]
$\text{Fe}^{3+} + \text{H}_2\text{O} \leftrightarrow \text{FeOH}^{2+} + \text{H}^+$	-2.15	NEA-TDB [108]

Table A. II SIT ion interaction coefficients for Fe species in NaCl solutions.

<i>i</i>	<i>j</i>	$\epsilon_{ij} (\text{mol kg}^{-1})$	Reference
H^+	Cl^-	0.12	NEA-TDB [35]
OH^-	Na^+	0.04	NEA-TDB [35]
Fe^{3+}	Cl^-	0.24	estimated from $\epsilon(\text{Fe}^{3+}, \text{ClO}_4^-) = 0.56$ ^{a)}
Fe^{2+}	Cl^-	0.16	estimated from $\epsilon(\text{Fe}^{2+}, \text{ClO}_4^-) = 0.38$ ^{a)}
FeCl^{2+}	Cl^-	0.15	estimated by charge correlation ^{b)}
FeCl_2^+	Cl^-	0.05	estimated by charge correlation ^{b)}
FeOH^{2+}	Cl^-	0.15	estimated by charge correlation ^{b)}

^{a)} The SIT coefficients for the interaction with Cl^- are estimated from the corresponding SIT coefficients for the interaction with ClO_4^- [35] according with the correlation: $\epsilon(\text{M}^{z+}, \text{Cl}^-) = 0.38 \epsilon(\text{M}^{z+}, \text{ClO}_4^-) \pm 0.02 \text{ mol kg}^{-1}$ [109].

^{b)} [53]

References

- [1] Bundesamt für Strahlenschutz; Radioactive waste disposal – survey of the geology of potential host rocks. 2013; Available from: <http://www.bfs.de/>.
- [2] Metz, V., Geckeis, H., Gonzalez-Robles, E., Loida, A., Bube, C. and Kienzler, B., Radionuclide behaviour in the near-field of a geological repository for spent nuclear fuel, *Radiochimica Acta*, **100**, 699-713, (2012).
- [3] Wieland, E. and Van Loon, L. R., Cementitious Near-Field Sorption Data Base for Performance Assessment of an ILW Repository in Opalinus Clay, PSI-Cericht 03-06, (2006).
- [4] Ackermann, J., Hagenbach, A. and Abram, U., Nitrosyltechnetium complexes with (2-aminomethylphenyl)diphenylphosphine, *Inorganica Chimica Acta*, **419**, 59-65, (2014).
- [5] Balasekaran, S. M., Fluorido complexes of technetium, 2013, Freie Universität Berlin Berlin.
- [6] Alberto, R., Schibli, R., Egli, A., Schubiger, A. P., Abram, U. and Kaden, T. A., A novel organometallic aqua complex of technetium for the labeling of biomolecules: Synthesis of $[\text{Tc}^{99\text{m}}(\text{OH}_2)_3(\text{CO})_3]^+$ from $[(\text{Tc}^{99\text{m}}\text{O}_4)]^-$ in aqueous solution and its reaction with a bifunctional ligand, *Journal of the American Chemical Society*, **120**, 7987-7988, (1998).
- [7] Fernandez, S., Gigio, J., Cerecetto, H. and Rey, A., Development of a $\text{Tc}^{99\text{m}}(\text{I})$ -tricarbonyl complex as potential agent for hypoxia imaging, *Nuclear Medicine and Biology*, **41**, 619-619, (2014).
- [8] Fernandez, L., Reyes, L. and Teran, M., Radiolabeling and biological evaluation of amphotericin using $\text{fac}[\text{Tc}^{99\text{m}}(\text{I})(\text{H}_2\text{O})_3(\text{CO})_3]^+$, *Nuclear Medicine and Biology*, **41**, 619-619, (2014).
- [9] El-Zaria, M. E., Janzen, N. and Valliant, J. F., Room-Temperature Synthesis of $\text{Re}(\text{I})$ and $\text{Tc}(\text{I})$ Metallocarboranes, *Organometallics*, **31**, 5940-5949, (2012).
- [10] Lukens, W. W., Shuh, D. K., Schroeder, N. C. and Ashley, K. R., Identification of the non-pertechnetate species in Hanford waste tanks, $\text{Tc}(\text{I})$ -carbonyl complexes, *Environmental Science & Technology*, **38**, 229-233, (2004).
- [11] Schroeder, N. C. and Ashley, K. R., Separation of non-pertechnetate species from Hanford AN-107 tank waste, *Journal of Radioanalytical and Nuclear Chemistry*, **263**, 567-573, (2005).
- [12] Lukens, W. W., Bucher, J. J., Edelstein, N. M. and Shuh, D. K., Products of pertechnetate radiolysis in highly alkaline solution: Structure of $\text{TcO}_2 \cdot \text{H}_2\text{O}$, *Environmental Science & Technology*, **36**, 1124-1129, (2002).
- [13] Poineau, F., Fattahi, M., Auwer, C. D., Hennig, C. and Grambow, B., Speciation of technetium and rhenium complexes by in situ XAS-electrochemistry, *Radiochimica Acta*, **94**, 283-289, (2006).

- [14] Rard, J. A., Rand, M. H., Anderegg, G. and Wanner, H., Chemical thermodynamics of technetium, ed. M. C. A. Sandino and E. Östhols. Vol. 3. North-Holland, Amsterdam, Elsevier, (1999).
- [15] Shannon, J. C. Database of ionic radii. 1976; Available from:
<http://abulafia.mt.ic.ac.uk/shannon/ptable.php>.
- [16] Abdelouas, A. and Grambow, B., Aquatic chemistry of long-lived mobile fission and activation products in the context of deep geological disposal. Aquatic chemistry in the context of deep geological disposal, ed. P. Christophe and G. Horst, Cambridge, UK, Woodhead Publishing, (2012).
- [17] LANL. Periodic Table of Elements: LANL. 2014; Available from:
<http://periodic.lanl.gov/43.shtml>.
- [18] Guillaumont, R., Fanghänel, T., Fuger, J., Grenthe, I., Neck, V., Palmer, D. A. and Rand, M. H., Update on the Chemical Thermodynamics of U, Np, Pu, Am and Tc. Vol.5 of Chemical Thermodynamics(2003), Amsterdam: Elsevier.
- [19] Chen, F. R., Burns, P. C. and Ewing, R. C., Near-field behavior of Tc-99 during the oxidative alteration of spent nuclear fuel, *Journal of Nuclear Materials*, **278**, 225-232, (2000).
- [20] Neck, V., Altmaier, M. and Fanghänel, T., Solubility of plutonium hydroxides/hydrous oxides under reducing conditions and in the presence of oxygen, *Comptes Rendus Chimie*, **10**, 959-977, (2007).
- [21] Poineau, F., Fattahi, M., Den Auwer, C., Hennig, C. and Grambow, B., Speciation of technetium and rhenium complexes by in situ XAS-electrochemistry, *Radiochimica Acta*, **94**, 283-289, (2006).
- [22] Chotkowski, M. and Czerwinski, A., Electrochemical and spectroelectrochemical studies of pertechnetate electroreduction in acidic media, *Electrochimica Acta*, **76**, 165-173, (2012).
- [23] Owunwanne, A., Marinsky, J. and Blau, M., Charge and nature of technetium species produced in reduction of pertechnetate by stannous Ion, *Journal of Nuclear Medicine*, **18**, 1099-1105, (1977).
- [24] Warwick, P., Aldridge, S., Evans, N. and Vines, S., The solubility of technetium(IV) at high pH, *Radiochimica Acta*, **95**, 709-716, (2007).
- [25] Cui, D. Q. and Eriksen, T. E., Reduction of pertechnetate by ferrous iron in solution: Influence of sorbed and precipitated Fe(II), *Environmental Science & Technology*, **30**, 2259-2262, (1996).
- [26] Zachara, J. M., Heald, S. M., Jeon, B. H., Kukkadapu, R. K., Liu, C. X., McKinley, J. P., Dohnalkova, A. C. and Moore, D. A., Reduction of pertechnetate [Tc(VII)] by aqueous Fe(II) and the nature of solid phase redox products, *Geochimica Et Cosmochimica Acta*, **71**, 2137-2157, (2007).
- [27] Ben Said, K., Fattahi, M., Musikas, C., Delorme-Hiver, A. and Abbe, J. C., A novel approach to the oxidation potential of the Tc(VII)/Tc(IV) couple in hydrochloric acid medium through the reduction of TcO_4^- by Fe^{2+} ion, *Radiochimica Acta*, **83**, 195-203, (1998).

- [28] Um, W., Chang, H. S., Icenhower, J. P., Lukens, W. W., Serne, R. J., Qafoku, N. P., Westsik, J. H., Buck, E. C. and Smith, S. C., Immobilization of 99-Techneium (VII) by Fe(II)-Goethite and Limited Reoxidation, *Environmental Science & Technology*, **45**, 4904-4913, (2011).
- [29] Wharton, M. J., Atkins, B., Charnock, J. M., Livens, F. R., Patrick, R. A. D. and Collison, D., An X-ray absorption spectroscopy study of the coprecipitation of Tc and Re with mackinawite (FeS), *Applied Geochemistry*, **15**, 347-354, (2000).
- [30] Liu, Y., Terry, J. and Jurisson, S., Pertechnetate immobilization with amorphous iron sulfide, *Radiochimica Acta*, **96**, 823-833, (2008).
- [31] Livens, F. R., Jones, M. J., Hynes, A. J., Charnock, J. M., Mosselmans, J. F. W., Hennig, C., Steele, H., Collison, D., Vaughan, D. J., Patrick, R. A. D., Reed, W. A. and Moyes, L. N., X-ray absorption spectroscopy studies of reactions of technetium, uranium and neptunium with mackinawite, *Journal of Environmental Radioactivity*, **74**, 211-219, (2004).
- [32] McBeth, J. M., Lloyd, J. R., Law, G. T. W., Livens, F. R., Burke, I. T. and Morris, K., Redox interactions of technetium with iron-bearing minerals, *Mineralogical Magazine*, **75**, 2419-2430, (2011).
- [33] Llorens, I. A., Deniard, P., Gautron, E., Olicard, A., Fattahi, M., Jobic, S. and Grambow, B., Structural investigation of coprecipitation of technetium-99 with iron phases, *Radiochimica Acta*, **96**, 569-574, (2008).
- [34] Kobayashi, T., Scheinost, A. C., Fellhauer, D., Gaona, X. and Altmaier, M., Redox behavior of Tc(VII)/Tc(IV) under various reducing conditions in 0.1 M NaCl solutions, *Radiochimica Acta*, **101**, 323-332, (2013).
- [35] Guillaumont, R., Fanghänel, T., Neck, V., Fuger, J., Palmer, D. A., Grenthe, I. and Rand, M. H., Update on the chemical thermodynamics of uranium, neptunium, plutonium, americium and technetium, ed. OECD Nuclear Energy Agency. Vol. 5. North-Holland, Amsterdam, Elsevier, (2003).
- [36] Ciavatta, L., The specific interaction theory in equilibrium-analysis - some empirical rules for estimating interaction coefficients of metal-ion complexes, *Annali Di Chimica*, **80**, 255-263, (1990).
- [37] Grenthe, I., Wanner, H. and Östhols, M., Guidelines for the extrapolation to zero ionic strength, Nuclear Energy Agency, OECD, (2000).
- [38] Neck, V., Altmaier, M., Rabung, T., Lützenkirchen, J. and Fanghänel, T., Thermodynamics of trivalent actinides and neodymium in NaCl, MgCl₂, and CaCl₂ solutions: Solubility, hydrolysis, and ternary Ca-M(III)-OH complexes, *Pure and Applied Chemistry*, **81**, 1555-1568, (2009).
- [39] Fellhauer, D., Neck, V., Altmaier, M., Lützenkirchen, J. and Fanghänel, T., Solubility of tetravalent actinides in alkaline CaCl₂ solutions and formation of Ca₄[An(OH)₈]⁴⁺ complexes: A study of Np(IV) and Pu(IV) under reducing conditions and the systematic trend in the An(IV) series, *Radiochimica Acta*, **98**, 541-548, (2010).

- [40] Brendebach, B., Altmaier, M., Rothe, J., Neck, V. and Denecke, M. A., EXAFS study of aqueous Zr-IV and Th-IV complexes in alkaline CaCl₂ solutions: Ca₃[Zr(OH)₆]⁴⁺ and Ca₄[Th(OH)₈]⁴⁺, *Inorganic Chemistry*, **46**, 6804-6810, (2007).
- [41] Pitzer, K. S., Activity coefficients in electrolyte solutions. Chap. 3, Boca Raton, FL, (1991).
- [42] Meyer, R. E., Arnold, W. D., Case, F. I. and Okelley, G. D., Solubilities of Tc(IV) Oxides, *Radiochimica Acta*, **55**, 11-18, (1991).
- [43] Eriksen, T. E., Ndalamba, P., Bruno, J. and Caceci, M., The Solubility of TcO₂ · nH₂O in Neutral to Alkaline-Solutions under Constant *p*CO₂, *Radiochimica Acta*, **58-9**, 67-70, (1992).
- [44] Vichot, L., Ouvrard, G., Montavon, G., Fattahi, M., Musikas, C. and Grambow, B., XAS study of technetium(IV) polymer formation in mixed sulphate/chloride media, *Radiochimica Acta*, **90**, 575-579, (2002).
- [45] Vichot, L., Fattahi, M., Musikas, C. and Grambow, B., Tc(IV) chemistry in mixed chloride/sulphate acidic media. Formation of polyoxopolymetallic species, *Radiochimica Acta*, **91**, 263-271, (2003).
- [46] Poineau, F., Fattahi, M. and Grambow, B., Correlation between X-ray chemical shift and partial charge in Tc(IV) complexes: Determination of Tc partial charge in Tc_nO_y^{(4n-2y)+}, *Radiochimica Acta*, **94**, 559-563, (2006).
- [47] Poineau, F., Fattahi, M. and Grambow, B., Photochemical behaviour of Tc₂OCl₁₀⁴⁻ and Tc_nO_y^{4n-2y+} in chloride media, *Radiochimica Acta*, **94**, 91-95, (2006).
- [48] Geckeis, H., Lutzenkirchen, J., Polly, R., Rabung, T. and Schmidt, M., Mineral-Water Interface Reactions of Actinides, *Chemical Reviews*, **113**, 1016-1062, (2013).
- [49] Cui, D. Q. and Eriksen, T. E., Reduction of pertechnetate in solution by heterogeneous electron transfer from Fe(II)-containing geological material, *Environmental Science & Technology*, **30**, 2263-2269, (1996).
- [50] Geraedts, K., Bruggeman, C., Maes, A., Van Loon, L. R., Rossberg, A. and Reich, T., Evidence for the existence of Tc(IV) - humic substance species by X-ray absorption near-edge spectroscopy, *Radiochimica Acta*, **90**, 879-884, (2002).
- [51] Maes, A., Geraedts, K., Bruggeman, C., Vancluysen, J., Rossberg, A. and Hennig, C., Evidence for the interaction of technetium colloids with humic substances by X-ray absorption spectroscopy, *Environmental Science & Technology*, **38**, 2044-2051, (2004).
- [52] Peretyazhko, T. S., Zachara, J. M., Kukkadapu, R. K., Heald, S. M., Kutnyakov, I. V., Resch, C. T., Arey, B. W., Wang, C. M., Kovarik, L., Phillips, J. L. and Moore, D. A., Pertechnetate (TcO₄⁻) reduction by reactive ferrous iron forms in naturally anoxic, redox transition zone sediments from the Hanford Site, USA, *Geochimica Et Cosmochimica Acta*, **92**, 48-66, (2012).

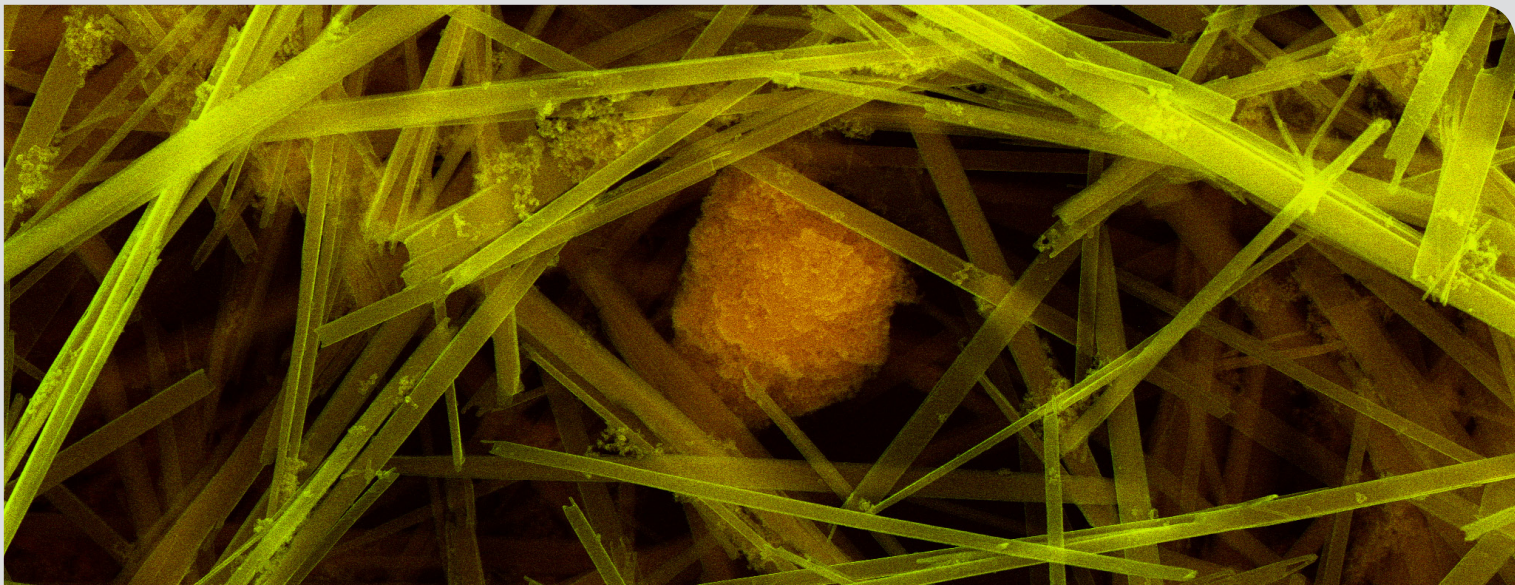
- [53] Hummel, W., Ionic strength corrections and estimation of SIT ion interaction coefficients, TM-44-09-01, (2009).
- [54] Jolivet, J. P., Belleville, P., Tronc, E. and Livage, J., Influence of Fe(II) on the Formation of the Spinel Iron-Oxide in Alkaline-Medium, Clays and Clay Minerals, **40**, 531-539, (1992).
- [55] Rickard, D., Characteristics of mackinawite, tetragonal FeS, *Geochimica Et Cosmochimica Acta*, **70**, A533-A533, (2006).
- [56] Thamdrup, B., Finster, K., Hansen, J. W. and Bak, F., Bacterial Disproportionation of Elemental Sulfur Coupled to Chemical-Reduction of Iron or Manganese, *Applied and Environmental Microbiology*, **59**, 101-108, (1993).
- [57] Sørensen, S. P. L. and Linderstrøm-Lang, K., On the determination and values of π_0 in electromotoric measurements of hydrogen ion concentrations, *C. R. Lab. Carlsberg* **15**, 1-40, (1924).
- [58] Bates, R. G., Definitions of pH Scales, *Chemical Reviews*, **42**, 1-61, (1948).
- [59] Covington, A. K., Bates, R. G. and Durst, R. A., Definition of pH Scales, Standard Reference Values, Measurement of pH and Related Terminology - (Recommendations 1984), *Pure and Applied Chemistry*, **57**, 531-542, (1985).
- [60] Buck, R. P., Rondinini, S., Covington, A. K., Baucke, F. G. K., Brett, C. M. A., Camoes, M. F., Milton, M. J. T., Mussini, T., Naumann, R., Pratt, K. W., Spitzer, P. and Wilson, G. S., Measurement of pH. Definition, standards, and procedures (IUPAC Recommendations 2002), *Pure and Applied Chemistry*, **74**, 2169-2200, (2002).
- [61] Butler, J. N., *Ionic equilibrium: solubility and pH calculations*, John Wiley & Sons, New York, (1998).
- [62] Knauss, K. G., Wolery, T. J. and Jackson, K. J., A New Approach to Measuring pH in Brines and Other Concentrated Electrolytes, *Geochimica Et Cosmochimica Acta*, **54**, 1519-1523, (1990).
- [63] Altmaier, M., Neck, V. and Fanghänel, T., Solubility of Zr(IV), Th(IV) and Pu(IV) hydrous oxides in CaCl₂ solutions and the formation of ternary Ca-M(IV)-OH complexes, *Radiochimica Acta*, **96**, 541-550, (2008).
- [64] Altmaier, M., Metz, V., Neck, V., Muller, R. and Fanghänel, T., Solid-liquid equilibria of Mg(OH)₂(cr) and Mg₂(OH)₃Cl·4H₂O(cr) in the system Mg-Na-H-OH-O-Cl-H₂O at 25°C, *Geochimica et Cosmochimica Acta*, **67**, 3595-3601, (2003).
- [65] Bischofer, B. P., Hagemann, S., Hühne, C., Schönwiese, D. and Scharge, T., Influence of chloride concentrations on the signal of redox electrode and on UV-spectrophotometric determination of Fe species, in 1st Annual Workshop Proceedings 7th EC FP- Recosy CP, Barcelona, (2009).

- [66] Scharge, T., Bischofer, B. P., Hagemann, S. and Schönwiese, D., Spectrophotometric and potentiometric determination of the redox potential in solutions of high ionic strength, in 2nd Annual Workshop Proceeding 7th EC FP-RecoSy CP, Cyprus, (2010).
- [67] Barry, P. H., Jpcalc, a software package for calculating liquid-junction potential corrections in patch-clamp, intracellular, epithelial and bilayer measurements and for correcting junction potential measurements, *Journal of Neuroscience Methods*, **51**, 107-116, (1994).
- [68] Kopunec, R., Abudeab, F. N. and Skraskova, S., Extraction of pertechnetate with tetraphenylphosphonium in the presence of various acids, salts and hydroxides, *Journal of Radioanalytical and Nuclear Chemistry*, **230**, 51-60, (1998).
- [69] Morrison, G. H. and Freiser, H., *Solvent Extraction in Analytical Chemistry*, London, John Willey & Sons, Inc., (1957).
- [70] JCPDS, Powder diffraction files. Joint Committee on Powder Diffraction Standards. Swarthmore, 2001: USA (2001).
- [71] Gaona, X., Dahn, R., Tits, J., Scheinost, A. C. and Wieland, E., Uptake of Np(IV) by C-S-H phases and cement paste: an EXAFS study, *Environmental Science & Technology*, **45**, 8765-8771, (2011).
- [72] Kirsch, R., Fellhauer, D., Altmaier, M., Neck, V., Rossberg, A., Charlet, L. and Scheinost, A. C., Reaction of Pu(III) and (V) with magnetite and mackinawite: A XANES/EXAFS investigation, *Geochimica Et Cosmochimica Acta*, **74**, A520-A520, (2010).
- [73] Kobayashi, T., Scheinost, A. C., Fellhauer, D., Gaona, X. and Altmaier, M., Redox behavior of Tc(VII)/Tc(IV) under various reducing conditions in 0.1M NaCl solutions, *Radiochim. Acta*, (2013).
- [74] Ravel, B. and Newville, M., ATHENA, ARTEMIS, HEPHAESTUS: data analysis for X-ray absorption spectroscopy using IFEFFIT, *Journal of Synchrotron Radiation*, **12**, 537-541, (2005).
- [75] Kirsch, R., Fellhauer, D., Altmaier, M., Neck, V., Rossberg, A., Fanghänel, T., Charlet, L. and Scheinost, A. C., Oxidation state and local structure of plutonium reacted with magnetite, mackinawite and chukanovite, *Environmental Science & Technology*, **45**, 7267-7274, (2011).
- [76] Saeki, M., Sasaki, Y., Nakai, A., Ohashi, A., Banerjee, D., Scheinost, A. C. and Foerstendorf, H., Structural study on complex of MIDOA with $M(VII)O_4^-$ ($M=Re$ and Tc) by ¹H-NMR, EXFAS and IR spectroscopy, *Inorg. Chem.*, (2012).
- [77] Rossberg, A., Reich, T. and Bernhard, G., Complexation of uranium(VI) with protocatechuic acid - application of iterative transformation factor analysis to EXAFS spectroscopy, *Analytical and Bioanalytical Chemistry*, **376**, 631-638, (2003).
- [78] Ressler, T., WinXAS: a program for X-ray absorption spectroscopy data analysis under MS-Windows, *Journal of Synchrotron Radiation*, **5**, 118-122, (1998).

- [79] Harvie, C. E., Moller, N. and Weare, J. H., The prediction of mineral solubilities in natural-waters - the Na-K-Mg-Ca-H-Cl-SO₄-OH-HCO₃-CO₃-CO₂-H₂O system to high ionic strengths at 25°C, *Geochimica Et Cosmochimica Acta*, **48**, 723-751, (1984).
- [80] Konnecke, T., Neck, V., Fanghänel, T. and Kim, J. I., Activity coefficients and Pitzer parameters in the systems Na⁺/Cs⁺/Cl⁻/TcO₄⁻ or ClO₄⁻/H₂O at 25°C, *Journal of Solution Chemistry*, **26**, 561-577, (1997).
- [81] Neck, V., Konnecke, T., Fanghänel, T. and Kim, J. I., Pitzer parameters for the pertechnetate ion in the system Na⁺/K⁺/Mg²⁺/Ca²⁺/Cl⁻/SO₄²⁻/TcO₄⁻/H₂O at 25°C, *Journal of Solution Chemistry*, **27**, 107-120, (1998).
- [82] Meyer, R. E. and Arnold, W. D., The electrode potential of the Tc(IV)-Tc(VII) couple, *Radiochimica Acta*, **55**, 19-22, (1991).
- [83] Lem, W. J. and Wayman, M., Decomposition of aqueous dithionite 1. kinetics of decomposition of aqueous sodium dithionite, *Canadian Journal of Chemistry*, **48**, 776-&, (1970).
- [84] Wayman, M. and Lem, W. J., Decomposition of aqueous dithionite 2. a reaction mechanism for decomposition of aqueous sodium dithionite, *Canadian Journal of Chemistry*, **48**, 782-&, (1970).
- [85] Stern, H. S., McAfee, J. G. and Subraman.G, Preparation distribution and utilization of technetium-99m-sulfur colloid, *Journal of Nuclear Medicine*, **7**, 665-&, (1966).
- [86] Felmy, A. R., Rai, D., Schramke, J. A. and Ryan, J. L., The solubility of plutonium hydroxide in dilute-solution and in high-ionic-strength chloride brines, *Radiochimica Acta*, **48**, 29-35, (1989).
- [87] Altmaier, M., Neck, V. and Fanghänel, T., Solubility and colloid formation of Th(IV) in concentrated NaCl and MgCl₂ solution, *Radiochimica Acta*, **92**, 537-543, (2004).
- [88] Hess, N. J., Xia, Y. X., Rai, D. and Conradson, S. D., Thermodynamic model for the solubility of TcO₂.xH₂O(am) in the aqueous Tc(IV)-Na⁺-Cl⁻-H⁺-OH⁻-H₂O system, *Journal of Solution Chemistry*, **33**, 199-226, (2004).
- [89] Fellhauer, D., Untersuchungen zur Redoxchemie und Löslichkeit von Neptunium und Plutonium, 2013, University of Heidelberg , Germany.
- [90] Almahamid, I., Bryan, J. C., Bucher, J. J., Burrell, A. K., Edelstein, N. M., Hudson, E. A., Kaltsoyannis, N., Lukens, W. W., Shuh, D. K., Nitsche, H. and Reich, T., Electronic and Structural Investigations of Technetium Compounds by X-Ray-Absorption Spectroscopy, *Inorganic Chemistry*, **34**, 193-198, (1995).
- [91] Rodriguez, E. E., Poineau, F., Llobet, A., Sattelberger, A. P., Bhattacharjee, J., Waghmare, U. V., Hartmann, T. and Cheetham, A. K., Structural studies of TcO₂ by neutron powder diffraction and first-principles calculations, *Journal of the American Chemical Society*, **129**, 10244-10248, (2007).

- [92] Neck, V., Fanghänel, T. and Kim, J., Thermodynamische Modellierung von Technetium in Natürlichen Aquatischen Systemen, Wissenschaftliche Berichte FZKA 6340, (1999).
- [93] Pitzer, K. S., Electrolyte Theory - Improvements since Debye and Huckel, Accounts of Chemical Research, **10**, 371-377, (1977).
- [94] Poineau, F., Johnstone, E. V., Sattelberger, A. P. and Czerwinski, K. R., Characterization of $TcCl_4$ and $\beta\text{-}TcCl_3$ by X-ray absorption fine structure spectroscopy, Journal of Radioanalytical and Nuclear Chemistry, **299**, 235-239, (2014).
- [95] Sundrehagen, E., Polymer Formation and Hydrolyzation of Tc(IV)-99, International Journal of Applied Radiation and Isotopes, **30**, 739-743, (1979).
- [96] Brown, P. L., Curti, E. and Grambow, B., Chemical thermodynamics of zirconium, ed. OECD Nuclear Energy Agency. Vol. 8. Issy-les-Moulineaux, France, Elsevier, (2005).
- [97] Rabung, T., Altmaier, M., Neck, V. and Fanghanel, T., A TRLFS study of Cm(III) hydroxide complexes in alkaline $CaCl_2$ solutions, Radiochimica Acta, **96**, 551-559, (2008).
- [98] Shannon, R. D., Revised Effective Ionic-Radii and Systematic Studies of Interatomic Distances in Halides and Chalcogenides, Acta Crystallographica Section A, **32**, 751-767, (1976).
- [99] Neck, V., Kim, J. I., Seidel, B. S., Marquardt, C. M., Dardenne, K., Jensen, M. P. and Hauser, W., A spectroscopic study of the hydrolysis, colloid formation and solubility of Np(IV), Radiochimica Acta, **89**, 439-446, (2001).
- [100] Grenthe, I. and Puigdomenech, I., Modelling in aquatic chemistry, ed. OECD Nuclear Energy Agency, Paris, Elsevier, (1997).
- [101] Scheinost, A. C., Kirsch, R., Banerjee, D., Fernandez-Martinez, A., Zaenker, H., Funke, H. and Charlet, L., X-ray absorption and photoelectron spectroscopy investigation of selenite reduction by Fe-II-bearing minerals, Journal of Contaminant Hydrology, **102**, 228-245, (2008).
- [102] Dulnee, S., Banerjee, D., Merkel, B. J. and Scheinost, A. C., Surface Complexation and Oxidation of Sn-II by Nanomagnetite, Environmental Science & Technology, **47**, 12852-12859, (2013).
- [103] Schwertmann, U. and Cornell, R. M., Iron Oxides in the Laboratory, ed. OECD Nuclear Energy Agency, Weinheim, Germany, (2000).
- [104] Fleet, M. E., The Structure of Magnetite - Symmetry of Cubic Spinels, Journal of Solid State Chemistry, **62**, 75-82, (1986).
- [105] Rodriguez, E. E., Poineau, F., Sattelberger, A. P., Llobet, A., Czerwinski, K. and Cheetham, A. K., INOR 173-Synthesis and characterization of technetium oxides, Abstracts of Papers of the American Chemical Society, **233**, 19-19, (2007).

-
- [106] Giffaut, E., Grive, M., Blanc, P., Vieillard, P., Colas, E., Gailhanou, H., Gaboreau, S., Marty, N., Made, B. and Duro, L., Andra thermodynamic database for performance assessment: ThermoChimie, Applied Geochemistry (in press), (2014).
- [107] Lamfers, H. J., Meetsma, A., Wiegers, G. A. and deBoer, J. L., The crystal structure of some rhenium and technetium dichalcogenides, Journal of Alloys and Compounds, **241**, 34-39, (1996).
- [108] Lemire, R. J., Berner, U., Musikas, C., Palmer, D. A., Taylor, P. and Tochiyama, O., Chemical thermodynamics of iron, ed. OECD Nuclear Energy Agency. Vol. 13a. Issy-les-Moulineaux, France, (2013).
- [109] Neck, V., Altmaier, M. and Fanghänel, T., Ion interaction (SIT) coefficients for the Th⁴⁺ ion and trace activity coefficients in NaClO₄, NaNO₃ and NaCl solution determined by solvent extraction with TBP, Radiochimica Acta, **94**, 501-507, (2006).



ISSN 1869-9669
ISBN 978-3-7315-0412-2

ISBN 978-3-7315-0412-2

